

**Continuous detection and prediction of  
grasp states and kinematics from primate  
motor, premotor, and parietal cortex**

**Dissertation**

for the award of the degree

**“Doctor rerum naturalium”**

of the Georg-August-Universität Göttingen

within the doctoral program *Theoretical and Computational Neuroscience*  
of the Georg-August University School of Science (GAUSS)

submitted by

**Veera Katharina Menz**

from Hünfeld, Germany

Göttingen, 2015

## **Thesis Committee**

Prof. Dr. Hansjörg Scherberger  
Research Group Neurobiology  
German Primate Center  
Kellnerweg 4  
37077 Göttingen

Prof. Dr. Fred Wolf  
Theoretical Neurophysics  
Max Planck Institute for Dynamics and Self-Organization  
Am Faßberg 17  
37077 Göttingen

Prof. Dr. Alexander Gail  
Cognitive Neuroscience Laboratory  
German Primate Center  
Kellnerweg 4  
37077 Göttingen

## **Members of the Examination Board**

Referee: Prof. Dr. Florentin Wörgötter  
Department of Computational Neuroscience  
Drittes Physikalisches Institut/BCCN  
Georg-August Universität  
Friedrich-Hund-Platz 1  
37077 Göttingen

2<sup>nd</sup> Referee: Prof. Dr. Julia Fischer  
Kognitive Ethologie  
German Primate Center  
Kellnerweg 4  
37077 Göttingen

3<sup>rd</sup> Referee: Dr. Igor Kagan  
Decision and Awareness Group  
German Primate Center  
Kellnerweg 4  
37077 Göttingen

Date of oral examination: April 29, 2015

Herewith I declare that I have written this thesis independently and with no other aids and sources than quoted.

Göttingen, February 27, 2015

Veera Katharina Menz



## Acknowledgements

Although it is my name that is written in front of this thesis, a work like this is never the product of only one person. In fact, it is the connections between many people that make such a project possible; I am just one part of this big network of people. Each person in this network contributed in one way or another to the realization of this work and I want to take the opportunity here to mention those people who wove this net together with me.

First of all, there was of course Hans, my supervisor, who gave me, as a mathematician, the opportunity to dive into this strange, yet fascinating world of monkeys and brains. Throughout this project he gave me the freedom to take my own decisions, directed me when it was necessary, and always was there with help and support, regardless of the issue.

Then, there was Stefan, who agreed to show and explain to me all kinds of things about monkey training and recording, and who let me work with him when I was new in the lab and needed to learn. Only thanks to Hans and Stefan, who had the confidence in me to realize this project and who gave me the data so that I could do it, I was able to take on this project.

Furthermore, there was my thesis committee consisting of Hans, Prof. Fred Wolf, and Prof. Alexander Gail, which were very supportive towards me, be it by means of scientific criticism or the friendly atmosphere of our meetings.

Apart from this scientific part of the net, there were many other connections to people, friends and family, which were equally important for this project, because they were important to me. The first ones to mention here are of course my present and former colleagues from the Neurobiology Lab who are at least as much friends to me as they are colleagues: Ricarda and Natalie, with whom I could always laugh and cry, Andres, Anja, Ben, Matthias, Sabine, Stefan, Wei-an, Yves, as well as Tanya and Sebastian, who empathized from across the ocean, and the Movie-Nighters Jeroen and Janine, Rijk, Josey, and Jonathan, who always provided a good start to the week. You guys made work a good place to be!

Then, there were Antonio, Caio, Clio, and Valeska from the befriended labs, with whom I could make and experience awesome art, be it music, movies, books, design, tv, or acting; all the awesome people I played theatre with; and my Flamenco girls. All these people supported me indirectly in my work by being there for me and backing me in all my other important projects that I had apart from work. You made me feel that I belong here.

The people who proof read parts of my thesis, Annabelle, Janine, Jonathan.

My friends from Köln and home, Annabelle, Martina, Sebi, Tina, and Anne, who gave me advise or distracted me or supported me in any other necessary way.

My parents, who supported my decisions, gave me love, advice, and helping hands.

And of course Jonathan, who was always there, always supportive, always understanding, always showing me that it's gonna be alright.

Thanks to all of you.

# Table of Contents

<b>Chapter I - Introduction</b> .....	<b>1</b>
1. Introduction.....	3
1.1. Cortical mechanisms involved in the planning and execution of grasping.....	4
1.1.1. Dorsal and ventral stream.....	5
1.1.2. Area AIP in the parietal cortex.....	6
1.1.3. Area F5 in the premotor cortex.....	9
1.1.4. Primary motor cortex M1.....	11
1.1.5. The fronto-parietal grasping network.....	13
1.2. Neuroprosthetics.....	15
1.2.1. Limitations and restrictions of previous decoding studies.....	17
1.3. Motivation and overview of thesis.....	20
<b>Chapter II - Kinematic decoding</b> .....	<b>23</b>
2. Materials and Methods.....	25
2.1. Basic procedures.....	25
2.2. Experimental setup.....	26
2.3. Behavioural paradigm.....	28
2.4. Signal procedures and imaging.....	28
2.5. Hand kinematics.....	30
2.6. Neural recordings.....	31
2.7. Decoding.....	31
2.7.1. Decoding algorithm.....	31
2.7.2. Decoding procedure.....	32
2.7.3. Variation of decoding parameters.....	33
2.7.4. Evaluation of decoding performance.....	34
2.7.5. Chance decoding performance.....	35
3. Results.....	37
3.1. Kinematic and neuronal data.....	37
3.2. Decoding of 27 DOF.....	38
3.3. Decoding performance of different areas.....	41
3.4. Influence of number of units on decoding performance.....	44
3.5. Decoding performance of proximal and distal movements.....	46
3.6. Optimal decoding parameters.....	48
4. Discussion.....	51

4.1. Movement reconstruction with primary and premotor cortex.....	51
4.2. Movement reconstruction with parietal cortex.....	55
4.3. Influence of unit number on decoding performance .....	57
4.4. Reconstruction of proximal and distal joints.....	58
4.5. Optimal decoding parameters and their network implications.....	60
4.6. Conclusion.....	65
<b>Chapter III - State decoding.....</b>	<b>67</b>
5. Materials and Methods .....	69
5.1. Decoding algorithm.....	69
5.2. Decoding procedure .....	71
5.3. Variation of decoding parameters .....	72
5.4. Evaluation of decoding performance .....	72
5.5. Accuracy of movement onset prediction.....	73
5.6. Chance level performance .....	74
6. Results .....	77
6.1. State detection performance of different areas.....	77
6.2. Detection performance for individual states .....	79
6.3. Resting state detection during passive resting phases and active hold epochs.....	81
6.4. Decoding of movement onset.....	83
6.5. Optimal decoding parameters.....	86
7. Discussion .....	89
7.1. State reconstruction with primary and premotor cortex.....	89
7.2. State reconstruction with parietal cortex .....	91
7.3. Reconstruction of individual states .....	92
7.4. Active and passive resting.....	94
7.5. Decoding of movement onset.....	96
7.6. Optimal decoding parameters.....	98
7.7. Conclusion.....	99
<b>Chapter IV - Conclusions .....</b>	<b>101</b>
8. Conclusions and Outlook .....	103
9. Summary .....	107
References .....	109
Abbreviations .....	121
Curriculum Vitae.....	123







# **Chapter I**

**- Introduction**



## 1. Introduction

Manipulation of objects and interaction with our environment by means of our hands is an essential part of our everyday lives. How much we actually rely on the use of our hands becomes most apparent when we lose the ability to perform hand and arm movements. Consequently, it comes as no surprise that the recovery of exactly these functions ranges as number one on the list of abilities which are wished to be regained by affected people (Anderson 2004). Hand and arm functions are essential to fulfil our physical and emotional needs as well as to establish and maintain an independent and self-directed life and are thus a significant contributor to the quality of life.

In order to restore the skill of everyday hand movements in patients who have lost this function due to spinal cord injuries, loss of limbs or other motor diseases, the development of neuroprostheses has come more and more into focus. The goal of these devices is the translation of neural activity arising during attempted movement generation into an output for controlling an external actuator like a robot hand as a hand and arm replacement.

However, grasping is a highly evolved behaviour, and the underlying mechanisms both on the mechanical and brain level are highly complex. The generation of movement and especially of finger kinematics is distributed across many areas within the cortex and subcortical structures. Besides the actual control of muscles to perform a movement, these areas code a variety of other aspects involved in the planning and execution of hand movements, such as features of the environment in which the action is going to take place in, features about the object the action is directed at, internal states like current hand position, muscle fatigue or motivational states, mechanical restrictions of the environment and the body, knowledge and expectations about the action to be performed, etc. All of these aspects need to be brought together in order to generate a movement plan which then can be executed.

Also on the mechanical level, the human hand shows a lot of complexity. Almost 40 muscles are engaged in the movement of the hand, acting to both extend and flex as well as stabilizing

individual joints (Lemon 1999, Raos *et al* 2006). In conjunction with several proximal muscles, the human hand and wrist are able to exhibit a total number of 27 degrees of freedom (DOF) (Lin *et al* 2000, Rehg and Kanade 1994). So far, neuroprosthetic devices have only been able to reproduce a fraction of this number.

This thesis is devoted to addressing this and other problems which are faced in the development of neuroprosthetics. However, before describing these challenges in more detail, I will first give an overview of the cortical mechanisms involved in the planning and execution of grasps (section 1.1). We will focus particularly on three different areas in the neocortex (M1, F5, and AIP, sections 1.1.2-1.1.4), which play important roles in this process, and describe their particular contributions to the planning and execution of hand movements (section 1.1.5).

Following, I will give an introduction to the state of the art of neuroprosthetics restoring hand and arm movements (section 1.2). Strengths and achievements of this technology are discussed, but also problems which have not been solved yet are addressed (section 1.2.1). Finally, I will delineate which of the current problems I will address in this thesis and give an outline of the structure of the thesis (section 1.3).

### ***1.1. Cortical mechanisms involved in the planning and execution of grasping***

Although the generation of hand and arm movements seems trivial to us while we perform hundreds of them every day, they involve a highly complex network of brain areas and computations carried out in those areas.

Imagine for example the mundane action of picking up a cup of coffee from the table. In order to bring the hand to the cup and grasp it, a visuomotor transformation needs to be performed in the brain in order to convert visual information about the object to be grasped or manipulated into a movement plan which then can be executed. We will now follow the processing of visual information through the brain and its transformation into a movement.

*1.1.1. Dorsal and ventral stream.* First, the gaze fixates onto the cup so that the image of the cup and its environment falls onto the retina. From there, information about the image is forwarded via the optic tract, through the lateral geniculate nucleus to primary visual cortex (V1) where features like the orientation of edges are detected (Hubel and Wiesel 1968). From there, information is forwarded into two major processing pathways, the ventral (temporal) and the dorsal (parietal) stream. These pathways are hierarchically organized: information from lower visual areas (early on within the stream) is projected to higher ones and this way integrated there into representations of more complex and abstract features (e.g. information of orientation of individual edges is combined into the representation of a geometric shape).

The two pathways differ from each other in terms of information they code: whereas the ventral pathway is concerned with object recognition (*what* do I see? a cup with delicious coffee!) and thus associated with perception, the dorsal pathway deals with information relevant to action generation, like the location or shape of the object to be grasped (*where* is the object? on the table in front me! what shape does it have? it is a cylinder with a circular extension on the right side!) (Goodale and Milner 1992, Norman 2002).

The significance of these two pathways and the information they code becomes apparent in the following two patient cases, described by Goodale *et al* (1994) and Goodale *et al* (1991), in which either of the streams was disrupted: in the first case, patient DF suffering from a lesion from a bilateral damage in the ventrolateral occipital region interrupting the ventral visual pathway, was not able to visually discriminate irregularly shaped objects, but could shape her hand according to the respective objects in order to grasp them with her fingers. In contrast, patient RV who suffered from a lesion of the occipitoparietal cortex disrupting the dorsal visual pathway, was able to visually discriminate the objects, however could not grasp those objects properly. In the following,

we will therefore focus on the latter of the two pathways, the dorsal stream, in our journey of tracing the generation of hand movement through the brain.

The dorsal pathway extends to the posterior parietal cortex (PPC) which contains several brain areas involved in the planning of movement: neurons in the lateral intraparietal area (LIP) become active during planning of saccadic eye movements (Andersen *et al* 1990b, Gnadt and Andersen 1988, Pesaran *et al* 2002), the parietal reach region (PRR) (medial and posterior to LIP; Snyder *et al* 1997) has been shown to be modulated during planning of reaching movements as well as to be tuned to the direction of reaches (Batista and Andersen 2001, Snyder *et al* 1997), and the medial intraparietal sulcus (MIP) (part of PRR; Musallam *et al* 2004) has been shown to encode the location of a reach target in an eye-centred reference frame (Pesaran *et al* 2006). The anterior intraparietal area (AIP) has been found to be specialized for the visual guidance of hand movements (Gallese *et al* 1994, Murata *et al* 2000, Sakata *et al* 1995) and forms the fronto-parietal grasping network, together with area F5 in the premotor cortex and primary motor cortex (M1) (Jeannerod *et al* 1995). Therefore, in the following three chapters, we will take a closer look at areas AIP, F5, and M1 and their contributions to the generation of grasping movements. Afterward, we will summarize the major points and shed more light on the fronto-parietal grasping network itself (section 1.1.5).

*1.1.2. Area AIP in the parietal cortex.* Area AIP plays an important role in the visuomotor transformation for grasping. It receives input from the caudal intraparietal area (CIP) (Borra *et al* 2008, Sakata *et al* 1999, Sakata *et al* 1995) which has been shown to be involved in the integration of information about texture and gradient signals of a stimulus in order to produce a representation of surface orientation in 3D space (Sakata *et al* 1997, Sakata *et al* 1999, Tsutsui *et al* 2001, Tsutsui *et al* 2002), as well as from areas PG and PFG (Borra *et al* 2008). PG and PFG, located in the rostral part of area 7a and the caudal part of 7b, have been shown to be involved in the execution of goal-directed hand and mouth movements (Fogassi and Luppino 2005). Information about eye



movements is sent to AIP from the rostral part of LIP (Andersen *et al* 1990a, Borra *et al* 2008) as well as from the ventral part of the frontal eye field (FEF) (Borra *et al* 2008). Furthermore, AIP shows strong reciprocal connections to the secondary somatosensory area (SII) (Borra *et al* 2008), a higher order somatosensory area involved in tactile object exploration and recognition as well as in expectation of a tactile stimulus (Carlsson *et al* 2000, Reed *et al* 2004).

Although the ventral and dorsal visual streams are considered as separate pathways encoding different aspects of visual information (see section 1.1.1), there is also evidence that areas within the streams communicate with each other across the two pathways. AIP is one of these brain regions (Borra *et al* 2008), suggesting that AIP receives information about object recognition and discrimination and at the same time contributes to the representation of 3D objects and surfaces in the inferotemporal cortex (Janssen *et al* 2001). In addition, AIP is reciprocally connected with area 12 (Borra *et al* 2008, Schwartz and Goldman-Rakic 1984) and area 46 (Borra *et al* 2008, Petrides and Pandya 1984, Schwartz and Goldman-Rakic 1984) in the prefrontal cortex. Wilson *et al* (1993) showed that area 12 acts as a working memory for keeping a representation of spatial stimuli.

In conclusion, as an area integrating information about eye position, object surface information, expected tactile sensation, object meaning, goal-directed hand movements, and with access to the representation of objects in the working memory, AIP seems to play a significant role in the generation of hand movements. Indeed, inactivation and lesions of area AIP in monkeys or humans resulted in deficits of hand preshaping and mismatch of hand orientation when grasping an object (Binkofski *et al* 1998, Faugier-Grimaud *et al* 1978, Gallese *et al* 1994).

Murata *et al* (2000) and Sakata *et al* (1995) studied the response of single units recorded in macaque area AIP while monkeys performed a delayed reach and grasp task in which different objects were presented to the animals one at a time. After a short delay period, the monkeys reached to the object and grasped it. The grasping was either performed in light or in dark. In addition, in a

separate task condition, the monkeys only fixated on the presented object without performing the motor action.

Depending on their response throughout the different task conditions, Murata, Sakata and colleagues assigned neurons in AIP into five different categories: the first class of cells consisted of “object-type visual-motor” neurons that responded to the presentation of objects regardless of subsequent movement or not, and that were also active during movement execution. However, activity was decreased if the movement was performed in the dark compared to movement performed in the light (Baumann *et al* 2009, Lehmann and Scherberger 2013, Townsend *et al* 2011). The same effect of illumination was also present in the activity of the second class of neurons, the “nonobject-type visual-motor” cells, however the response during presentation of the object was only present if a movement followed. Neurons of the third and fourth class, the “object-type” and “nonobject-type visual-dominant” cells, respectively, showed activity during movement execution only if the movement was performed in the light. “Object-type visual-dominant” neurons did not require a subsequent motor execution to become active during object presentation whereas “nonobject-type visual-dominant” cells did. According to Borra *et al* (2008), the visual response of these four neuron types could be driven by projections from the lateral superior temporal sulcus (ISTS). Last but not least, the neurons of the fifth category, the “motor-dominant” cells, were active during movement execution and did not exhibit any difference in activity if the movement was performed in the light or in the dark. Together with the “object-type visual-motor” neurons, these cells were the most common ones.

Furthermore, neurons in AIP have been shown to be selective in their response for object shape (Murata *et al* 2000, Sakata *et al* 1995, Schaffelhofer *et al* 2015), object size (Murata *et al* 2000, Schaffelhofer *et al* 2015), and object orientation (Baumann *et al* 2009, Murata *et al* 2000). However, not only visual features of objects to be grasped were found to be encoded in AIP, but also aspects of the performed hand action like grip types and target position in space (Baumann *et*

*al* 2009, Jeannerod *et al* 1995, Lehmann and Scherberger 2013, Murata *et al* 2000, Sakata *et al* 1995).

Based on these findings, it has been suggested that activity in AIP could already reflect a motor plan based on visual and somatosensory information (Borra *et al* 2008, Debowy *et al* 2001, Murata *et al* 2000) instead of solely extracting visual cues relevant for grasping.

Information is then projected from AIP to area F5 in the premotor cortex where a pattern of hand movements or grip type is selected. The chosen action command is sent back to AIP as an efference copy where it can be compared to spatial features of the object and the initial motor plan and be upgraded if necessary (Borra *et al* 2008, Murata *et al* 2000, Sakata *et al* 1995).

*1.1.3. Area F5 in the premotor cortex.* Area F5 is located rostrally in the ventral premotor cortex (PMv) and as already mentioned above, is strongly connected with area AIP in a reciprocal way (Borra *et al* 2008, Gerbella *et al* 2011, Luppino *et al* 1999). Similarly to area AIP (as described in the previous section 1.1.2), F5 receives input from areas PFG, SII, and area 12 (Gerbella *et al* 2011) providing F5 with information about the goal of a hand action (Fogassi and Luppino 2005), the tactile expectation of a stimulus (Carlsson *et al* 2000, Reed *et al* 2004), and access to upheld information about spatial stimuli (Wilson *et al* 1993), respectively. Furthermore, area 46v in the prefrontal cortex coding goals of a motor action (Mushiake *et al* 2006, Saito *et al* 2005) is projecting to F5 and area GrFO in the granular postarcuate cortex has been suggested to convey motivational information to F5 (Gerbella *et al* 2011). Connections from area F6/pre-SMA in the medial rostral premotor cortex provide F5 with higher order aspects of motor control (Gerbella *et al* 2011) like temporal sequencing of a motor action (Rizzolatti and Luppino 2001, Saito *et al* 2005).

F5 can be divided into three anatomically distinct parts: the first part lying in the posterior (and dorsal) part of the postarcuate bank (F5p), the second one in the anterior (and ventral) part of the postarcuate bank (F5a), and the third located on the postarcuate convexity cortex (F5c). The three

parts are strongly interconnected (Belmalih *et al* 2009, Gerbella *et al* 2011, Rizzolatti and Luppino 2001).

The different parts of F5 also show functional differences: cells in the convexity become active, when the subject is observing someone else's hand actions ("mirror" neurons), whereas cells in the bank of F5 respond to the presentation of 3D objects and while the subject is grasping an object ("canonical" neurons) (Rizzolatti and Fadiga 1998). More precisely, "canonical" neurons have been shown to code the goal of an action rather than the individual components comprising an action. Examples are "Grasping-with-the-hand neurons", "Holding neurons" or "Tearing neurons" (Rizzolatti *et al* 1988). These neurons have also been shown to exhibit selectivity for different grip types and hand shapes involved in a hand action (Fluet *et al* 2010, Lehmann and Scherberger 2013, Raos *et al* 2006, Rizzolatti *et al* 1988, Rizzolatti and Fadiga 1998, Schaffelhofer *et al* 2015). Furthermore, wrist orientation has been found to be coded as part of the hand configuration in F5 neurons (Kakei *et al* 1999, 2001, Raos *et al* 2006).

Raos *et al* (2006) and Murata *et al* (1997) recorded grasping neurons in macaque brains while animals performed a delayed grasping task and examined the responses of the cells more thoroughly. Similarly to the experiment performed by Murata *et al* (2000) and Sakata *et al* (1995) with which the activity of AIP neurons was investigated (see section 1.1.2), animals were trained to grasp different objects that were presented in front of them either in the light or in the dark. In addition, in a separate task condition, the animals were only required to observe the presented object without grasping it.

Based on these experiments, Raos, Murata, and colleagues grouped the neurons into "motor" and "visuomotor" cells: both neuron types were active during movement execution. However "visuomotor" cells also responded before movement onset while the object was presented to the animal regardless if an actual movement was following or not (Murata *et al* 1997), whereas "motor" neurons only discharged during movement execution. Interestingly, "visuomotor" cells showed

tuning towards certain objects. However, the selectivity did not appear to correspond to visual features of the object as was observed in AIP, but rather to the type of grip used to grasp the object (Raos *et al* 2006, Schaffelhofer *et al* 2015).

According to Raos *et al* (2006), the number of recorded “motor” and “visuomotor” cells in F5 was about the same. Compared to AIP, the amount of motor-dominant cells was higher in F5 (Murata *et al* 2000).

Based on these findings, it has been concluded that sensorimotor information projected from the parietal cortex to F5 is integrated with higher order motor information in order to select an action plan, motor pattern, or grip type (Belmalih *et al* 2009, Fluet *et al* 2010, Gerbella *et al* 2011, Kakei *et al* 2001, Murata *et al* 1997, Raos *et al* 2006, Rizzolatti *et al* 1988, Rizzolatti *et al* 1987, Stark *et al* 2007). This information is then forwarded to the hand field in primary motor cortex (Borra *et al* 2010, Dum and Strick 2005, Matelli *et al* 1986, Muakkassa and Strick 1979), layers of the superior colliculus, sectors of the mesencephalic, pontine, the bulbar reticular formation, and hand muscle motoneurons in the spinal cord (Borra *et al* 2010, Dum and Strick 1991, Galea and Darian-Smith 1994, He *et al* 1993) as well as back to area AIP as already mentioned above (Borra *et al* 2008, Murata *et al* 2000, Sakata *et al* 1995).

In conclusion, area F5 plays an important role for movement generation. Patient studies in which recovery of independent finger movement impairments due to a lesion in M1 or its corticospinal projections could be attributed to F5, support the notion that this area is highly involved in the generation of hand movements (Fridman *et al* 2004, Nudo 2007). Indeed, studies in which area F5 was inactivated confirm that the ability to shape the hand in order to grasp an object was severely impaired (Fogassi *et al* 2001).

*1.1.4. Primary motor cortex M1.* Area M1 is located rostral to the central sulcus and is somatotopically organized: experiments conducted as early as 1870 demonstrated that electrical

stimulation of the motor cortex was able to elicit muscle twitches and movements in different parts of the contralateral side of the body. Which exact region was excited was determined by the location of stimulation within the motor cortex – stimulation from medial to lateral in M1 elicited movements in the lower body parts up to the trunk, to the head and the face. Conversely, patients with lesions in primary motor cortex experience a complete loss of the ability to perform voluntary movements with the respective contralateral body part (Kandel *et al* 2000). For example, differently to the inactivation of ventral premotor cortex, where the ability of proper hand shaping to perform grasp is impaired, a lesion of the M1 hand and digit area results in the inability to perform independent finger movements or finger movements at all (Fulton 1949, Travis 1955).

M1's hand area receives its strongest input from area F5 to which it is reciprocally connected (Dum and Strick 2005, Matelli *et al* 1986, Muakkassa and Strick 1979) and the neurons located there have been subject to extensive studies in the past. They have been found to be modulated by various aspects of motor actions like joint angles and muscle activation (Bennett and Lemon 1996, Holdefer and Miller 2002, Morrow and Miller 2003, Rathelot and Strick 2006, Thach 1978, Umilta *et al* 2007) together with more abstract kinematic features like movement direction (Ashe and Georgopoulos 1994, Georgopoulos *et al* 1986, Kakei *et al* 1999, Thach 1978), position of the wrist (Ashe and Georgopoulos 1994, Kakei *et al* 1999, 2001, Thach 1978), and force (Ashe 1997, Cheney and Fetz 1980, Taira *et al* 1996).

Contrary to area F5, where elevated activity is present already in pre-movement periods, cells in M1 only become active shortly before movement onset and during movement execution. Furthermore, M1 neurons are modulated by different motor components of a performed action, i.e. they exhibit different activity patterns for reaching, grasping, holding and releasing an object, whereas units in F5 show a continuous tuning throughout the entire movement execution (Umilta *et al* 2007). In conclusion, while F5 seems to represent an action plan or grip type as already described

above (section 1.1.3), cells in M1 seem to code individual steps of movement execution in order to realise the movement plan or hand shape.

Information is then projected from M1 via the pyramidal tract to motor neurons and interneurons in the spinal cord. Interneurons are interposed to motor neurons which then in turn innervate respective muscle fibres in order to execute a movement (Bennett and Lemon 1996, Dum and Strick 1991, Holdefer and Miller 2002, Morrow and Miller 2003, Rathelot and Strick 2009). Rathelot and Strick (2009) discovered that area M1 can be partitioned into two subdivisions with different influences on motor output based on their connections to the spinal cord: one part (termed “old” M1 and located in the rostral region of M1) contains cells that contact spinal interneurons and is therefore considered to have a mainly indirect influence on motor commands. In contrast, neurons making direct, monosynaptic connections with motoneurons in the spinal cord (CM cells) are almost exclusively located in the caudal region of M1 (termed “new” M1). It has been suggested that the latter type of cells is necessary for primates to execute highly developed muscle activity patterns like precision grips (Rathelot and Strick 2009).

*1.1.5. The fronto-parietal grasping network.* In 1998, Fagg and Arbib proposed a computational model to describe the cortical involvement in grasping, termed the FARS model (Fagg 1996, Fagg and Arbib 1998). Based on previous findings (Jeannerod *et al* 1995), this model attempted to depict the roles of areas AIP and F5 and their contribution to the generation of grasping movements.

According to the FARS model, visual input is projected via the dorsal stream to area AIP in which visual dominant neurons extract 3D features of the object to be grasped. Then, specific, grasping relevant features (object affordances) are selected by visuomotor cells and forwarded to visuomotor neurons in area F5. According to Fagg and Arbib (1998), multiple visual descriptions are delivered by AIP in order to provide a selection of possibilities of how an object may be grasped. Coming back to our example of the coffee mug, the cup may be grasped for example with

all fingers clasped around the cup's body or only with thumb and index finger held at the cup's handle. The most appropriate choice depends on different aspects, such as the goal of the action (is the cup to be moved on the table or to be brought to the mouth for drinking, etc.) or external factors (is the cup empty or filled, is the content hot or cold, etc.). All these aspects are brought together in area F5 which receives input from prefrontal and premotor cortex like areas as F6 and area 24 (see section 1.1.3 for a more detailed description) including for example the meaning of the object to be grasped which is delivered to the prefrontal cortex by the inferotemporal lobe (IT) (ventral stream). Visuomotor cells in F5 choose one of the grasping prototypes provided by AIP that satisfies the requirements best. Motor neurons in F5 then dissect this prototype into temporally segmented sequences which are forwarded to M1 and the spinal cord. In M1, movement execution is initiated and detailed execution information is projected to the spinal cord (Fagg 1996, Fagg and Arbib 1998, Rizzolatti and Luppino 2001). In addition, F5 sends information about motor prototypes to motor dominant neurons in area AIP where it is stored in a working-memory-like fashion and can be compared to the affordances of the object.

The computational implementation of the FARS model and its comparison to actual observed data was able to rectify the general layout of the model. Based on later studies and observations, modifications have been suggested to it: since area AIP exhibits stronger connections to the prefrontal cortex than F5, additionally to receiving projections directly from IT, it has been proposed that the appropriate object description is not chosen in F5, but instead already selected in AIP and forwarded to area F5 where it is translated into the respective motor prototype by visuomotor neurons (Rizzolatti and Luppino 2001).

In conclusion, together with the hand area of M1, areas F5 and AIP form the fronto-parietal grasping circuit in which visual information is utilized and transformed into a grasping plan (visuomotor transformation) which then can be executed by projections to the spinal cord to adequately innervate muscles in the arm and hand. Finally, after briefly looking at our cup filled



with hot coffee, we stretch our arm and grasp it to reward ourselves after this long and complex journey through the brain.

### ***1.2. Neuroprosthetics***

In order to translate neural activity into a motor command to control a robot hand or another actuator, two different approaches have been pursued depending on the medical condition of the subject causing the motor impairment. In the case of remaining functioning nerves in the peripheral nervous system (e.g. in a stump of an arm or the trunk), neural activity formerly activating muscles in the hand and arm can be recorded from the peripheral nerves and used to control a prosthetic, robotic limb (Raspopovic *et al* 2014, Rossini *et al* 2010). However, in patients in which the communication between the central and peripheral nervous system is interrupted (e.g. due to a spinal cord injury), peripheral activity cannot be accessed. Instead, neural activity is recorded directly from the brain.

Reading activity from the brain can be done in multiple ways: the least invasive method to record neural activity are electroencephalogram (EEG) recordings carried out by scalp electrodes attached to the skull by means of a head cap. Although 3D arm position in space (Bradberry *et al* 2010, Kim *et al* 2014) has been successfully predicted from EEG signals, the method also contains several disadvantages: depending on the parameters to be decoded, the neural signals originally encoding these parameters might not be accessible to the EEG electrodes or the recorded neural signals might be disturbed by brain activity encoding unrelated parameters (Kim *et al* 2014). Therefore, brain activity unrelated to the actual parameters to be predicted often has to be used for prediction instead (Hochberg and Donoghue 2006). Consequently, the patient needs to learn to modulate his or her brain activity accordingly (Hochberg and Donoghue 2006), which in some cases requires extensive training (Neumann and Kubler 2003, Wolpaw and McFarland 2004). Furthermore, since the information transfer of EEG signals is limited (Hochberg and Donoghue

2006, Lal *et al* 2005), the complexity of the output into which the EEG activity is to be translated, is limited as well. Naturalistic hand movements that are composed of a high number of degrees of freedom and show a high kinematic variability can therefore not be predicted accurately by means of EEG signals (Bradberry *et al* 2010).

Electrocorticographic (ECoG) recordings obtained by an electrode grid placed on top of the cortex underneath the dura mater deliver a volume-averaged neural signal similarly to EEG, but have a much higher spectral and spatial resolution (Hochberg and Donoghue 2006, Liu *et al* 2010). The ability to decode hand and finger movements from ECoG signals is subject to ongoing research. For example, patients with temporally implanted subdural electrode arrays due to other, unrelated medical reasons were instructed to perform individual finger movements. Researchers were able to read out from the brain activity when fingers were moved and could distinguish which finger was moved (Kubaneck *et al* 2009, Liu *et al* 2010). In other studies, movements performed with a joystick or reaches to lift a cup were successfully detected (Pistohl *et al* 2013, Wang *et al* 2012) or grip types to grasp a cup were decoded (Pistohl *et al* 2012).

However, in none of the mentioned studies has the detected or decoded movement been translated into an actual movement of a robot arm so far. Instead, this has been realised with neural activity recorded by electrode arrays implanted into the cortex. With this method, action potentials from individual cells can be picked up and activity from multiple, up to several hundred neurons can be recorded simultaneously (Maynard *et al* 1997, Williams *et al* 1999). This technique provides the highest spatial and temporal resolution compared to the recording methods described above. As a consequence, the “original” neural signal from areas involved in the generation of arm and hand movements can be utilized to control a prosthetic limb, ideally similarly as a healthy person would use his or her brain activity to move the arm and hand. Furthermore, the control signal for prosthetic control is separated (at least to a certain extent) from brain activity involved in other tasks of motor control like talking or looking around. Therefore, these tasks can be carried out by the subject at the

same time as moving the prosthetic without affecting the control of the artificial limb (Hochberg and Donoghue 2006).

First successful studies have been conducted with monkeys in which neural activity was translated into movements of a virtual or robot arm. The animals were able to perform reaching movements without using their own limbs or even managed to perform self-feeding actions (Velliste *et al* 2008, Wessberg *et al* 2000).

Recently, this method was also transferred to human patients. Chadwick *et al* (2011) recorded spiking activity in the arm area of primary motor cortex of a tetraplegic person which was translated into arm movements in a virtual environment. The movements were restricted to elbow and shoulder joints in the horizontal plane (2 DOF in total) with which the subject performed reaches to virtual objects.

In a study conducted by Hochberg *et al* (2012), two tetraplegic participants were able to control the arm endpoint position of a robot arm to perform reaches towards an object and grasp it. These movements included 4 DOF in total. The number of parameters controlled by neural activity was increased in study carried out by Collinger *et al* (2013) in which a tetraplegic patient performed reaching, grasping and manipulative movements with a robot arm. A total number of 7 DOF were controlled by the patient and allowed more natural and flexible actions with the neuroprosthesis.

*1.2.1. Limitations and restrictions of previous decoding studies.* In the electrophysiological decoding studies described above, four major problems arise which need to be addressed in order to develop more natural and robust neuroprosthetics in the future.

First, as already described above, the number of DOF decoded from or controlled by neural signals remained relatively low. Human online control achieved 7 DOF (Collinger *et al* 2013) and only one monkey study so far was able to predict an almost full description of hand and arm movements offline continuously over time: there, 18 DOF of the hand and fingers were decoded

together with 7 other wrist and arm joints. Additionally, arm endpoint position and grasp aperture was reconstructed (Vargas-Irwin *et al* 2010). However, the human hand and wrist alone exhibits a total number of 27 DOF (Lin *et al* 2000, Rehg and Kanade 1994). A neuroprosthetic needs to offer the possibility of a variety of hand and arm movements to achieve versatile and natural hand movements.

Second, most of the decoding studies with humans and monkeys so far have focused on utilizing neural activity from M1 (Ben Hamed *et al* 2007, Carmena *et al* 2003, Chadwick *et al* 2011, Collinger *et al* 2013, Hochberg *et al* 2012, Vargas-Irwin *et al* 2010, Velliste *et al* 2008) and premotor cortex or F5 for their predictions (Aggarwal *et al* 2013, Bansal *et al* 2012). Most of the studies recording from primary motor cortex used activity from the rostral part of M1. However, as already mentioned in section 1.1.4, neurons in this area of M1 might only have an indirect influence on motor control as opposed to cells in the caudal region with direct connections to motoneurons in the spinal cord (Rathelot and Strick 2009). Higher decoding performance might therefore be achieved if activity from the latter part of M1 was used for decoding.

Furthermore, other areas than M1 and F5 might have the potential to be suited for prediction of hand and arm movements. As described in section 1.1.2, area AIP in the parietal cortex is also highly involved in the generation of hand and arm movements and has been found to carry motor related information. Nevertheless, so far only very few studies investigated the suitability of AIP for decoding of grasping kinematics: Townsend *et al* (2011) as well as Lehmann and Scherberger (2013) were able to decode two different grip types with an accuracy of ~70% and 75% (averaged), respectively. However, the result was considerably lower than for decoding from area F5 (performance: >90%). A similar result was obtained by Schaffelhofer *et al* (2015) who predicted 20 different grip types with both F5 and AIP and obtained higher decoding accuracy with F5 than with AIP. In contrast, decoding the grip type together with object position in space or object orientation could be performed with higher accuracy with AIP than F5 (Lehmann and Scherberger 2013,

Townsend *et al* 2011). However, all of these studies only decoded grip types and hand shape categories from activity in AIP. A prediction of continuous kinematics is still lacking. So far, only signals from the posterior part of parietal cortex (PPC) like the parietal reach region (PRR) and area 5d have been used for predicting hand positions in 3D space (Hauschild *et al* 2012, Wessberg *et al* 2000).

The third problem concerns the decoding scheme of the neuroprosthesis. All decoding studies mentioned above used a continuous kinematic decoding scheme, i.e. a motor output was continuously decoded and translated into robot movement over time. However, in phases of resting or no movement many decoding algorithms still have been found to produce a noisy, jittering output resulting in a slight tremble of the hand. Furthermore, it might be advantageous to the patient to be able to turn the prostheses on or off depending on whether the patient wants to engage in a motor action or not. Therefore, it has been suggested to combine the continuous kinematic decoding with a state decoder working in parallel monitoring the cognitive state the patient is in (Achtman *et al* 2007, Darmanjian *et al* 2003, Ethier *et al* 2011, Hudson and Burdick 2007, Kemere *et al* 2008). Depending on the predicted state, the robotic arm could be turned on or off or switched into other configurations needed to perform a specific task.

In monkeys, state decoding has already begun to be explored. Typically, either different epochs related to the specific course of a behavioural task have been decoded (Achtman *et al* 2007, Aggarwal *et al* 2013, Kemere *et al* 2008), or more general behavioural states like “movement” or “no movement” (Aggarwal *et al* 2008, Ethier *et al* 2011, Lebedev *et al* 2008, Velliste *et al* 2014). Again, all these studies recorded activity from motor and premotor cortex to make state predictions. In parietal cortex, only area PRR has been used to decode behavioural categories during reaching movements (Hudson and Burdick 2007, Hwang and Andersen 2009, Shenoy *et al* 2003); no comparable investigation has been conducted with area AIP so far.

The fourth and final point concerns the feedback the patient receives from the prosthetic. By visually inspecting the decoded hand actions, errors can be counteracted by the patient and control can be maintained. However, without tactile feedback the ability to perform natural movements is greatly diminished (Flanagan and Wing 1993, Johansson and Westling 1984, Johansson and Flanagan 2009). Currently, methods to deliver haptic information from the prosthesis back to the brain are being investigated in monkeys (O'Doherty *et al* 2009, O'Doherty *et al* 2011) but at the moment any elicited haptic sensations still remain far from natural experience.

### ***1.3. Motivation and overview of thesis***

This thesis aims to address the first three points described in the previous section. To do so, we recorded spiking activity simultaneously from the three areas AIP, F5, and M1 which are involved in the fronto-parietal grasping network (see section 1.1). The electrode arrays located in the hand area of M1 were placed into the anterior bank of the central sulcus ("new" M1, Rathelot and Strick 2009) to be able to record from CM cells.

Using a delayed grasping task which aimed to elicit a variety of different hand and finger movements, we decoded 27 DOF of reaching and grasping kinematics from the recorded spiking activity. To our knowledge, this is the most complete decoding of finger, wrist, and arm joints so far. Furthermore, we predicted two different behavioural states, *resting* and *movement*, with activity from the three brain areas. For the first time, decoding could be carried out with simultaneously recorded spiking activity from areas M1, F5, and AIP. This provided the unique opportunity to investigate the areas' suitability for decoding and their information content with respect to grasping kinematics comparatively.

Due to the two different types of decodings carried out in this study, this thesis is divided into two major chapters: in the first part (chapter II), the continuous decoding of 27 DOF of the hand and arm is presented. It is composed of a section describing the materials and methods (section 2), a

section in which the results are illustrated (section 3) as well as a section in which the results are interpreted and discussed in the context of previous research findings (section 4). The results presented in this chapter have also been submitted for publication (Menz *et al* 2015) and are currently under review.

The second part, chapter III, consists of the materials and methods (section 5), results (section 6), and discussion (section 7) of the state decoding. Finally, in chapter IV, section 8, the results of both individual decodings are brought together and an outlook towards future research is given based on the findings presented in this thesis. A summary of all the findings of this study is presented at the end of this thesis in section 9.





# **Chapter II**

**- Kinematic decoding**



## 2. Materials and Methods

In the following sections, the basic procedures, experimental setup, behavioural paradigm, signal procedures and imaging, recording of the hand kinematics, neural recordings, and the decoding are described.

Animal training (as described in section 2.1), neural and kinematic recordings during experimental sessions (as described in sections 2.2 and 2.3) were performed by Stefan Schaffelhofer and were partly assisted by me. The processing of the kinematic and neural data (except for the principal component analysis shown in figure 1 (e), as well as the filtering of neural signals and spike sorting as described in section 2.6, which was also carried out by Stefan Schaffelhofer), the implementation of decoding algorithms and procedures, the decodings (both kinematic decodings as described in this chapter and state decodings as described in chapter III), performance evaluations of decodings and all further analyses were performed by me.

Furthermore, although the results presented in section 3 and parts of the discussion in section 4 were submitted for publication (Menz *et al* 2015), they were entirely written by me.

### 2.1. Basic procedures

For decoding hand movements, two purpose-bred macaque monkeys (*Macaca mulatta*, animal Z: female, 7.0 kg; animal M: male, 10.5 kg) were trained to grasp a wide range of different objects while wearing an instrumented glove (Schaffelhofer and Scherberger 2012). After training was accomplished, both animals were implanted with head holders on the skull and with microelectrode arrays in cortical areas AIP, F5, and M1. In the following recording sessions, spiking activity was recorded from these electrodes together with the kinematics of the primate hand.

Animal care and all experimental procedures were conducted in accordance with German and European law and were in agreement with the Guidelines for the Care and Use of mammals in Neuroscience and Behavioral Research (National Research Council 2003).

### 2.2. Experimental setup

During training and experimental sessions the animals were sitting upright in a customized animal chair with their head fixed. In order to protect the instrumented glove, we constrained the passive (non-grasping) hand with a plastic tube that encompassed the forearm in a natural posture. A

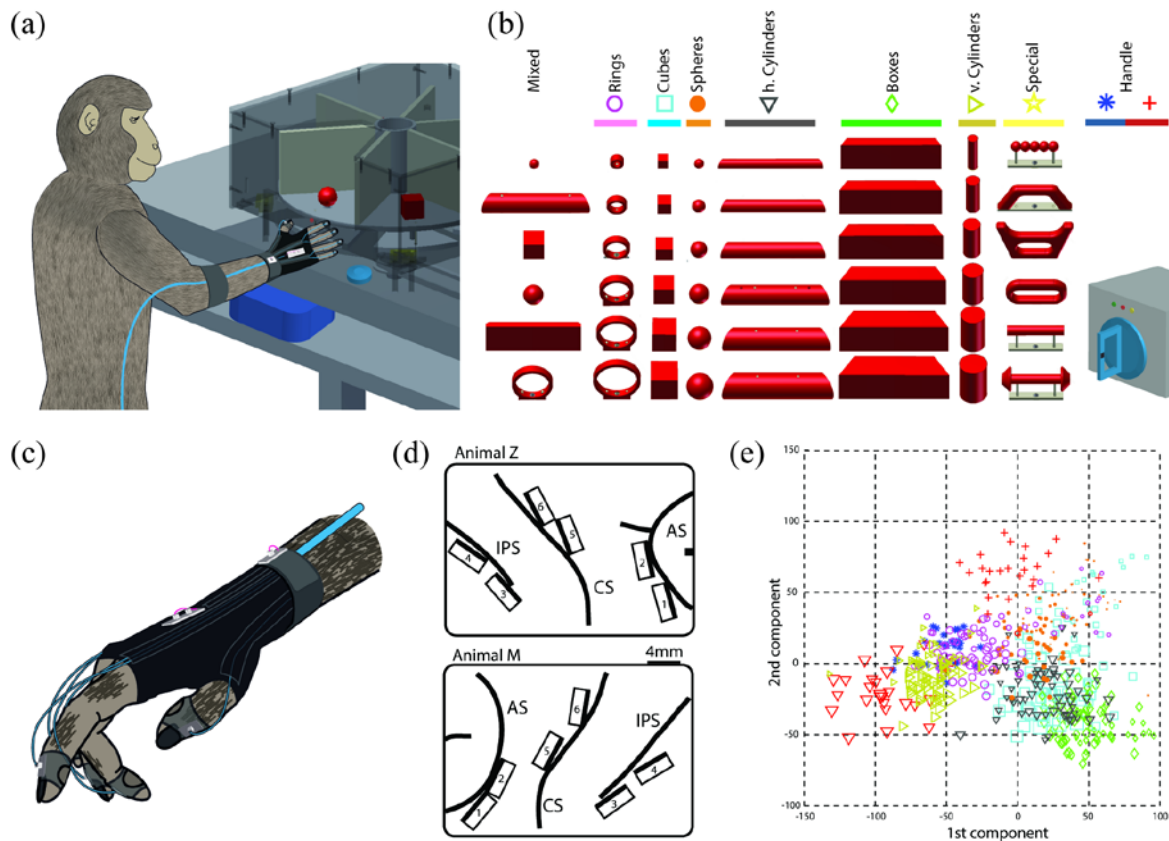


**Figure 1.** (a) 48 different objects were presented on a turntable in front of the monkey. Each turntable held a set of six different objects as shown in columns in (b) which had to be grasped, lifted, and held for 500 ms (*Turntable task*). Furthermore, the turntable could be replaced by a handle box (rightmost object in (b)) on which the animal had to perform precision or power grips (*Grasping Box task*). Hand kinematics were monitored by a data glove as shown in (c). Array implantation locations are illustrated in (d) (IPS, intraparietal sulcus; CS, central sulcus; AS, arcuate sulcus). 1<sup>st</sup> and 2<sup>nd</sup> principal components of recorded kinematics (recording Z032012) are shown in (e). Each marker corresponds to the first two principal components of the 27 DOF averaged across a hold epoch while the monkey was holding a specific object. Symbols correspond to objects as depicted in (b), marker size reflects object size.

capacitive switch at the side of the active (performing) hand allowed detecting the animal's hand position at rest. All graspable objects (figure 1 (b)) were placed at a distance of ~25 cm in front of the animal at chest level. We used a PC-controlled turntable (figure 1 (a)) to pseudo randomly present the objects. Light barriers on top of the ceiling and a step motor ensured precise object positioning. Additional light barriers beneath the turntable detected when the monkey lifted the displayed object.

Eight exchangeable turntables allowed presentation of a total of 48 objects. To obtain a high variation of hand kinematics, we designed the objects to have different shape and size (figure 1 (b)) including *rings* (outer diameter: 10 mm, 20 mm, 30 mm, 40 mm, 50 mm, 60 mm), *cubes* (length: 15 mm, 20 mm, 25 mm, 30 mm, 35 mm, 40 mm), *spheres* (diameter: 15 mm, 20 mm, 25 mm, 30 mm, 35 mm, 40 mm), *cylinders* (length: 140 mm; diameter: 15 mm, 20 mm, 25 mm, 30 mm, 35 mm, 40 mm), and *bars* (length: 140 mm; height 50 mm; depth: 15 mm, 20 mm, 25 mm, 30 mm, 35 mm, 40 mm). Furthermore, a *mixed* turntable was used, holding mid-sized objects of various shapes for fast exchange (sphere 15 mm, horizontal cylinder 30 mm, cube 30 mm, bar 10 mm, ring 50 mm), as well as a *special turntable* that contained objects of abstract forms (figure 1 (b)). All objects had a uniform weight of 120 g, independent of their size and shape.

In addition to these 48 objects, we also trained the monkeys to grasp a handle object in two different ways, either with a precision grip (using thumb and index finger) or with a power grip (enclosure of handle using all digits). These grip types were detected by sensors in cavities the middle of the handle and a light barrier behind the handle, respectively.

Eye position was measured with an optical eye tracker (ISCAN, Woburn, MA, USA), and hand kinematics were recorded by a custom-made hand tracking device (Schaffelhofer and Scherberger 2012; see section 2.5.). To avoid interference with the electro-magnetic based hand tracker, no ferromagnetic materials were used in the experimental setup, including animal chair, table and manipulanda (Kirsch *et al* 2006, Raab *et al* 1979). All task relevant behavioural parameters (eye

position, stimulus presentation, switch activation) were controlled by custom-written behavioural control software that was implemented in LabView (National Instruments).

### **2.3. Behavioural paradigm**

Monkeys were trained to perform grasping actions in the dark in order to observe motor signals in the absence of visual information. To realize this approach, a delayed grasping paradigm (*Turntable task*) was implemented (Schaffelhofer *et al* 2015): monkeys initialized a trial by pressing a capacitive switch in front of them. This action turned on a red LED that the animals had to fixate. After fixating for 500-800 ms, a target object located next to the fixation LED was illuminated for 700 ms (cue epoch), followed by a waiting period in the dark (planning epoch, 500-1000 ms) in which the animals had to withhold movement execution but continue to fixate until the fixation LED blinked (“go” signal). Then, the animals grasped the object and held it up for 500 ms (hold epoch).

Grasp movements performed on the handle (*Grasping Box task*, see figure 1 (b) “Handle”) were executed with the same paradigm with the exception that one of two additional LEDs instructed the monkeys during cue period to perform either a precision grip (yellow LED) or a power grip (green LED).

Incorrect trials were aborted immediately; correct trials were rewarded with juice.

### **2.4. Signal procedures and imaging**

Prior to surgery, we performed a 3D anatomical MRI scan of the animal’s skull and brain to locate anatomical landmarks (Townsend *et al* 2011). For this, the animal was sedated (10 mg/kg ketamine and 0.5 mg/kg xylazine, i.m.), placed in the scanner (GE Signa HD or Siemens TrioTim; 1.5 Tesla) in a prone position, and T1-weighted images were acquired (iso-voxel size: 0.7 mm<sup>3</sup>).

Then, in an initial procedure, a head post (titanium cylinder; diameter 18 mm) was implanted on top of the skull (approximate stereotaxic position: midline, 40mm anterior, 20° forward tilted) and secured with bone cement (Refobacin Plus, BioMed, Berlin) and orthopedic bone screws (Synthes, Switzerland). After recovery from this procedure and subsequent training with head fixation, each animal was implanted in a second procedure with six floating microelectrode arrays (FMAs; MicroProbes for Life Science, Gaithersburg, MD, USA). Specifically, two FMAs were inserted in each area AIP, F5, and M1 (see figure 1 (d)). FMAs consisted of 32 non-moveable monopolar platinum-iridium electrodes (impedance: 300-600 k $\Omega$  at 1 kHz) as well as two ground and two reference electrodes per array (impedance < 10 k $\Omega$ ). Electrode lengths ranged between 1.5 and 7.1 mm and were configured as in Townsend *et al* (2011).

Electrode array implantation locations are depicted in figure 1 (d). In both animals the lateral array in AIP was located at the end of the intraparietal sulcus at level of PF, whereas the medial array was placed more posteriorly and medially at the level of PFG (Borra *et al* 2008). In area F5, the lateral array was positioned approximately in area F5a (Belmalih *et al* 2009, Borra *et al* 2010), whereas the medial array was located in F5p in animal Z and at the border of F5a and F5p in animal M. Finally, both arrays in M1 were positioned in the hand area of M1 (anterior bank of the central sulcus at the level of the spur of the arcuate sulcus and medial to it) (Rathelot and Strick 2009).

All surgical procedures were performed under aseptic conditions and general anaesthesia (e.g. induction with 10 mg/kg ketamine, i.m., and 0.05 mg/kg atropine, s.c., followed by intubation, 1-2% isoflurane, and analgesia with 0.01 mg/kg buprenorphine, s.c.). Heart and respiration rate, electrocardiogram, oxygen saturation, and body temperature were monitored continuously. Systemic antibiotics and analgesics were administered for several days after each surgery. To prevent brain swelling while the dura was open, the animal was mildly hyperventilated (end-tidal CO<sub>2</sub> < 30 mmHg) and mannitol kept at hand. Animals were allowed to recover for at least 2 weeks before behavioural training or recording experiments recommenced.

### **2.5. Hand kinematics**

To monitor the animal's movements, an instrumented glove for small primates was used that allowed recording the animal's finger, hand and arm movements in 27 DOF (Schaffelhofer and Scherberger 2012). The glove was equipped with 7 electro-magnetic sensor coils that enabled hand and arm movement tracking at a temporal resolution of 100 Hz without depending on light or sight to a camera (figure 1 (c)). In this way, finger movements could be tracked continuously even when the sensors were behind or below objects. The method has been described in detail in Schaffelhofer and Scherberger (2012). In short, the technique exploits the anatomical constraints of the primate hand and the 3D position and orientation information of the sensors located at the fingertips, the hand's dorsum and the lower forearm.

Recorded 3D positions of the finger, hand, and arm joints were compared to the animal's anatomy. Rarely occurring errors (e.g. due to short freezing of the kinematic tracking) were set to NaN. Then, each joint angle was calculated for every recorded time step and afterward linearly resampled to exactly 100 Hz. This way, also recorded and previously added NaNs were eliminated by linear interpolation.

Specifically, the following 27 joint angles were extracted: spread (extension/flexion), carpometacarpal (CMC), metacarpophalangeal (MCP), and interphalangeal (IP) joint of the thumb; spread (adduction/abduction), metacarpophalangeal (MCP), proximal interphalangeal (PIP), and distal interphalangeal (DIP) joint of index, middle, ring, and little finger; radial/ulnar deviation (yaw), flexion/extension (pitch), and pronation/supination (roll) of the wrist; flexion/extension of the elbow; as well as adduction/abduction (yaw), flexion/extension (pitch), and lateral/medial rotation (roll) of the shoulder.

Furthermore, the speed of every DOF at each time sample was calculated and added to the kinematics. This resulted in a  $54 \times T$ -matrix with  $T$  as the total number of samples. Note, that only



data recorded while the monkey was exposed to the handle or turntable task was used and concatenated into one matrix, including both correctly and incorrectly performed trials, reward epochs, as well as the time between trials (inter-trial intervals). Data recorded while turntables or the Grasping Box were exchanged by the experimenter were not included.

For illustration purposes, the 27 DOF were averaged during the hold epoch of each successful trial of recording *Z032012*, and a principal component analysis was performed. The first two principal components of the kinematics of each trial are illustrated in figure 1 (e), demonstrating that we were able to cover a wide range of hand configurations together with sampling very small differences in hand kinematics.

### **2.6. Neural recordings**

Extracellular signals were simultaneously recorded from six FMAs (6 x 32 channels) that were permanently implanted into area AIP, F5, and M1 (two arrays in each area). Raw signals were sampled at a rate of 24 kHz with a resolution of 16 bit, and stored to disk together with the behavioural and the kinematic data using a RZ2 Biosignal Processor (Tucker Davis Technologies, FL, USA). Offline, the raw data was bandpass filtered (0.3-7 kHz) and spikes were detected (threshold: > 3.5 standard deviation). Spike sorting was performed with WaveClus (Quiroga *et al* 2004) for automatic sorting and OfflineSorter (Plexon TX, USA) for subsequent manual inspection and revision. Only single and multiunits were considered for further analyses.

### **2.7. Decoding**

**2.7.1. Decoding algorithm.** For offline prediction of the hand and arm kinematics, we employed a Kalman filter (Kalman 1960) as described in Wu *et al.* (2006, 2004). A Kalman filter assumes a linear relationship between the kinematics at time instant  $k$  and the following time instant  $k+1$  (step size: 10 ms), as well as between the kinematics and the neural data at time  $k$ :

$$x_{k+1} = Ax_k + w_k,$$

$$z_k = Hx_k + q_k.$$

Here,  $x_{k+1}$  is the 54x1-vector of the 27 angles and their velocities at time  $k+1$ ,  $A$  a 54x54-matrix relating the kinematics of one time step to the following one,  $z_k$  a vector of length  $N$  containing the neural data at time  $k$  where  $N$  denotes the total number of recorded units,  $H$  a  $N \times 54$ -matrix relating the kinematics at time  $k$  to the corresponding neural information at time  $k$ , and  $w_k$  and  $q_k$  noise terms that are assumed to be normally distributed with zero mean, i.e.  $w_k \sim N(0, W)$  and  $q_k \sim N(0, Q)$ , with  $W \in \mathbb{R}^{54 \times 54}$  and  $Q \in \mathbb{R}^{N \times N}$  covariance matrices.

*2.7.2. Decoding procedure.* For decoding a complete recording session, we used 7-fold cross-validation. For this, the recording session was divided into seven data sets of equal length and composition: each task type (i.e. *Grasping Box task* and data from each turntable) was divided into seven parts of equal length and these parts were randomly attributed to the seven sets, so that eventually each set contained data of each turntable and the *Grasping Box task*.

To decode the kinematics of the  $i$ -th of the seven sets, the parameters of the Kalman filter, namely  $A$ ,  $H$ ,  $W$ , and  $Q$ , were calculated by using the neural and kinematic data of the remaining six sets (decoder training). Then, the kinematic data of the  $i$ -th set (27 DOF and their respective velocities) were iteratively predicted by the Kalman filter. The initial value of each DOF (and velocity) was randomly set within the observed range of the respective DOF/velocity during the recording (interval between the smallest and highest value). For each subsequent time step, the Kalman filter first calculated an a-priori estimation of the kinematics based on the kinematic state of the previous time step. Then, an update of this prediction based on the corresponding neural activity was performed (a-posteriori estimation) (Welch and Bishop 2006).

This procedure was carried out for each of the seven data sets, hence leading to the decoding of the entire recording session. The decoding procedure was implemented in a custom-written software in Matlab (MathWorks Inc., Natick, MA, USA).

*2.7.3. Variation of decoding parameters.* The neural data used for decoding was varied in the following way in order to systematically investigate the impact on decoding performance:

- (1) For each unit, spike times were binned in specific time intervals, i.e. the number of occurring spikes in a specific time bin was counted. Since the kinematic data was predicted by the Kalman filter with a frequency of 100 Hz, the bins for counting the spikes were shifted in time steps of 10 ms which resulted in overlapping bins if the window length was larger than 10 ms. To test the impact of bin length on the decoding performance, it was systematically varied.
- (2) In addition to bin length, we tested whether the introduction of a time lag (gap) between the time series of the kinematics and the series of spike counts would lead to changes in decoding performance. We therefore systematically varied gap length (using both positive and negative values). Using a gap length  $g < 0$  and a bin length  $b > 0$  translated into predicting the kinematics at time point  $t_k$  with the spike count in the time window  $[t_k+g-b \ t_k+g]$  in the a-posteriori step of the Kalman filter, meaning that neural activity preceded the kinematics. Positive gap lengths where the neural data used for decoding succeeded the kinematic prediction were tested as well. A positive gap length  $g > 0$  and bin length  $b > 0$  would then take the spikes in the time window  $[t_k+g \ t_k+g+b]$  into account. For the purpose of clarity, we used the notation  $g = -0, b > 0$  to refer to the time window  $[t_k-b \ t_k]$  and  $g = (+)0, b > 0$  for the time window  $[t_k \ t_k+b]$  of spike counting.

For each recording and area/combination of areas, we tested different combinations of bin and gap lengths, ranging from 0 to  $\pm 180$  sec for gaps and 10–250 ms for bin lengths, and evaluated them with respect to their decoding performance.

*2.7.4. Evaluation of decoding performance.* To assess decoding performance, we calculated both Pearson's correlation coefficient (CC) and the relative root mean squared error (rRMSE) for each DOF across the entire decoded recording session to compare the measured trajectory of a joint angle with the decoded trajectory as predicted by the Kalman filter.

CC was defined as

$$CC = \left[ \sum_{k=1}^N (x_k - \bar{x})(\hat{x}_k - \hat{\bar{x}}) \right] \cdot \left[ \sqrt{\sum_{k=1}^N (x_k - \bar{x})^2 \cdot \sum_{k=1}^N (\hat{x}_k - \hat{\bar{x}})^2} \right]^{-1},$$

where  $N$  is the total number of samples,  $x_k$  and  $\hat{x}_k$  denote the true and decoded DOF at time  $k$ , respectively, and  $\bar{x}$  and  $\hat{\bar{x}}$  are the means across all  $N$  samples of the true and decoded DOF, respectively.

rRMSE was determined by calculating the root mean squared error (RMSE)

$$RMSE = \sqrt{\frac{1}{N} \sum_{k=1}^N (x_k - \hat{x}_k)^2}$$

for each DOF and then normalizing it by the range of the respective DOF:

$$rRMSE = RMSE / (d_{95} - d_5),$$

where  $d_5$  and  $d_{95}$  are the 5<sup>th</sup> and 95<sup>th</sup> percentile of all recorded data samples of the respective DOF. The normalization allowed us to compare prediction errors of joint angles that differed in their operational range.

For each neuronal dataset we determined the optimal gap and bin length combination that maximized CC and minimized rRMSE. Most of the times, the optimal combinations matched for CC and rRMSE. Both CC and rRMSE are important measures for performance, however, a

trajectory prediction that captures the movement shape with an offset bias might have a high CC, but will also have a high rRMSE. In cases where the optimal parameter combination did not match for CC and rRMSE, we therefore favoured the parameter combination yielding better rRMSE, which generally also had a high CC. The optimal parameter combination was selected to evaluate the information content that can be utilized by the Kalman filter to predict continuous movements.

*2.7.5. Chance decoding performance.* Since the Kalman filter used the previous kinematic state as the first part of its prediction (a-priori estimation), in case of very regular movement, the filter might be able to already achieve a high performance simply by utilizing the regularity of the oscillatory kinematics, i.e. without having to rely on the neural information at all. In such a case, a high decoding performance might then be falsely attributed to the neural data. To avoid such an effect, we included both correct and incorrect trials (where the kinematics often did not follow the typical temporal structure of the correct trials) in the decoding.

Furthermore, we calculated a chance level performance to get an estimation of how much the filter was utilizing potentially encoded information in the neural data to predict the continuous kinematics, as opposed to relying solely on the inherent kinematic information. For this, we removed any potential task-relevant information contained in the spike train population by applying the following *random shift method*: We shifted the spike sequence of each unit individually by a random gap length of at least 20 sec in either positive or negative time direction. Neural data that was shifted beyond the end or the beginning of the kinematic data was circularly reinserted at the beginning or end, respectively. This way, we destroyed any potential relationship between the kinematics of the limb and spike sequence, while keeping the inherent temporal structure of the spike sequence intact. Importantly, we used different randomly determined gap lengths for each unit, thus destroying also any potential correlations in the neuronal population. Using this

temporally reshuffled neural data, we carried out decodings and calculated the performance measures, CC and rRMSE, from which we determined the chance level performance as follows:

By repeating this surrogate method ten times, we established the probability distribution of CC and rRMSE during chance performance for each area and recording session. To test if the CC or rRMSE obtained from the respective standard decoding differed significantly from chance, we compared the respective CC or rRMSE value to the median of the chance probability distribution by means of a two-sided sign test. If  $p < 0.05$ , we considered the performance of the standard decoding to be significantly different from chance.

When comparing the mean performance across all ten recording sessions to chance (as in the analysis of decoding performance for proximal and distal groups of joints, figure 6), a chance distribution across recording sessions was composed out of the means of the chance distributions of each recording. Then, a two-sided sign test was performed to determine whether the median of that chance distribution differed significantly from the mean performance of the standard decoding across all ten recording sessions.

### 3. Results

We recorded 27 DOF of the hand, wrist, and arm simultaneously over time together with single and multiunit spiking activity in the hand areas of primate motor (M1), premotor (F5), and parietal cortex (AIP). In total, ten recording sessions were analyzed for this study (monkey Z: six sessions, monkey M: four sessions). Table 1 provides an overview of the number of single and multiunits recorded during each session in the cortical areas M1, F5, and AIP.

#### 3.1. Kinematic and neuronal data

Representative example trajectories of the 27 DOF from recording *Z032012* while the monkey grasped and lifted a horizontal bar, a cube, and a small ball are shown in figure 2. As can be clearly observed, different hand and arm configurations occurred for grasping the objects which was an important goal of the task design. In total, 49 distinct objects in various sizes and shapes were tested (see section 2.2) covering a wide range of hand configurations and hence allowed to sample very

**Table 1.** Number of single and multiunits recorded in each brain area in each recording session as well as the mean and standard deviation (std) across recordings.

		M1	F5	AIP
Monkey Z	<i>Z120511</i>	66	88	45
	<i>Z011312</i>	61	71	64
	<i>Z012312</i>	70	77	52
	<i>Z030212</i>	64	76	67
	<i>Z032012</i>	79	75	61
	<i>Z033112</i>	64	74	60
mean $\pm$ std		67.3 $\pm$ 6.4	76.8 $\pm$ 5.8	58.2 $\pm$ 8.2
Monkey M	<i>M110813</i>	148	112	97
	<i>M111913</i>	164	114	82
	<i>M112013</i>	176	119	81
	<i>M112113</i>	153	119	90
	mean $\pm$ std		160.3 $\pm$ 12.4	116.0 $\pm$ 3.6

small differences in hand kinematics (see also figure 1 (e) in Materials and Methods).

In addition to the kinematic data, neural activity of the recorded units is shown at the bottom of figure 2 (rasterplot). As expected, units in M1 displayed a clear modulation of firing rate during movement execution, whereas they exhibited a decreased activity during periods with no movement. An increase of spiking activity was also observed during movement periods for units in F5 and AIP. The extent however was smaller than in M1 and was smallest in AIP. In contrast, AIP showed a higher firing rate during periods where the object was presented to the monkey and while the animal was planning the movement. A similar behaviour could be observed for F5 although the planning activity was decreased compared to AIP. Such activity patterns have been reported previously for single units in M1 (Bansal *et al* 2011, Poliakov and Schieber 1999, Umilta *et al* 2007, Vargas-Irwin *et al* 2010), F5 (Fluet *et al* 2010, Lehmann and Scherberger 2013, Murata *et al* 1997, Raos *et al* 2006, Rizzolatti *et al* 1988, Umilta *et al* 2007), and AIP (Baumann *et al* 2009, Lehmann and Scherberger 2013, Murata *et al* 2000, Townsend *et al* 2011), hence confirming the validity of the observed patterns within these areas.

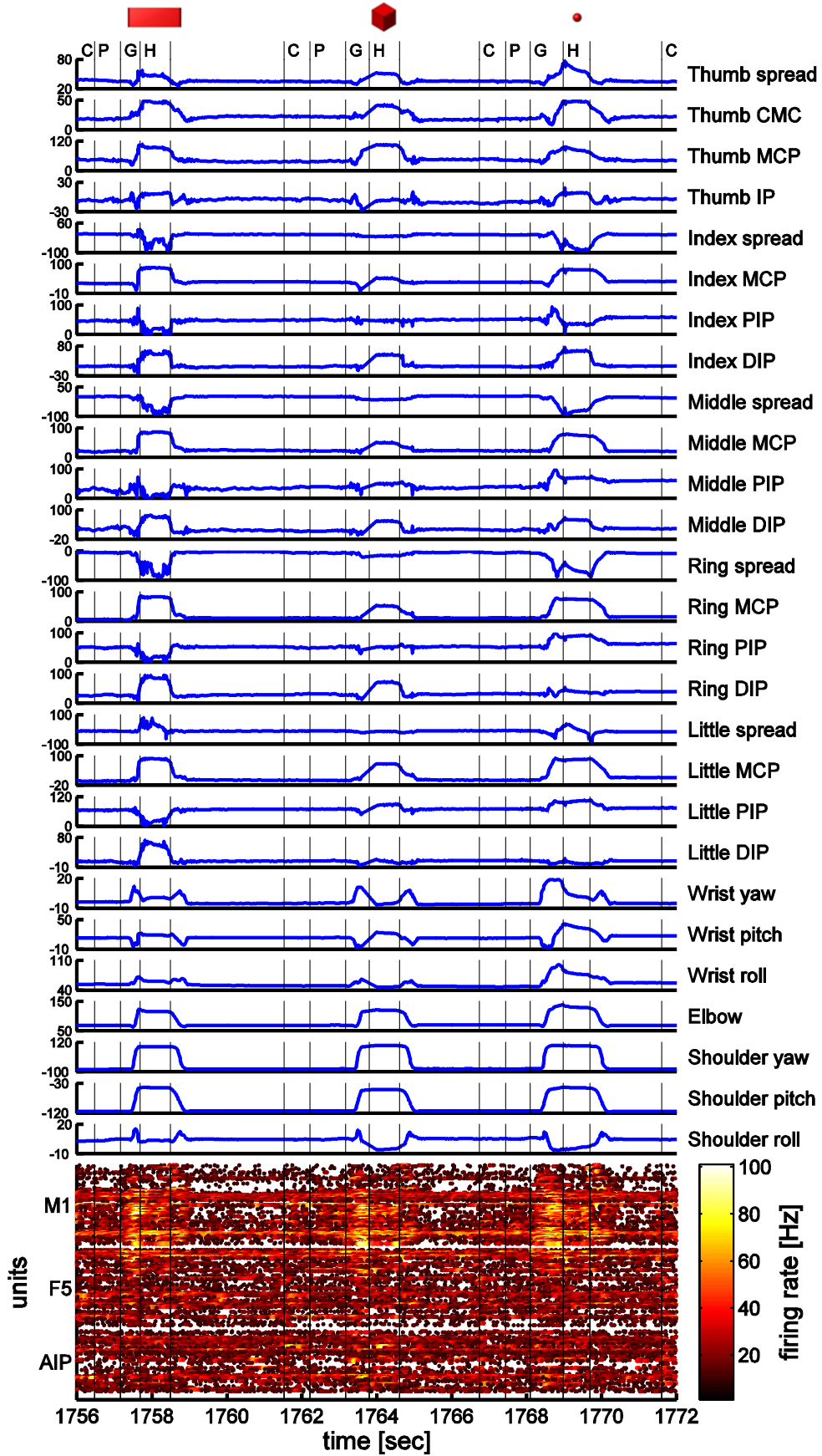
#### **3.2. Decoding of 27 DOF**

Since a clear relationship between neural activity and kinematics could be observed, we decoded 27 DOF of the hand, wrist and arm continuously over time using single unit activity from areas M1, F5, and AIP. Figure 3 shows example trajectories from recording *Z032012* of hand, wrist and shoulder joints over a time course of 80 sec while the monkey was lifting objects of the *mixed*

---

**Figure 2.** Joint angle kinematics of all recorded 27 DOF of recording *Z032012* during 3 trials. Hand, wrist, and arm DOF are shown while the monkey grasped a horizontal bar, a cube, and a small ball (objects on top). Task epochs are marked by black vertical lines and labelled (“C”, cue; “P”, planning; “G”, “go” signal; “H”, hold epoch). Simultaneously recorded neural activity from M1, F5, and AIP is presented as a rasterplot below. Each unit is represented by one row of dots, and each dot represents the occurrence of a spike. Colour code indicates the firing rate of a unit in Hz.



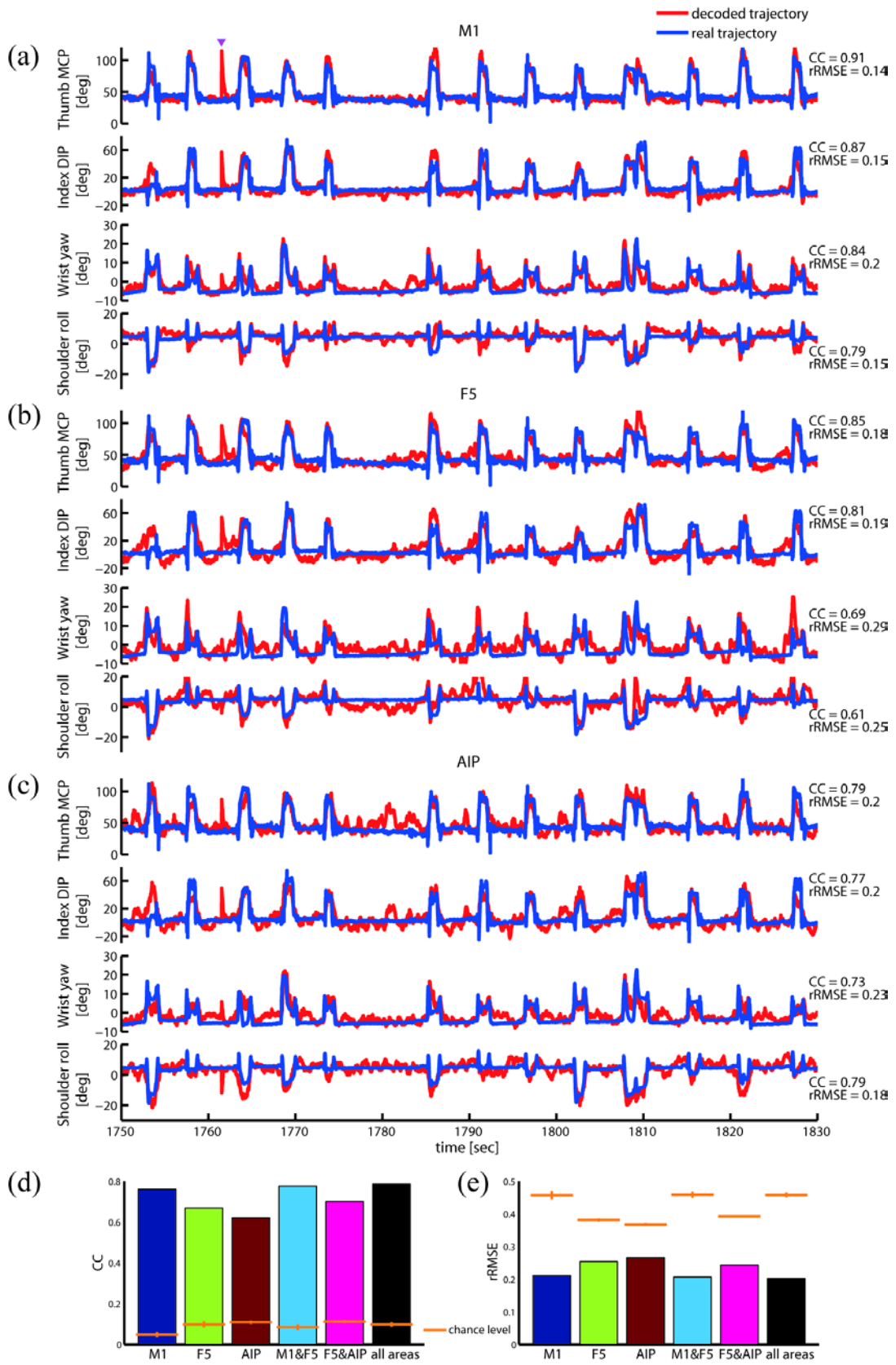


turntable. Both the true and the predicted joint angles are shown. Decodings were performed with either single units from area M1 (figure 3 (a)), F5 (figure 3 (b)), or AIP (figure 3 (c)). For all three areas, the estimated trajectory followed the real one accurately: the timing of both movement onset and termination were captured in a very precise way. The movement amplitude seemed to be reproduced best when decoding with data from area M1 and was slightly diminished when predicting from areas F5 or AIP, respectively. Furthermore, in time periods without movement (inter-trial intervals) the predicted trajectory contained more jittering when decoding from AIP than when decoding with M1 or F5.

$t_{\text{div}} = 1761.5$  sec (marked with a pink triangle on top) is one of the time instants when the data was divided in order to carry out the 7-fold cross-validation: here the Kalman filter was re-trained and decoding was restarted with new initial values within the range of the respective DOF (see section 2.7.2 in Materials and Methods). This led to discontinuities in most curves, since the decoding trajectory was placed far off the actual trajectory at this time instant. However, the Kalman filter managed to bring the trajectory back close to the true amplitude within 300-400 ms, hence illustrating the power of the algorithm.

---

**Figure 3.** Examples of real and decoded trajectories of four example DOF (thumb MCP, index DIP, wrist yaw, and shoulder roll) are shown over a duration of 80 sec (recording *Z032012*). Blue lines: recorded trajectories, red lines: decoded kinematics using neural activity from (a) area M1 (bin length 10 ms, gap length -50 ms, 79 single units), (b) area F5 (bin length 10 ms, gap length -30 ms, 75 single units), and (c) area AIP (bin length 10 ms, gap length -10 ms, 61 single units). Decoding performance (CC and rRMSE) during these 80 sec is indicated separately for each trajectory. Pink triangle: time point when data was divided for 7-fold cross-validation, leading to brief (re-)initialization errors in the decoded trajectories. Decoding performance across the entire recording session and across all 27 DOF are shown in (d) for CC and (e) for rRMSE for individual areas or combinations thereof. Orange lines and errorbars in (d)-(e) indicate chance level and standard deviation (see section 2.7.5 in Materials and Methods).



#### ***3.3. Decoding performance of different areas***

To quantify the decoding performance of the different areas more precisely, we calculated the CC and rRMSE for each DOF over the entire recording session (Z032012) and averaged the CCs across all 27 DOF (figure 3 (d)-(e)). As expected, decoding with neural signals from area M1 yielded the best decoding performance in comparison to decoding from F5 or AIP. However, there was no significant difference in mean between M1 and F5, neither for CC nor rRMSE (one-way ANOVA and Tukey-Kramer multicomparison test,  $p > 0.05$ ). The similar CC shows that the actual movement could be captured similarly precisely when decoding from M1 or F5. Still, predictions made with F5 did not seem to capture the amplitude of the movement as well as when decoding with M1, and there was more noise during resting phases (see also figure 3 (a)-(b)), which was reflected in a higher rRMSE for F5. AIP yielded good performance values as well which did not differ significantly from those obtained with area F5. However, when comparing AIP and M1, a significant difference was found in the mean correlation coefficients ( $p < 0.05$ ).

In addition to predicting from one brain area alone, we also decoded with pairs of areas (AIP&F5 and M1&F5) and with all three areas combined to investigate if the decoding performance could be improved by combining information from different brain areas. Decoding from M1 and F5 in combination increased the mean CC and decreased the mean rRMSE slightly, but not significantly in comparison to decoding with M1 alone. Similarly, there was no significant improvement when decoding from F5 and AIP in combination compared to decoding from F5 alone. As expected, decoding performance was best when all three areas were used for decoding. However, there was no significant improvement in comparison to using only data from M1.

We were curious to evaluate to which extent the decoding performance could be attributed to movement information contained in a brain area as opposed to information inherent in the kinematics themselves. In other words, we wanted to determine a decoding performance based on neural information that did not contain any meaningful information with respect to movement. If

the resulting decoding accuracy was comparable to the performance presented in bars in figure 3 (d)-(e), the performance must have been obtained by the Kalman filter solely relying on the information within the kinematics (a-priori estimation, see section 2.7.2 in Materials and Methods). In contrast, if the decoding performance was significantly lower when using meaningless spiking activity, additional movement information must have been present in the brain areas which the decoder was able to translate into kinematic predictions in order to yield the accuracy in figure 3 (d)-(e). Therefore, we performed simulated decodings with randomly reshuffled spiking activity in which neural information is unrelated to movement kinematics to determine a chance level performance, (*random shift method*, see section 2.7.5 in Materials and Methods for further explanation). This method was repeated ten times for each neuronal dataset (area or combination of areas), and CC and rRMSE were calculated for each DOF and then averaged across all 27 DOF. Mean and standard deviation (across ten repetitions) are shown in figure 3 (d)-(e) (orange lines). Clearly, decoding with the original neural data significantly outperformed chance performance both in terms of CC and rRMSE (two-sided sign test, see section 2.7.5 in Materials and Methods,  $p < 0.002$ ). This demonstrated that significant movement information was present in these brain areas that the decoder was able to translate into accurate movement predictions.

Figure 4 illustrates the combined results across all recording sessions (six sessions for monkey Z, four sessions for monkey M; see also table 1). Overall, they confirm the findings of the example recording shown in figure 3 (d)-(e). When decoding with neural activity from a single area, M1 yielded best results, followed by F5 and AIP, all differing significantly from each other in their accuracies (one-way ANOVA and Tukey-Kramer multicomparison analysis;  $p < 0.05$ ). Combining two or three areas for decoding improved the decoding performance only slightly (but not significantly) compared to using only the better performing single area.

Finally, we also compared the performances between monkeys for each area. There were no differences in means or variances for M1 and F5 (two-sample t-test,  $p > 0.10$ , and Bartlett's test,

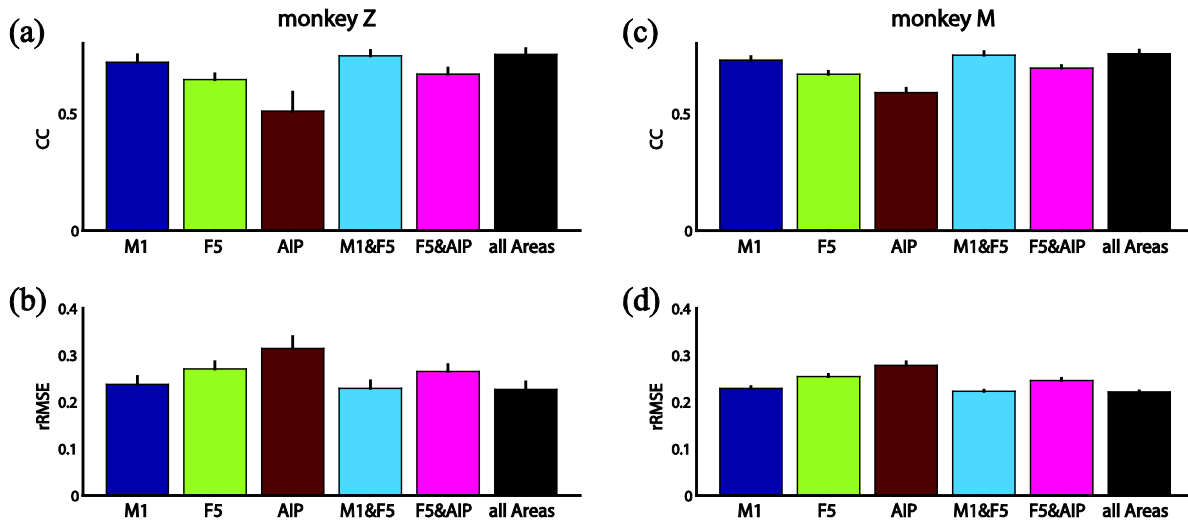


**Figure 4.** Decoding performance of individual recording sessions (as in figure 3 (d)-(e)) was averaged across all 10 sessions for CC (a), (c) and rRMSE (b), (d), separately for monkey Z (a)-(b) and M (c)-(d). Bars and errorbars indicate mean and standard deviation.

$p > 0.05$ , respectively). However for area AIP, the variances differed significantly between monkeys (Bartlett's test,  $p < 0.04$ ).

In conclusion, we were able to perform accurate movement prediction with all three areas with significantly better precision than chance. Combining areas increased accuracy to a small extent compared to decoding with the respective best performing area but improvements were not significant. With the exception of area AIP, decoding results were highly comparable between monkeys.

### 3.4. Influence of number of units on decoding performance

Since the amount of units was lowest for area AIP (see table 1), we wanted to rule out that AIP's lower decoding performance was simply due to a lower number of recorded units. To address this question, we randomly selected a fixed number of units from each area M1, F5, and AIP and decoded with this data set. This was done repeatedly (ten times) for each area and resulting performances were averaged across all 27 DOF and repetitions. Figure 5 shows the mean decoder

performance across all recording sessions for randomly selecting 5, 15, 25, and 35 units. In addition, the rightmost bars (“max”) show the decoding performance when, for each recording session, the maximum amount of units available in all of the areas, i.e. the smallest of the three set sizes of units in M1, F5, and AIP, was randomly selected for each session (i.e. 45 units for session *Z120511*, 61 units for session *Z011312*, etc., see table 1).

Regardless of the actual number of units, M1 yielded the best decoding performance for both CC and rRMSE, followed by F5 and AIP. The ranking of areas in decoding performance therefore did not depend on the number of available units. Furthermore, as expected, decoding performance increased with the number of units used for decoding, and in individual recording sessions (data not

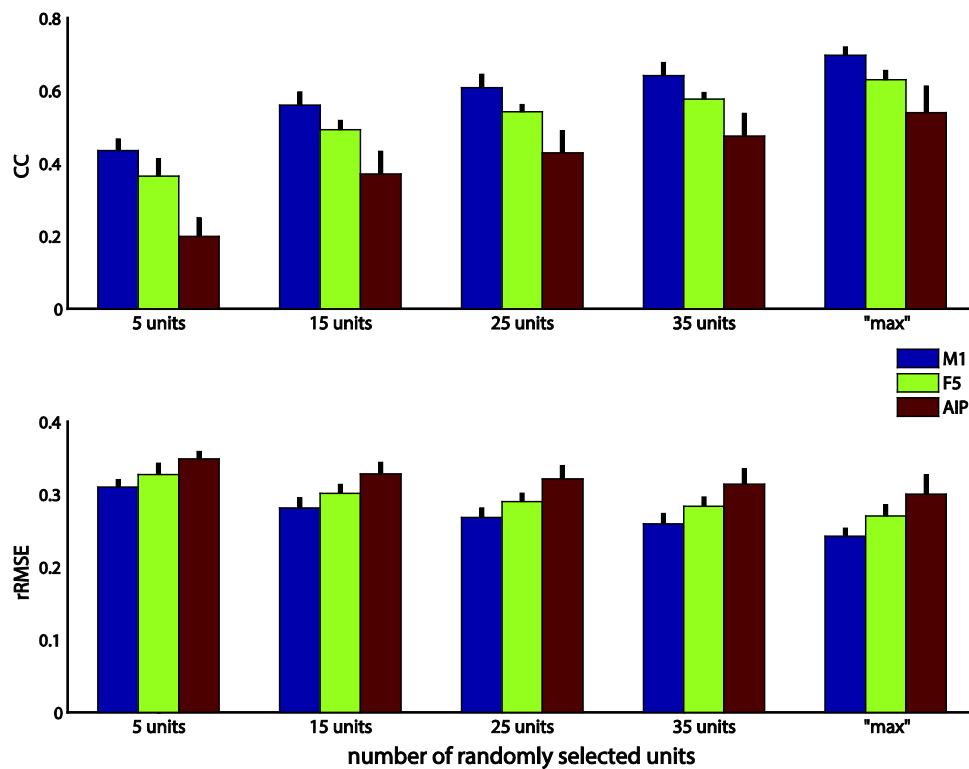


**Figure 5.** CC and rRMSE was determined for decoding with a fixed number of randomly selected units (5, 15, 25, and 35 units) from each area and averaged across all DOF. This procedure was repeated 10 times for each recording session and mean CC and rRMSE was determined across all repetitions and recording sessions (bars and errorbars: mean and standard deviation). Different colours indicate the three recording areas (M1, F5, and AIP). In the rightmost group of bars (“max”) the number of randomly selected units in the three areas was maximized for each session (i.e. the minimum number of available units in M1, F5, and AIP).

shown) the standard deviation of CC and rRMSE decreased with growing number of units, hence demonstrating that results became more consistent.

Remarkably, performance already lay above chance when choosing only a small number of single units (like five). For each recording, we compared the distribution of performance levels obtained by ten repetitions of the random selection of five units with the distribution of chance levels obtained by ten repetitions of the *random shift method* obtained by using all available units in an area (Mann-Whitney U-test): when using M1 for decoding, the performances (both CC and rRMSE) differed significantly from chance for all ten recording sessions ( $p < 0.001$ ). For F5, there was a significant performance difference to chance in 9 and 10 of 10 recordings for CC and rRMSE, respectively ( $p < 0.05$ ). For area AIP, decoding with five units was able to yield a significantly better performance than chance level in eight out of ten recordings for CC ( $p < 0.05$ ) and in all recordings for rRMSE ( $p < 0.05$ ).

Thus we can conclude that all areas carry substantial amount of information about hand and arm kinematics which enabled kinematic prediction that was better than chance already with a small number of units. Decoding accuracy improved monotonically with increasing number of units used for decoding whereas the ranking of areas in decoding performance was independent of the amount of recorded units.

#### ***3.5. Decoding performance of proximal and distal movements***

Decoding performance for different groups of joints was compared in figure 6. Although the electrode arrays were carefully placed in the hand area of motor, premotor, and parietal cortex, decoding of elbow and shoulder joints (“arm joints” in figure 6) generally performed best for all areas. Decoding performance was significantly higher than for all other groups of DOF except for wrist angles when decoding with AIP and using rRMSE for judgement (one-way ANOVA and Tukey-Kramer multicomparison analysis,  $p < 0.05$ ). The high decoding accuracy is likely due to the



task design which concentrated on eliciting a high variability in finger kinematics but showed a more stereotypical demand on elbow and shoulder movements. Therefore, these trajectories were easier to predict. Recordings of those angles also contained less noise which might have affected the decoding performance. However, as this group consisted of only 4 of all 27 total DOF, bias towards high prediction accuracy in the overall result, as presented in figure 4, was only marginal.

Besides the difference between proximal and distal joint angles, there was only little variation in the decoding performance between hand and wrist joints. Thumb and little finger joints tended to be predicted with slightly less accuracy than the other DOF of the wrist and hand. Thumb performance could be attributed to the fact that the thumb was the finger with most variation in movement and therefore was also most prone to (kinematic) recording noise. Compared to middle and ring finger, which tended to move in correlation (sometimes also together with the index finger), both thumb

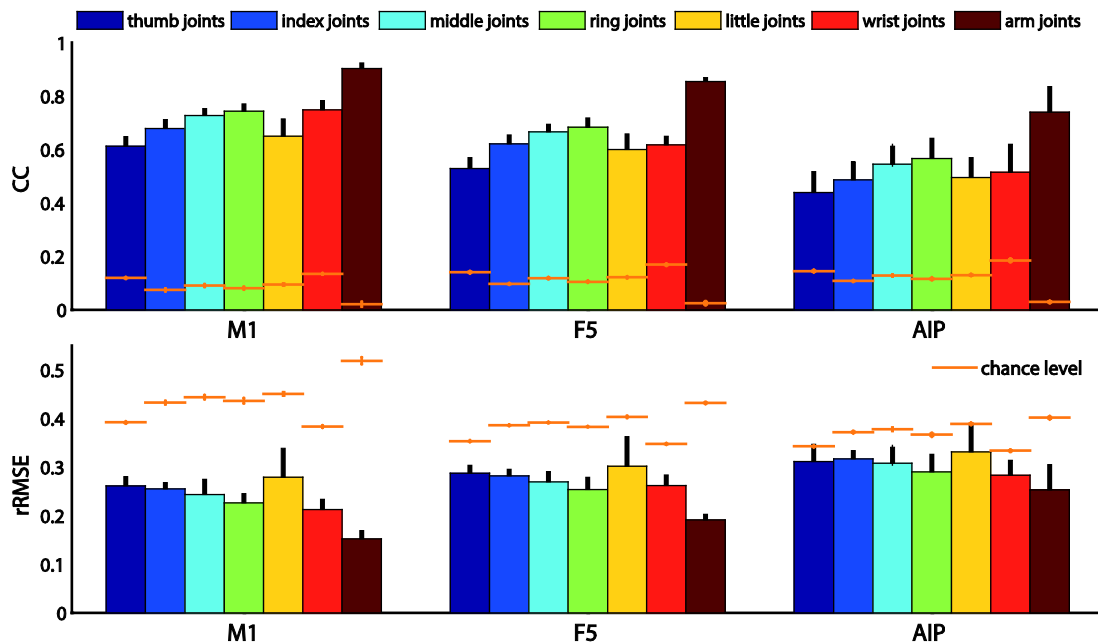


**Figure 6.** Mean CC's and rRMSE's were averaged across groups of joints (thumb joints, index finger joints, middle finger joints, ring finger joints, little finger joints, wrist joints, and arm joints including shoulder and elbow joints) and recording sessions separately for M1, F5, and AIP. Bars and errorbars: mean and standard deviations. Orange lines and errorbars: chance decoding mean and standard deviations (see section 2.7.5).

and small finger movements were more independent. When grasping, the little finger often did not clasp the object as the other fingers did, but was positioned more loosely next to the object. It therefore exhibited, similarly to the thumb, a movement pattern with higher variation across the tested grip types.

In addition, figure 6 shows the respective chance performance levels. As it is clearly visible, decoding performance of all joint groups was significantly better than chance level (two-sided sign test, see section 2.7.5 in Materials and Methods,  $p < 0.002$ ).

#### ***3.6. Optimal decoding parameters***

As mentioned above, different parameter combinations (varying gap and bin lengths) were tested for decoding and evaluated in terms of CC and rRMSE. Bin lengths of 10-250 ms were systematically combined with gap lengths ranging from 0 to  $\pm 180$  sec and the best combination with respect to CC and rRMSE was determined. This procedure was repeated for all recording sessions and areas. In 95% of these optimal combinations a bin length of 10 ms was the best duration for counting spikes. Gap lengths, however, varied more strongly between areas and recordings. Figure 7 (a)-(b) illustrates the decoding performance of M1, F5, and AIP as a function of gap lengths while bin length was kept constant at 10 ms. Furthermore, the cumulative distribution of optimal gap lengths (across recording sessions) for each area is provided in figure 7 (c)-(d).

For area M1, the gap lengths yielding the best decoding performance for each recording clustered around durations from -70 to 10 ms. A two-sided sign test showed that the median of these gap lengths (-10 ms) was not significantly different from zero for CC ( $p = 0.07$ ), but was for rRMSE (median: -50 ms,  $p = 0.04$ ). For area F5, the optimal gap lengths were shifted more into the negative range, indicating that neural data used for decoding preceded the kinematic prediction: for both CC and rRMSE, the median (-40 ms for CC, -60 ms for rRMSE) was significantly different

from zero ( $p = 0.002$  for both CC and rRMSE). However, this was not true for AIP: there, the median of optimal gap lengths was not at all significantly differing from zero ( $p = 1$  for CC, median:  $-0$  ms;  $p = 0.45$  for rRMSE, median:  $-15$  ms). Together, optimal gap lengths for decoding with area M1 were close to zero with a shift into the negative range, which became even larger for decoding with F5. Optimal gap lengths for decoding with AIP however clustered around zero. This becomes also apparent in figure 7 (c)-(d) where the lines for F5 are shifted furthest to the negative range, followed by the lines for M1 and AIP.

Moreover, these plots demonstrate that there was much more variation in optimal gap length for area AIP than for the other two areas: for CC the respective standard deviation of optimal gap

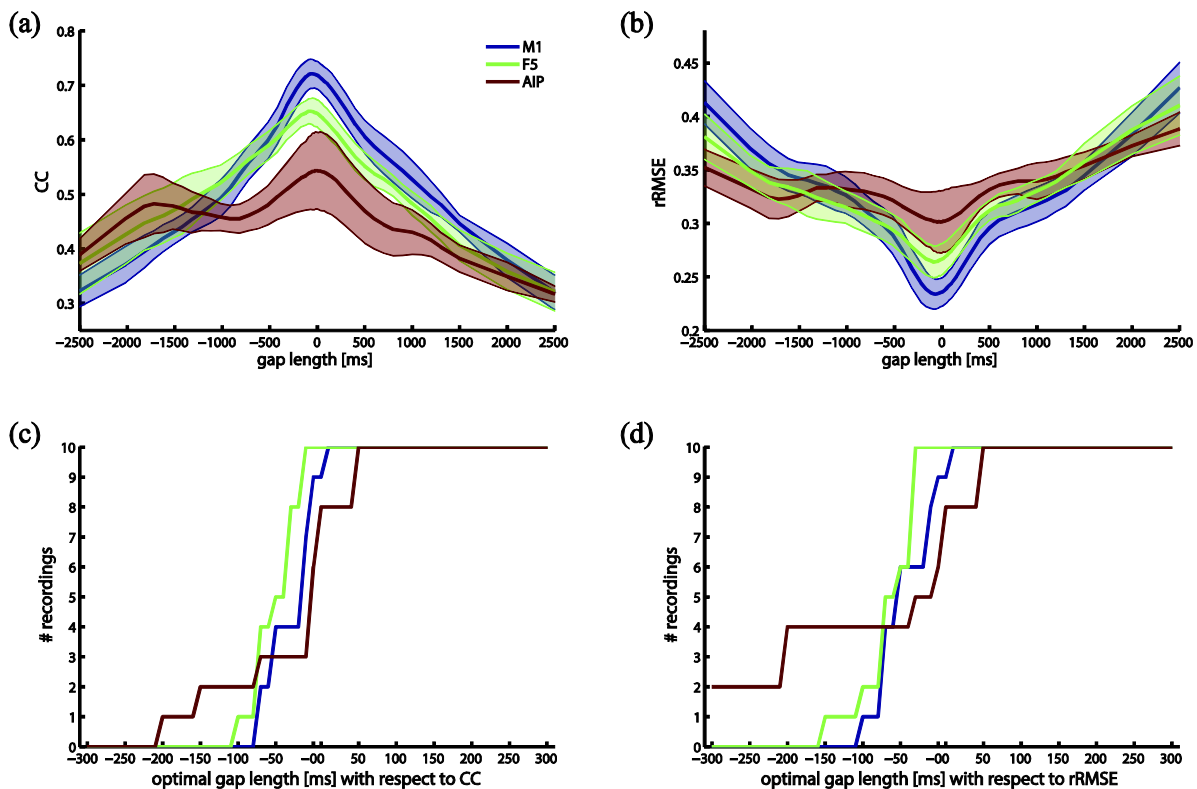


**Figure 7.** CC (a) and rRMSE (b) is plotted as a function of gap lengths (bin length: 10 ms). Lines show the mean value averaged across all ten recordings, shaded regions depict the respective standard deviation. Gap lengths yielding the highest CC/rRMSE were determined for each recording and area and cumulative distributions of the optimal gap lengths are shown for CC (c) and rRMSE (d).

### 3. Results of kinematic decoding

---

length distributions were 30.62 ms (M1), 29.83 ms (F5), and 83.11 ms (AIP). This difference was significant (non-parametric Levene's test,  $p < 0.03$ ). Similar results were observed for rRMSE with standard deviations of 37.06 ms (M1), 38.89 ms (F5), and 452.86 ms (AIP), also significantly different (non-parametric Levene's test,  $p < 0.01$ ).

Furthermore, when decoding with data from AIP, a second, but smaller peak in performance appeared for gap lengths around -1700 ms (figure 7 (a)-(b)). The ranking of the three areas in terms of decoding performance was reversed for these long gap lengths. Contrary to AIP, the performances for F5 and M1 improved steadily the closer the neural data used for decoding lay in time compared to the kinematics to be predicted. For gap lengths longer than approximately -600 ms, F5 still yielded higher decoding accuracy than M1. For positive gap lengths, decoding performance monotonically decreased and there was no second peak in either area.

In conclusion, while consistently observing a bin length of 10 ms as optimal throughout areas, the impact of specific gap lengths on decoding performance varied largely. Consequently, the gap lengths yielding highest decoding performance differed to a great extent for M1, F5, and AIP.

## 4. Discussion

Our goal was to investigate the possibility of decoding complete hand, wrist, and arm movements (represented by 27 DOF) from single and multiunit activity in the hand areas of motor (M1), premotor (F5), and parietal cortex (AIP) in a comparative way. To our knowledge, this is the first study that combines and compares these three grasping areas for prediction of versatile, continuous hand kinematics. Simultaneous recordings of population activity from three areas by multi-electrode arrays gave us the possibility to examine differences between these areas and evaluate the information content with respect to hand and arm kinematics in these areas.

Our task design required the monkey to grasp a high number of distinct objects of different sizes and shapes. Our goal was to elicit versatile hand and finger movements to investigate the information content in each of the brain areas by means of decoding naturalistic grasping movements with a high number of dimensionalities. Brochier *et al* (2004) demonstrated with a similar, smaller set of objects that for each of them distinctive patterns of EMG activity in shoulder, arm, hand, and digit muscles and thus different kinds of hand movements and configurations were elicited. By including similar and more objects in our study, we hoped to achieve distinctive and various hand movements and shapes. The PCA analysis of the performed kinematics in each trial demonstrated that we succeeded in covering a wide range of hand configurations while also sampling small differences in hand kinematics (see figure 1 in Materials and Methods).

### ***4.1. Movement reconstruction with primary and premotor cortex***

Continuous trajectories of 27 joint angles could be reconstructed accurately over time by using single and multiunit activity from M1, F5, or AIP. However, decoding performance varied between the areas. Highest performance was achieved when using M1 for decoding, followed by F5 (figures 3 and 4). These results were very consistent between monkeys.

It is known that various parameters regarding hand and arm movements such as joint and muscle representations, wrist position, and grasp configurations are encoded in both M1 (Ashe 1997, Ashe and Georgopoulos 1994, Georgopoulos *et al* 1986, Kakei *et al* 1999, Rathelot and Strick 2006, Taira *et al* 1996, Thach 1978, Umiltà *et al* 2007) and F5 (Fluet *et al* 2010, Kakei *et al* 2001, Raos *et al* 2006, Rizzolatti *et al* 1988). Furthermore, F5 has strong projections to the digit area of M1 (Borra *et al* 2010, Dum and Strick 2005, Matelli *et al* 1986, Muakkassa and Strick 1979) as well as direct connections to motoneurons in the spinal cord (Galea and Darian-Smith 1994, He *et al* 1993). F5 has therefore been considered to operate – to some extent – at the same hierarchical level as M1 (Dum and Strick 2005). Based on these findings, it is not surprising that both M1 and F5 were able to predict joint kinematics in a precise way (figures 3 and 4). Resting epochs were reconstructed better with activity from M1 than when using F5. This might be connected to the fact that contrary to units in M1, a group of neurons in F5 already responded to object representation as shown previously (Lehmann and Scherberger 2013, Murata *et al* 1997, Raos *et al* 2006) which might have mistakenly been interpreted by the decoder as movement information.

The suitability of areas M1 and F5 for decoding of continuous arm and hand kinematics has previously been investigated (Aggarwal *et al* 2013, Bansal *et al* 2012, Ben Hamed *et al* 2007, Carmena *et al* 2003, Vargas-Irwin *et al* 2010). However, different decoding algorithms, task types and parameters for decoding (such as bin and gap lengths) were employed which makes it difficult to compare these results to ours. Furthermore, the number of decoded DOF was much lower in most of these studies. However, the three following studies were closest related to ours: first, Aggarwal *et al* (2013) trained two monkeys to grasp four different objects in different locations in front of them and decoded 18 DOF (15 DOF of the hand and three DOF of the wrist) additionally to the hand endpoint position with a Kalman filter. For prediction, they used single and multiunit activity simultaneously recorded from M1, dorsal premotor cortex (PMd), and ventral premotor cortex (PMv). Very similarly to our results, they obtained a CC of 0.76 (averaged across all sessions and

DOF) when combining both M1 and F5 for decoding which fits very well with our respective CC of 0.75 when averaging across monkeys (figure 4 (a), (c)). When decoding kinematics with brain areas separately, both their and our studies came to similar conclusions as well: decoding with area M1 produced a higher CC than when using activity from premotor cortex and combining both areas barely improved the decoding performance compared to using only M1 (Aggarwal *et al* 2013).

Second and third, Vargas-Irwin *et al* (2010) and Bansal *et al* (2012) trained two monkeys to grasp six to nine different objects that swung on a string in front of the animals. Vargas-Irwin and colleagues recorded single unit activity from the hand regions of M1 and decoded 25 DOF (3 DOF of the shoulder, 1 elbow DOF, 3 wrist DOF, 18 hand DOF) with a linear state-space model. Their mean CC across all these decoded joint angles reached a value of 0.72 which corresponds to our CC of 0.72 for kinematic reconstruction with M1 averaged across all sessions.

Bansal and colleagues additionally recorded from PMv (F4/F5 boundary) but reconstructed only eight kinematic DOF (3D hand position, 3D velocity, aperture and speed of the hand) with a Kalman filter. In their study, no significant difference in decoding accuracy between M1 and PMv was observed and the average CC (across brain areas) had a value of 0.66 (Bansal *et al* 2012).

Note that all three studies included circumstances not present in our study that might have influenced the decoding performance in the positive direction: first, in all three studies, the number of objects used for grasping was substantially lower than in our task. It is therefore likely, that we were able to elicit more versatile grasping kinematics and finger configurations. However, more variance in the kinematics will increase the difficulty for precise decoding and is therefore likely to affect the decoding performance in a negative way.

Second, Aggarwal and colleagues only decoded time periods from cue onset to beginning of holding the object during correct trials. No other epochs of the task or inter-trial intervals were considered and incorrect trials were discarded. In contrast, in our study all occurring movement and resting kinematics were included. We deliberately chose to do so in order to mimic a more natural

behaviour, where also unexpected movements could occur in addition to the ones demanded by the task design. Again, this introduced variance in the kinematics in our study and increased the difficulty for precise decoding.

Third, in Bansal *et al*'s study the decoding was performed using only a specific subset of units. The units were selected by a greedy selection algorithm aiming to improve the CC. Bansal and colleagues showed in their paper that this method indeed outperformed an average selection approach (Bansal *et al* 2012). Similarly, Vargas-Irwin and colleagues chose a subset of units for decoding that was selected by a greedy selection algorithm evaluating the correlation between firing rate and kinematics. Moreover, each DOF was decoded separately enabling the selection the most suitable subset of units for each DOF individually. Additionally, the optimal time lag between each unit and a specific DOF was determined. In our study none of these optimization steps were carried out, only a general optimal bin and gap length was selected for an entire neuronal population. Evaluation of unit contribution to kinematic features was left to the automated training of the Kalman filter. Despite all these points, our decoding accuracy was the same, or even higher, than reported in those studies.

On the one hand, this might be contributed to the mathematical power of the Kalman filter. On the other hand, our decoding results might have benefited from the fact that our M1 electrodes were located in the anterior bank of the central sulcus ("new" M1) as opposed to the surface anterior to the central sulcus ("old" M1) where Aggarwal's and Bansal's arrays were placed. Rathelot and Strick (2009) demonstrated that units in the "old" M1 project to spinal interneurons and therefore might only have an indirect influence on motor execution. In contrast, cells in the "new" M1 part were found to make monosynaptic connections with motoneurons in the spinal cord (and were hence termed cortico-motoneuronal cells, in short *CM cells*). It has been suggested that these cells enable primates to execute highly developed muscle activity patterns (Rathelot and Strick 2009). Information coded by these cells therefore might contain a more direct motor control signal than the



information encoded in cells in the rostral region of M1 and might therefore be particularly beneficial for the decoding of hand kinematics.

#### ***4.2. Movement reconstruction with parietal cortex***

Decoding with AIP yielded the lowest decoding performance even though it was significantly above chance (figures 3 and 4), suggesting that AIP carries substantial information about movement kinematics that can be decoded. The signals in AIP do not necessarily have to be movement commands, but could also represent other information related to movement execution like object features relevant for grasping. However, the temporal characteristics of movement appeared to be precisely captured by AIP, which supports the notion that motor related information in AIP is not exclusively categorical information, like visual features, but also includes temporal aspects of movement execution.

Predicted trajectories during resting periods often showed undesired jittering when decoding from AIP. This might be accounted for by the fact that AIP responded to the visual presentation of objects and therefore exhibited higher activity already much before the actual movement execution (Baumann *et al* 2009, Lehmann and Scherberger 2013, Murata *et al* 2000, Sakata *et al* 1995, Townsend *et al* 2011). This visual activity could have affected the decoder and might have caused noisy movement residuals during periods of resting.

To our knowledge, this is the first study investigating area AIP as a potential brain region for continuous decoding of versatile hand and finger movements. Previously, other areas in the parietal cortex have been subject of decoding studies, mostly with emphasis on arm and reaching movements: the parietal reach region (PRR), area 5d (Hauschild *et al* 2012) and posterior parietal cortex (PPC) (Wessberg *et al* 2000) have been used for prediction of hand position in 3D space. Hauschild *et al* (2012) obtained respective CC values that were very close to ours when decoding from AIP (figure 4), whereas Wessberg *et al* (2000) reported that PPC and M1 performed equally

well and were only outperformed in accuracy when decoding from PMd. Carmena *et al* (2003) predicted 2D cursor position elicited by hand manipulations of a vertical pole from neuronal firing rates in the medial intraparietal area in PPC and compared them to trajectories reconstructed from other brain areas, such as M1 and PMd. Similarly to our results, they found M1 to deliver the best decoding results (same CC as in our results) followed by PMd and PPC. However, the decoding performance of cursor position predicted from PMd and PPC did not reach the performance levels we were able to obtain for prediction of 27 joint angles of the arm and the hand with areas F5 and AIP, respectively.

Other studies focusing directly on areas AIP and F5 for decoding only predicted categorical variables like grip types: Lehmann and Scherberger (2013), Schaffelhofer *et al* (2015) as well as Townsend *et al* (2011) found that F5 was better suited for decoding of grip types than AIP. Furthermore, Townsend and colleagues were able to observe that decoding from combined activity of F5 and AIP did not increase decoding performance significantly in comparison to F5 alone. Both points correspond well with our results (figures 3 and 4). The fact that decoding performance did not improve when neural activities from F5 and AIP were combined suggests that AIP largely shares its kinematics-related information with area F5.

Another point we noticed in our results was that the decoding performance of AIP was not as consistent between monkeys as it was for M1 and F5. Monkey Z showed a higher variability in prediction accuracy than monkey M when decoding from AIP. One reason could be that two more recording sessions were used for monkey Z (six sessions) which were spread over a longer time duration (3.5 months) than for monkey M (four sessions in one month). However, this difference in recording numbers and periods did not seem to affect the decoding performance of M1 and F5 as much. Also, high variability in decoding performance could not be observed in monkey M for any of the three tested areas. Therefore we suspect that the observed prediction variance for AIP in monkey Z could have been associated with the array implanted in AIP in that monkey. For example,

the array could have changed its position over time. An indication for this could be the number of units recorded in AIP in each session (see table 1) and its variability from session to session. As we were able to observe in the random neuron selection procedure (figure 5) and others have shown before with neuron dropping analyses (Aggarwal *et al* 2013, Bansal *et al* 2012), decoding accuracy increases with number of neurons and saturates after a certain amount of units. Therefore changes in number of recorded units do not affect the decoding performance largely as long as the overall number of neurons stays on a high level. This was the case for both monkeys for M1 and F5 as well as in AIP for monkey M (see table 1). However, for lower numbers of recorded units as in area AIP in monkey Z, the effect of a small change in unit number on decoding performance is bigger and thus might have introduced a higher variability between decodings.

#### ***4.3. Influence of unit number on decoding performance***

We demonstrated that differences in decoding performance between AIP, F5, and M1 did not primarily depend on the number of neurons available for decoding, but strongly reflected the type of information encoded in these areas (figure 5).

Furthermore, we found that already a very small number of randomly selected single units raised decoding accuracy above chance. As suggested previously (Vargas-Irwin *et al* 2010), neurons in M1 and F5 do not seem to be reflect a specific kinematic variable but instead carry information about a broader range of movement parameters, which would allow reasonable movement reconstruction even with a few neurons. This seemed to hold true also for units in AIP.

Neuron dropping analyses in previous studies suggested that only a limited amount of units is necessary for making accurate predictions of hand and arm movements: Ben Hamed *et al* (2007) concluded that 30-40 neurons from M1 were enough to discriminate finger movements and Vargas-Irwin *et al* (2010) found 10-30 cells from primary motor cortex to be enough to decode continuous joint kinematics. However, as already mentioned above (section 4.1), Vargas-Irwin and colleagues

had selected neurons according to their decoding performance. Thus, the subset of aforementioned 10-30 neurons contained only cells that were optimally suited for movement prediction. A random selection of units as performed in our study therefore most likely requires a higher number of units to provide a comparable amount of information to the decoder and achieve a similarly high decoding accuracy. Indeed, a random selection of 35 units produced an average decoding performance of  $\approx 90\%$  of the accuracy obtained when using all available units for prediction.

#### ***4.4. Reconstruction of proximal and distal joints***

Although the task demanded a wide variety of finger movements and hand configurations, no substantial difference was found between decoding finger and wrist joints (figure 6). However, a slight tendency towards a higher decoding performance for index, middle, and ring finger was observed. These fingers showed higher synergies in their movements. Since the Kalman filter used combined state information of all DOF for predicting a single joint (*a priori estimate*), more information was available for joints moving in a correlated fashion and therefore the algorithm could predict such DOF more accurately. In contrast, thumb movements were more independent from the other fingers and showed more variation and were therefore harder to predict by the decoder. Furthermore, the little finger was not actively used for grasping in many conditions and played a rather subordinated role. The finger tended to be moved along with the other fingers but often did not clasp the object properly as the other fingers did. Since it was used more passively, its movement intention might have been underrepresented in the brain activity, which might explain the slightly reduced decoding performance. For a few objects like the ones from the “special” turntable (see figure 1 (b) in Materials and Methods) where the grasp was mainly carried out with fingers 2-4 (similarly to the “spherical power grasp” described in Cutkosky and Wright (1986)), this was also true for the thumb.

In contrast, shoulder and elbow movements were predicted with significantly higher accuracy. Since our task was designed to focus on eliciting dexterous grasping kinematics, arm movements were more stereotypical than those of finger and wrist kinematics. Therefore, they also might have been less prone to noise in the kinematic tracking. This might have facilitated the prediction of shoulder and elbow movements. Nevertheless, by including incorrect trials that were often aborted in the middle or contained unexpected movements (due to the monkey moving its arm away from the object instead of towards it, or executing no movement at all), we tried to prevent the occurrence of a stereotypical temporal structure in the kinematics. However, since we recorded from highly trained animals, the number of incorrect trials was generally low.

In conclusion, although the arrays were carefully placed in the hand areas of primary, premotor, and parietal cortex, both distal and proximal joints could be predicted with high accuracy. This finding is supported by the observation of Vargas-Irwin *et al* (2010) that individual neurons in primary motor cortex encode information about both proximal and distal kinematics. McKiernan *et al* (1998) showed that a large portion of CM cells have muscle fields in both distal and proximal muscles. Since we recorded in the “new” part of M1 (Rathelot and Strick 2009), it is likely that our recorded population contained a considerable portion of such cells. Furthermore, neurons in both F5 and M1 have been found to be tuned not only to hand kinematics but also to different wrist postures although the percentages of tuned units was lower in F5 than in area M1 (Kakei *et al* 1999, 2001). In F5, the wrist orientation seems to be encoded as an additional feature of the grip configuration (Raos *et al* 2006) and populations of units tuned to reaching movements have been identified in both F5 and AIP (Lehmann and Scherberger 2013, Rizzolatti *et al* 1988).

Moreover, our results go hand in hand with the finding that also on the mechanical level proximal and distal kinematics can hardly be disentangled (Jeannerod 1988, Lemon 1999): Stark *et al* (2007) measured EMG activity during reach and grasp movements in shoulder, elbow, wrist, and

extrinsic digit muscles and found that distal muscle activity cannot be exclusively related to either reaching or grasping movements, respectively, but are rather biomechanically dependent.

##### ***4.5. Optimal decoding parameters and their network implications***

In our study, a bin length of 10 ms yielded the highest decoding performance in 95% of the tested data sets, regardless of which brain area was used for prediction. Previous decoding studies used bin lengths of 100-150 ms, however without explaining their choice (Aggarwal *et al* 2013, Bansal *et al* 2012, Vargas-Irwin *et al* 2010). Long time windows will likely include the time point when information content is highest, but they also act like low-pass filters. In contrast, with a short window, changes in firing rate can be detected with higher temporal precision, which is advantageous especially for brain areas with lower tuning strength, like AIP. However, it is also crucial to combine the bin length with an adequate time lag to find the optimal relation between brain activity and actual movement execution. Indeed, we found the time point from which data was used for decoding to show high impact on decoding performance and the optimal time lag varied considerably for the three areas (figure 7).

When decoding from M1, we found the highest amount of information being present when neural data preceded the hand kinematics by 0-50 ms. Previous studies investigating the temporal lag between neural activity in primary motor cortex and movement execution reported a wide range of gap lengths both supporting and opposing our results:

Ashe and Georgopoulos (1994) decoded different movement parameters like direction, position, velocity, and acceleration of reaching movements to instantaneous single unit activity in primary motor cortex using a multiple linear regression method. They varied the time lag from 0 up to  $\pm 200$  ms systematically for each individual unit and described the median optimal time lag as -90 ms, although the distribution of optimal time lags of all cells covered the entire tested range of gap lengths. However, it is noteworthy to mention that contrary to our study, only time periods

during onset of target (i.e. immediately before movement onset) and 500 ms after reaching the target were decoded. These time periods did not include incorrect trials, inter-trial intervals or any other phases in which movement was withheld and/or planned.

A similarly broad result was obtained by Paninski *et al* (2004) who used a center-out-task to investigate M1 cells. They evaluated different time lags with respect to mutual information between firing rate and position in 2D space and obtained a heterogeneous range of optimal gap lengths (spanning the entire range of  $\pm 1$  sec). In contrast, Humphrey *et al* (1970) correlated spike frequencies of M1 cells to wrist movements and exerted force and reported a very specific time lag of -100 ms to yield the highest correlation.

Morrow and Miller (2003) decoded muscle activity from neurons in primary motor cortex by means of linear regression. 15 out of 50 recorded units were randomly selected for decoding and different delays were systematically tested for the respective subset of units with respect to their decoding performance. This method was repeated 50 times and a delay of -50 ms was determined to yield the highest decoding performance. In addition, they reported the CC of the decoding depending on the different tested gap lengths. Their findings are comparable to our results (figure 7 (a)) with small differences: their peak performance exceeded ours and dropped faster the more the gap lengths deviated from the optimal one, until levelling off at a time lag of around  $\pm 250$  ms to a CC of approximately 0.6. In contrast to our study however, they predicted only four distal muscles (i.e. four DOF of the hand only instead of a complete kinematic representation of both the hand and the arm as in our study) which showed very stereotypical behaviour since the monkey was only required to perform one type of grip. Therefore, a higher decoding accuracy was probably achieved. The faster drop of decoding accuracy for time lags around the optimal length could either be due to the fact that Morrow and colleagues used a different decoding algorithm than we did or that sequentially recorded neuronal activity was used for decoding (or both). Additional information encoded in the coherence or phase synchrony within the neuronal population (Averbeck and Lee

2004) was therefore not contained in their data. In our study however, this information was available to the decoder due to simultaneous array recordings and might have helped to maintain a relatively high decoding performance for gap lengths around the optimal ones. For a time gap of around  $\pm 500$  ms however, their decoding performance is comparable to ours. Unfortunately, no longer time gaps were tested in their study.

A similar optimal time lag as presented by Morrow and Miller (2003) was reported by Cheney and Fetz (1980) who investigated CM cells in precentral cortex and their relationship to EMG activation of forearm muscles. They found an average latency of -60 to -70 ms prior to EMG activation for most of the units; however the whole range of time lags from -200 ms to +80 ms with respect to EMG activity onset was present in the investigated sample of units. In contrast, McKiernan *et al* (1998), determining the latency between spikes of CM cells in primary motor cortex and the onset of muscle activity of elbow, wrist, digit, and intrinsic hand muscles, reported an onset of postspike effects around 8 ms and a peak of around 11 ms after neuronal activity. Similar results were obtained by Fetz and Cheney (1980), Kasser and Cheney (1985), as well as by Lemon *et al* (1986).

Our results fit well in this broad range of temporal relationships. Since we did not test for an optimal time lag for each recorded unit individually, but sought for a gap length accounting for the neural signal as a population, our result represents more an average across the population. We were recording in the anterior bank of the central sulcus, therefore it is very likely that our neuronal population contained CM cells which have direct projections to motoneurons in the spinal cord (Rathelot and Strick 2009). This might explain why we found a tendency towards shorter gap lengths as described by McKiernan *et al* (1998) to yield higher decoding accuracy in contrast to the other studies mentioned above which recorded almost exclusively from the “old” part (Rathelot and Strick 2009) of M1.



Optimal time gaps for F5 exhibited the same temporal order as M1 (namely neural activity preceding movement), but were longer than for M1. This indicates that information about grasping is present earlier in F5 than in primary motor cortex. Furthermore, F5 yielded higher decoding accuracies compared to M1 if neural activity preceding the movement with long time lags was used. However, for very short gap lengths (i.e. close to movement execution and during movement execution), M1 exceeded F5 in prediction strength (figure 7 (a)-(b)). These findings go hand in hand with the results of Schaffelhofer *et al* (2015) who found (using the same task design as described in our study) that grip type classification during planning epoch yielded higher decoding accuracy when using activity from F5 for prediction than when using M1, whereas during the hold epoch (i.e. during movement execution) M1 was better suited for decoding. Furthermore, these findings are supported by a study conducted by Umilta *et al* (2007) in which F5 units showed grasp/object related tuning earlier than units in M1. The preference index (PI), indicating the degree of selectivity for a certain object, was higher in F5 during periods immediately before and at the beginning of the movement, whereas peak selectivity in M1 occurred during grasping execution and holding of an object.

Furthermore, our time lag results are in line with the fronto-parietal grasp network hypothesis (Jeannerod *et al* 1995 and section 1.1.5), which states that visual information about an object to be grasped is projected from AIP to F5, where a grip type is selected. Grip type information is then forwarded to both M1 and the spinal cord. Neurons in M1 translate the grip type into a motor command which is projected to the spinal cord as well. According to this idea, the temporal peak of neural information with respect to grasping should be found in F5 earlier than in M1, which goes hand in hand with our results.

However, the role of AIP in this process seems to be more intricate. Decoding performance peaked for gap lengths close to zero and optimal gap lengths showed a much higher variance than when decoding with M1 or F5. Additionally, we found a smaller peak in decoding performance for

time lags around -1700 ms preceding movement. It is very unlikely that in natural grasping movements, AIP represents movement intentions more than 1.5 sec before execution. Instead, this second peak could be caused by the visual task instruction: the object is illuminated approximately 1.5 sec before movement onset (variable time duration due to a variable length of the planning epoch), which is known to cause a visual activation in AIP (Sakata *et al* 1995, Schaffelhofer *et al* 2015). Furthermore, Schaffelhofer *et al* (2015) showed that object information (and to a less extent grip type) could be decoded from single and multiunit activity during the cue epoch of the task. Clearly, object features and hand configurations were coupled in our task; therefore cue information could have been used by the decoder for movement prediction. However, an object can be grasped in different ways. Therefore, visual information could only be used as a rough guideline for the prediction of individual movement kinematics. Accordingly, decoding performance was lower for these long gap lengths compared to the accuracy peak when decoding with very short time lags.

Previous studies testing the temporal delay between activity in parietal cortex and movement found similar short durations for optimal time lags: the study by Ashe and Georgopoulos (1994) described above did not only test single unit activity in primary motor cortex, but also in the arm area of area 5. They obtained a median optimal time lag of +30 ms (neuronal activity following movement), although again the distribution of time lags of all investigated cells covered the entire tested time range from -200 to +200 ms. In contrast to M1, where 50% of the units showed an optimal gap length between -200 and approximately -100 ms, 50% of the units from the arm region in area 5 showed highest performance for time lags between approximately 20 to 200 ms. A different result was reported by Hauschild *et al* (2012) who evaluated time lags from -45 to -125 ms for prediction of arm endpoint position in 3D space from spiking activity in PRR and area 5d and found a gap length of  $\approx$  -80 ms to be optimal (with a bin length of 90 ms).

The closest experimental result to our findings was reported by Mulliken *et al* (2008) who performed a center-out-task with and without obstacles and recorded individual PPC neurons.

Based on mutual information, Mulliken and colleagues determined the optimal time lag between neural activity and movement angle for neurons which exhibited tuning to this movement parameter. The distribution of optimal time lags had a median  $\pm$  interquartile range of  $0 \pm 90$  ms and  $-30 \pm 90$  ms for the center-out task with and without obstacles, respectively (lags were tested approximately between  $\pm 180$  ms), showing again a wide spread across the entire tested gap length range. The authors argued that a motor command in PPC would require at least 90 ms to be translated into movement. Furthermore, a proprioceptive feedback would take at least 30-90 ms to reach PPC. Thus, the authors concluded that the information in parietal cortex at time lags close to zero could encode a forward estimate of movement and neurons in PPC were therefore not only involved in movement planning, but also in movement control by utilizing an efference copy from premotor and motor cortices and projections to and from the cerebellum (Mulliken *et al* 2008). The same is likely the case for AIP. It has been suggested that so-called motor neurons in AIP could represent a copy of the motor plan in F5 in order to compare it to the visual object properties. Depending on the result, a positive or negative feedback could be sent to the premotor cortex in order to facilitate or modify the motor command (Murata *et al* 2000, Sakata *et al* 1997, Sakata *et al* 1999, Sakata *et al* 1995). Our results are compatible with this hypothesis.

#### **4.6. Conclusion**

We were able to show for the first time that high-dimensional reaching and grasping movements could be decoded continuously over time with high precision not only from areas M1 and F5 but also from area AIP in the parietal cortex. Although the decoding performance from AIP was inferior to that from motor and premotor cortex, our results support the idea that AIP not only encodes categorical visual information, as shown previously by other studies, but that AIP also contains temporal movement information, at least to some extent. However, kinematic information in AIP seems to be redundant to movement intentions encoded in area F5.



# **Chapter III**

**- State decoding**



In this chapter the decoding of two different behavioural states, *resting* and *movement*, from neural activity in areas M1, F5, and AIP is presented. The chapter is structured in the following way: In section 5, we will describe the respective materials and methods, which are followed by the presentation of the results (section 6). In the end, the results will be discussed put into the greater scientific context (section 7).

## 5. Materials and Methods

The basic procedures, experimental setup, behavioural paradigm, signal procedure, imaging, kinematic and neural recordings were identical for state decoding as described in chapter II, sections 2.1-2.6. Methods and analyses that differed from the kinematic decoding such as decoding algorithm, decoding procedure, variation of decoding parameters, evaluation of decoding performance, and chance decoding performance are described below.

### 5.1. Decoding algorithm

In addition to the prediction of continuous kinematics, we performed a separate decoding to classify kinematic states. For this, we employed a weighted Support Vector Machine (wSVM) (Huang and Du 2005) to distinguish between *movement* and *resting* states based on neural activity.

A Support Vector Machine (SVM) is a binary, linear classification algorithm which constructs a hyperplane between two populations of vectors corresponding to two different classes (decoder training). The hyperplane can be described by points  $\mathbf{p}$  satisfying

$$\mathbf{w} \cdot \mathbf{p} - b = 0$$

with  $\mathbf{w}$  normal vector of the plane and  $\frac{b}{\|\mathbf{w}\|}$  offset of the hyperplane from the origin along  $\mathbf{w}$ . To separate the two populations of data samples, the plane is required to fulfil  $\mathbf{w} \cdot \mathbf{x}_i - b \geq 1$  for all data points  $\mathbf{x}_i$  belonging to class one and  $\mathbf{w} \cdot \mathbf{x}_i - b \leq -1$  for all data points  $\mathbf{x}_i$  belonging to class two. For

data sets, in which these requirements cannot be fulfilled because the two populations are not cleanly separated, a non-negative slack variable  $\xi_i$  can be introduced. In this way, the requirements become  $\mathbf{w} \cdot \mathbf{x}_i - b \geq 1 - \xi_i$  and  $\mathbf{w} \cdot \mathbf{x}_i - b \leq -1 + \xi_i$  for data points  $\mathbf{x}_i$  belonging to the two classes, respectively (Cortes and Vapnik 1995). In our decoding, we chose this “soft margin” approach. By means of quadratic programming methods, the variables  $\mathbf{w}$ ,  $b$ , and  $\xi_i$  can be optimized with subject to the described requirements while at the same time maximizing the distance between the hyperplane to the data points of the two populations (Platt 1999).

By mapping the vectors into a (higher dimensional) feature space with an appropriate kernel, the construction of the hyperplane can be carried out even for data points which are not linearly separable in the input space (Cortes and Vapnik 1995, Smola and Schölkopf 2004). For our decoding, we used a radial basis function kernel (RBF) defined by

$$K(\mathbf{x}_i, \mathbf{x}_j) = e^{-\gamma \|\mathbf{x}_i - \mathbf{x}_j\|^2},$$

with  $\mathbf{x}_i$  and  $\mathbf{x}_j$  data points, and  $\gamma$  free parameter,  $\gamma > 0$  (Chang *et al* 2010, Hsu *et al* 2003).

After the hyperplane has been determined, the class of a given test vector  $\mathbf{x}$  can then be decoded by simply calculating on which side of the hyperplane the vector is located, i.e. if  $\mathbf{w} \cdot \mathbf{x} - b$  greater or smaller than zero.

However, the standard SVM has been found to produce a prediction bias toward the class with the larger training sample size (Chew *et al* 2000). In our study, due to the task design, approximately two thirds of the neural data corresponds to *resting* as opposed to *movement*. Thus, to avoid the aforementioned bias, a weighted SVM was used for state prediction since it compensates for uneven sizes of training samples and minimizes misclassification errors (Huang and Du 2005).



### 5.2. Decoding procedure

The kinematic data was prepared for state decoding by calculating the speed of each kinematic dimension and smoothing each of the velocities with a Gaussian kernel (width:  $\sigma = 0.05$  sec). Next, each data sample of a DOF was classified as either *movement* and marked with “1” if the absolute speed exceeded an empirically set threshold of 0.9 °/sec, or as *resting* and marked with “0” if otherwise. This yielded a kinematic state information vector for each individual DOF. To obtain a general kinematic state information vector, a time sample was classified as *movement* if more than a third of the individual movement vectors displayed a “1” at that time instant, otherwise it was classified as *resting*. This threshold was empirically determined. In a last step, very short sequences of *movement* or *resting* were deleted by reversing the state class if the sequence was shorter than nine time samples (i.e. shorter than 90 ms).

This way, the neural activity of each time step was assigned to a state of either *resting* or *movement*. Using both the neural activity and the kinematic state information, a wSVM was trained and employed to predict the kinematic state of the entire recording session by means of a 7-fold cross-validation as already described in the Methods and Materials section of the Kalman filter (see section 2.7.2). However, in contrast to the Kalman filter decoding, state decoding was not performed with a sampling rate of 100 Hz but with a rate of 20 Hz. Since the computational load for training the SVM is much higher than for the Kalman filter, computational time was saved using only every fifth time sample of the training data to calibrate the SVM. Similarly, prediction of the kinematic states was also performed only every 50 ms.

The decoding procedure was implemented with custom-written software in Matlab (MathWorks Inc., Natick, MA, USA) using the c-code library LIBSVM for Support Vector Machines (Chang and Lin 2011).

### 5.3. Variation of decoding parameters

Similar to the decoding of continuous kinematics, we varied parameters of the neural data such as bin length and gap length to test the impact on state prediction accuracy. At the same time, we optimised two SVM parameters with respect to decoding accuracy, which needed to be chosen by the experimenter prior to training of the algorithm, namely the regularization parameter  $C$  (Cortes and Vapnik 1995, Smola and Schölkopf 2004) and the free parameter  $\gamma$  of the RBF kernel (see section 5.1). We fixed the bin and gap length to specific initial values based on previous decoding results and tested combinations of exponentially growing sequences of  $C$  and  $\gamma$  for decoding (typically  $C = 2^0, 2^1, 2^3, \dots, 2^9$  and  $\gamma = 2^{-2}, 2^{-1}, \dots, 2^2$  following Hsu *et al* (2003)). The combination of  $C$  and  $\gamma$  yielding the highest decoding accuracy was determined and kept fixed. Then, various combinations of bin and gap lengths were tested (similarly as described in section 2.7.3) ranging from -1000 to 200 ms for gap lengths and 10-1400 ms for bin lengths (same notation as in section 2.7.3). Now, the best combination of bin and gap lengths was determined and kept fixed while again different combinations of  $C$  and  $\gamma$  were tested as described before. After that, keeping the resulting optimal combination of  $C$  and  $\gamma$ , again bin and gap lengths were optimised. This process was repeated iteratively until either none of the parameters were modified any more or decoding accuracy only changed marginally from one iteration to the next. The resulting set of four parameters was then considered as the optimal parameter combination.

### 5.4. Evaluation of decoding performance

To measure decoding performance, the accuracy was calculated as percent of correctly decoded samples:

$$\text{percent of correctly decoded samples} = \frac{\# \text{ correctly predicted samples}}{\# \text{ total testing samples}} \cdot 100 \% .$$

“# of total testing samples” referred to either the total number of predicted samples in a decoding (as in figure 10) or the total number of decoded samples in specific kinematic classes (as in figure 11) or trial/inter-trial epochs (as in figure 12).

### 5.5. Accuracy of movement onset prediction

To assess how precisely movement onset was detected by the decoder, we defined a window  $w_i$  centered around each true movement onset at time  $t_{\text{on}}^i$ , with  $i = 1, \dots, N_{\text{on}}$  and  $N_{\text{on}}$  number of movement onsets in a recording, i.e.  $w_i = [t_{\text{on}}^i - 400 \text{ ms}, t_{\text{on}}^i + 400 \text{ ms}]$ . Each sample within a window was checked for its state information so that for each window  $w_i$  a respective state information vector  $s_i = [s_i^1, s_i^2, \dots, s_i^N]$  could be created,  $s_i^n \in \{0, 1\}$  state information,  $n = 1, \dots, N$ , and  $N = 17$  number of samples in  $w_i$  ( $N = 17$  because the sample of movement onset is added to two times the number of samples in a 400 ms window corresponding to eight samples each). Then, an averaged state information vector  $\bar{s} = [\bar{s}^1, \bar{s}^2, \dots, \bar{s}^N]$  across all windows in a recording was calculated with  $\bar{s}^n = \frac{1}{N_{\text{on}}} \sum_{i=1}^{N_{\text{on}}} s_i^n$ ,  $n = 1, \dots, N$ . The parameters  $\bar{s}^n$  represented the probability of movement occurring relative to movement onset. By definition,  $\bar{s}^9$ , representing the likelihood at the time instant in which movement onsets took place, had a 100% probability to belong to the *movement* state, whereas the time sample directly before had a 0% probability of movement.

The probability of movement depending on the time relative to movement onset was then averaged across recordings and the mean values were fitted by a logistic curve with a vertical offset

$$p(t) = \frac{a}{1 + e^{-b(t-c)}} + d, \quad (1)$$

with  $p$  probability of movement,  $t$  time relative to movement onset, and four fitting parameters  $a$ ,  $b$ ,  $c$ , and  $d$ , .

Next, the probability of decoded movement in a 800 ms time window around each true movement onset was determined in the predicted data sets separately for each area used for

decoding in the same way as described above. Again, a logistic curve was fitted. The fit parameters  $b$  and  $c$  in equation (1), describing the slope and the horizontal shift of the respective functions, were analysed to assess the accuracy of movement onset prediction compared to true movement onset.

### 5.6. Chance level performance

In contrast to kinematic decoding with the Kalman filter, state prediction with the wSVM does not infer any information from the temporal structure in the data since the wSVM is not an iterative algorithm. Instead, each data sample is an independent vector in the input space and its classification does not depend on previous predictions. To assess chance level accuracy, it is therefore legitimate to assign the given distribution of states randomly to the neural data to create “meaningless” neural data.

In a decoding based on a data set like that, one could imagine a classifier that matches the frequency distribution of the states in the training data in its prediction. Average chance level decoding accuracy can then be calculated as the percentage of correctly classified samples in the following way:

Be  $s$  the total number of samples,  $p_R$  and  $p_M$  the probability in the true data set for a sample to belong to the *resting* or *movement* state, respectively (i.e.  $s = s \cdot p_R + s \cdot p_M$ ). The number of correctly classified samples will then (on average) be the sum of number of samples belonging to *movement* that are correctly classified as *movement* and the number of samples belonging to *resting* that are correctly classified as *resting*. The number of samples belonging to *movement* is  $s \cdot p_M$  and since the decoder has learned the distribution of classes, it will (on average) classify these samples as *movement* with a probability of  $p_M$ , assuming the classifier is an unbiased estimator. Therefore, the number of correctly classified samples will be  $s \cdot p_M \cdot p_M$ . The same is true for the number of correctly classified *resting* samples, namely  $s \cdot p_R \cdot p_R$ . The total proportion of correctly classified

samples is thus  $(s \cdot p_R \cdot p_R + s \cdot p_M \cdot p_M) / s = p_R \cdot p_R + p_M \cdot p_M$ . Knowing that  $p_R = 1 - p_M$ , the formula can be rewritten as

$$1 - 2p_R p_M, \quad (2)$$

which has its minimal value of 0.5 for the balanced case of  $p_R = p_M = 0.5$  (see green line in figure 8).

Another possibility of a classifier that predicts the kinematic state without reliable neural information is a decoder that always picks the most common class in the training set as its prediction. This way, a decoding accuracy of the percentage of the most common class is ensured. In our case, this would be the *resting* state and decoding accuracy would therefore be  $p_R$ . For  $p_R \geq 0.5$ , this would yield a higher decoding accuracy than the chance level described in equation (2) (see figure 8) and would therefore be a more conservative chance level estimation. However, this decoder would never predict the *movement* state, which is not desirable in a neuroprosthetic application. Therefore, we did not consider this decoder scenario further but chose the one described in the previous paragraph and determined average chance level performance for each recording session (as shown in figure 10) by evaluating equation (2). For chance level estimation for prediction of individual states (as shown in figure 11 and figure 12), the respective probabilities

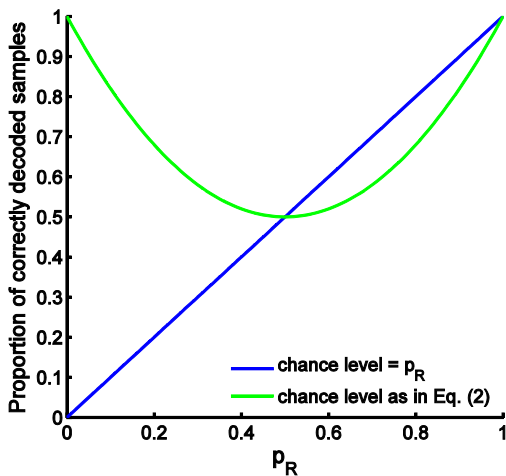


**Figure 8.** Proportion of correctly decoded samples as a function of  $p_R$ , the probability of resting in the true data set. The blue line depicts the accuracy of the chance decoder as described by equation (2), the green line shows the accuracy of a classifier always predicting the most common class in the training set.

of a class (i.e.  $p_R$  and  $p_M$ , respectively, in figure 11 for example) were used.

## 6. Results

In figure 3 (a)-(c) in chapter II, section 3.2, four example trajectories of the 27 decoded DOF were illustrated. As already described before, the Kalman filter was able to predict movement kinematics accurately with spiking activity from each of the three areas. However, during resting phases between trials and during fixation, cue, and planning epochs, the prediction of the Kalman filter did not exactly match the original trajectories. Instead, the decoded DOF exhibited jittering and undesired movement.

To address this problem, we performed a separate continuous prediction of the kinematic state, namely movement or resting states to distinguish between phases with and without movement. If information about the condition of the movement could be inferred from the neural data in addition to actual kinematic movement trajectories, this could enable the kinematic decoder to adjust its prediction during states of resting to prevent undesired movement by either pausing the decoding of the joint trajectories or overwriting its prediction with a desired stationary value.

### ***6.1. State detection performance of different areas***

Figure 9 illustrates state predictions from recording *M110813* over a time course of 55 sec. The trajectory of the index MCP joint is shown additionally as a reference to indicate when the monkey was resting or performing a movement. Decodings were carried out with units from either area M1 (figure 9 (a)), F5 (figure 9 (b)), or AIP (figure 9 (c)). For all three areas, the state prediction agreed largely with the trajectory: Each time the monkey reached to an object to grasp it, the decoder classified the state as *movement*. Even during phases after the monkey had lifted the object and held it for a few hundred milliseconds the decoder often detected the *resting* state. When decoding with AIP however, the classifier sometimes assigned the *movement* state to periods where the monkey was clearly resting. Furthermore, the onset of movement was not always detected exactly on time but showed a short delay.

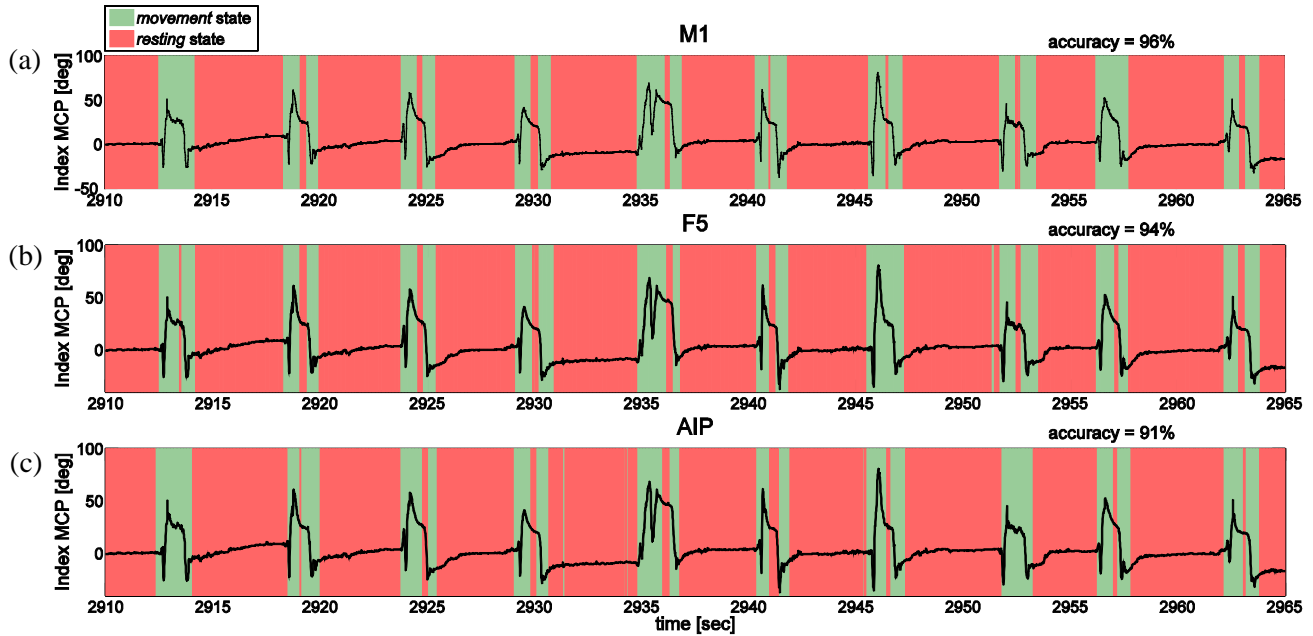


**Figure 9.** Examples of decoded kinematic states are shown over a duration of 55 sec (recording *M110813*) together with the kinematic trajectory of the index MCP joint as a reference (black line). Background colours indicate the decoded state using neural activity from (a) area M1 (bin length 300 ms, gap length -0 ms, 148 units), (b) area F5 (bin length 250 ms, gap length -0 ms, 112 units), or (c) area AIP (bin length 450 ms, gap length -0 ms, 97 units) for prediction: red colour represents *resting state*, green colour represents *movement state*. State decoding accuracy during these 55 sec is indicated at the top right of each subfigure.

To quantify the state decoding performance of the different areas more precisely, we calculated the percentage of correctly decoded samples of each recording session. The mean performances averaged across sessions are shown in figure 10 separately for each monkey.

Similar to the results obtained by the Kalman filter decoding, M1 yielded highest decoding performance, followed by F5 and AIP. However, the means of M1 and F5 did not differ significantly from each other. Only the state decoding accuracy of AIP was significantly different from M1 and F5 (one-way ANOVA and Tukey-Kramer multicomparison analysis,  $p < 0.05$ ). This was true for both monkeys.

Moreover, chance level performance was determined for each recording (see Materials and Methods, section 5.6) and the resulting chance level distribution across recordings was compared to



the performance distribution obtained by the standard decodings of each area. All areas yielded significantly better performance than chance (paired t-test,  $p < 0.0001$ ).

Furthermore, we compared the performance between monkeys for each area. There were no differences in means or variances for M1 (two-sample t-test,  $p > 0.05$ , and Bartlett's test,  $p > 0.05$ ). Similarly, for AIP there were no differences in variance (Bartlett's test,  $p > 0.05$ ) but means differed significantly (two-sample t-test,  $p < 0.001$ ). Finally, for F5 variances differed significantly between monkeys (Bartlett's test,  $p < 0.05$ ). In the following, we will therefore present the results for each animal separately.

### 6.2. Detection performance for individual states

Since the overall percentage of correctly predicted samples as presented in figure 10 only gives a coarse overview of the decoding performance, we examined the decoding accuracy of the individual kinematic states in more detail. Figure 11 illustrates the percentage of correctly decoded samples of each state separately, averaged across recording sessions of each monkey. For all three areas,

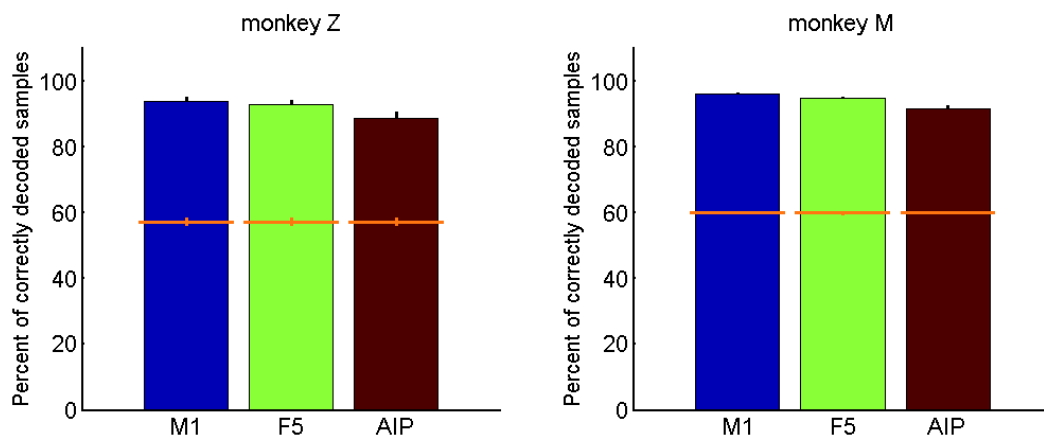


**Figure 10.** State detection performance averaged across all recordings sessions, shown separately for monkey Z (six sessions, see table 1 in chapter II, section 3.1) and M (four sessions, see table 1). Bars and errorbars indicate mean and standard deviation. Orange lines and errorbars indicate mean chance level and standard deviation, also averaged across recording sessions (see section 5.6 in Materials and Methods).

*resting* state was detected with a higher accuracy than *movement*. Medians of decoding performance differed significantly between both states, independent of which area was used for decoding (Mann-Whitney U-test,  $p < 0.03$ ).

However, prediction accuracy of both states lay substantially above chance level: for each recording, average chance level for predicting each state correctly was calculated (as described in Materials and Methods, section 5.6) and then chance levels were averaged across recordings. Median decoding performances of standard decodings differed significantly from the respective medians of the chance level distributions for all conditions (Mann-Whitney U-test,  $p < 0.03$ ).

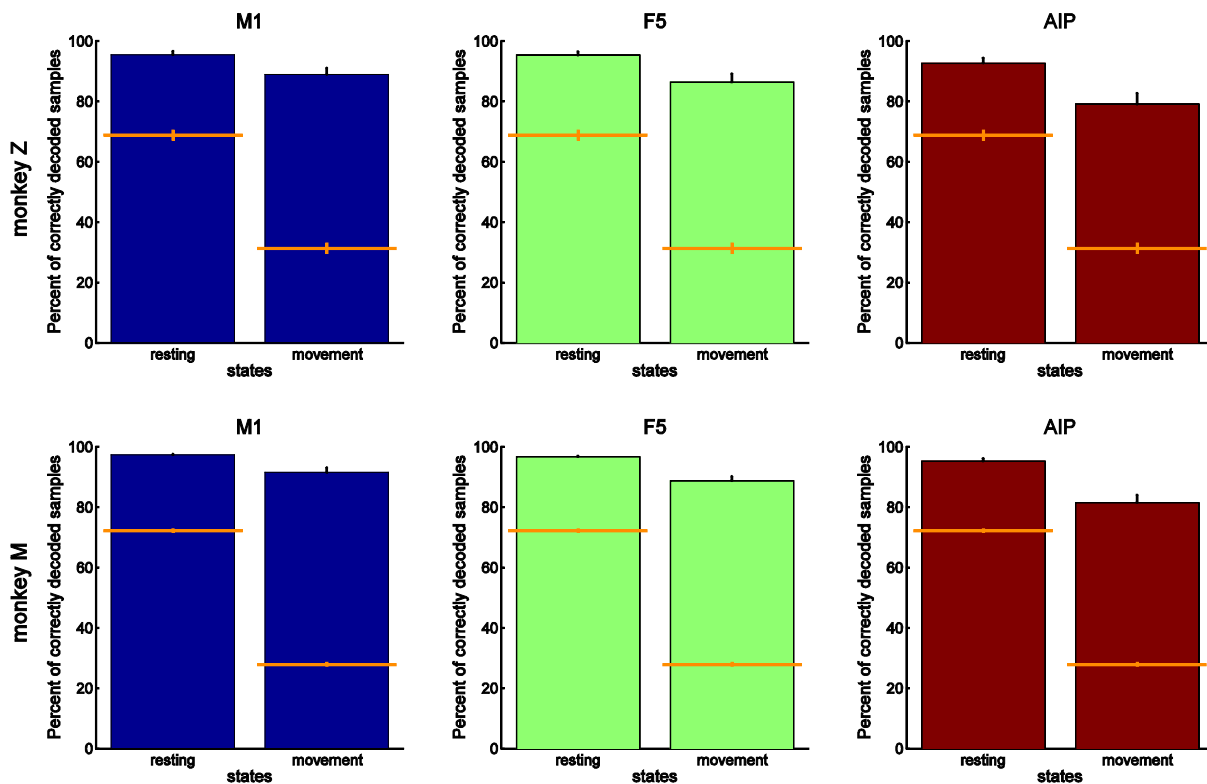


**Figure 11.** Decoding performance of individual states averaged across all recordings sessions, shown separately for monkey Z (upper row) and M (lower row) as well as for the different areas (columns). Bars and errorbars indicate mean and standard deviation. Orange lines and errorbars indicate mean chance level and standard deviation also averaged across recording sessions (see section 5.6 in Materials and Methods).

Comparing different brain areas for decoding yielded very similar results as already obtained for the overall decoding performance in figure 10: mean decoding accuracy for both *resting* and *movement* state did not differ significantly between M1 and F5, as well as not between F5 and AIP. However, there was a significant difference between AIP and M1, except for *resting* state detection in monkey Z, where medians did differ significantly between F5 and AIP (Kruskal-Wallis test and Tukey-Kramer multicomparison test,  $p < 0.05$ ).

Finally, we compared individual state detection accuracy between monkeys: Median performances did not differ significantly between animals (Mann-Whitney U-test,  $p > 0.05$ ) except for resting state prediction decoded from F5 and AIP where means were significantly different ( $p < 0.05$ ).

In conclusion, we were able to predict two separate kinematic states with single and multiunit activity from either of the three tested brain areas. Performance ranking of the areas corresponded to the ranking obtained for the continuous kinematic decoding with the Kalman filter except for the fact that the differences between M1 and F5 were non-significant.

### ***6.3. Resting state detection during passive resting phases and active hold epochs***

Since the *movement* and *resting* state was defined based on a velocity threshold, the *resting* state included on the one hand passive waiting phases between trials as well as during fixation, cue, and planning epochs, and on the other hand phases during hold epochs where the monkey was holding the grasped object without moving its hand and arm. Although kinematically similar, these phases might be different in terms of neural coding. Whereas the monkey is passively resting its hand while waiting for the go signal to perform its next movement, it is actively engaged by tensing muscles in the arm and hand while holding an object. In the following, we will therefore distinguish these two different categories of *resting* by the terms *passive* and *active resting*.

We were curious to see whether these two different *resting* states could be decoded with comparable accuracy or if a tentative change in neural and muscular state would be reflected in the decoding performance. To do so, we calculated the percentage of correctly decoded samples specifically during *passive resting* and compared it to the percentage of correctly decoded samples during *active resting* state in each recording session.

Figure 12 illustrates the respective means and standard deviations averaged across recording sessions separately for each monkey and each area used for decoding. Clearly, samples during *passive resting* phases, i.e. while the monkey was waiting to perform the next hand movement and the arm was lying on the hand rest button, could be detected with a much higher accuracy than

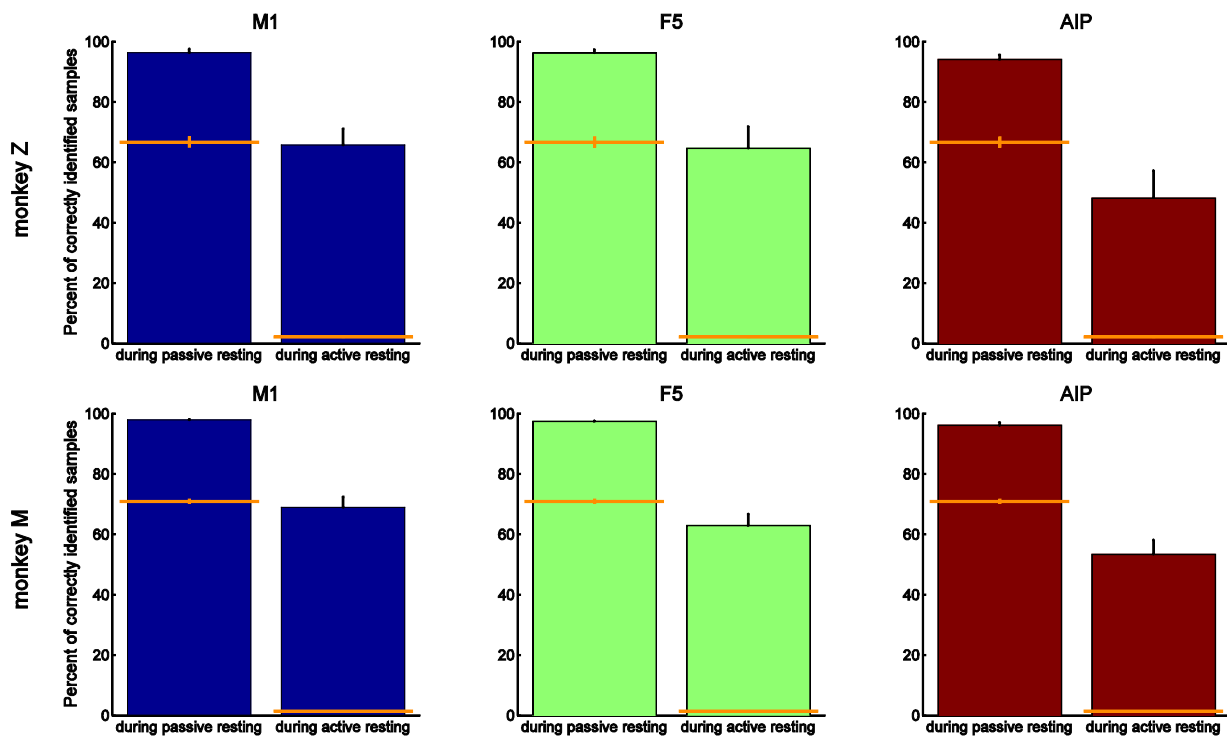


**Figure 12.** Decoding performance of *active* and *passive resting* state, averaged across all recording sessions and shown separately for monkey Z (upper row) and monkey M (lower row) as well as for the different areas used for decoding (columns). Bars and errorbars: mean and standard deviation. Orange lines and errorbars indicate mean chance level and standard deviation also averaged across recording sessions (see section 5.6 in Materials and Methods).

samples during hold phases (*active resting*). Medians differed significantly in both monkeys and independent from which area was used for decoding (Mann-Whitney U-test,  $p < 0.03$ ).

The performances of the three areas did not differ from the previous results: when comparing the decoding accuracy of *passive resting* among the areas, there was no significant difference in means between M1 and F5, but AIP was differing significantly from both M1 and F5 (Kruskal-Wallis test and Tukey-Kramer multicomparison test,  $p < 0.05$ ). The same was true when comparing the accuracy of predicting *active resting* between areas.

All decoding performances were significantly better than their respective chance level: again, for each recording, chance level for predicting *active* or *passive resting* were separately calculated (see section 5.6) and averaged across recordings. Median decoding performances of standard decodings differed significantly from the respective medians of the chance level distributions (Mann-Whitney U-test,  $p < 0.03$ ). This was true for both *passive* and *active resting*.

Finally, decoding results were compared between monkeys: there were no significant differences in the median decoding accuracies between monkeys for any conditions (Mann-Whitney U-test,  $p > 0.05$ ).

#### **6.4. Decoding of movement onset**

For a neuroprosthetic application, it is not only important to correctly distinguish between movement and resting phases but to catch the timing of movement onset precisely. As described in Materials and Methods (see section 5.5), we calculated the probability of true and decoded movement around each actual movement onset. Figure 13 shows the mean probabilities together with their standard deviations averaged across recordings. The results were fitted with logistic curves which are shown in addition.

As expected, there was a stepwise transition from resting to movement in the real data (figure 13 (a), (e)): by definition, since movement always started at  $t = 0$  ms, the probability of movement was

at a 100% level for this time point, whereas the preceding time sample at  $t = -50$  ms had a probability of 0%. For the decoded data sets however, the transition happened much more smoothly. The fit parameter  $b$  (see equation (1) in section 5.5 in Materials and Methods) describing the slope of the fitted function (larger values of  $b$  correspond to steeper graphs) decreased drastically from 3.5 and 1.8 in the actual data set (for monkeys Z and M, respectively) to 0.05 and 0.07 when decoding with M1 (figure 13 (b), (f)), 0.03 and 0.05 when decoding with F5

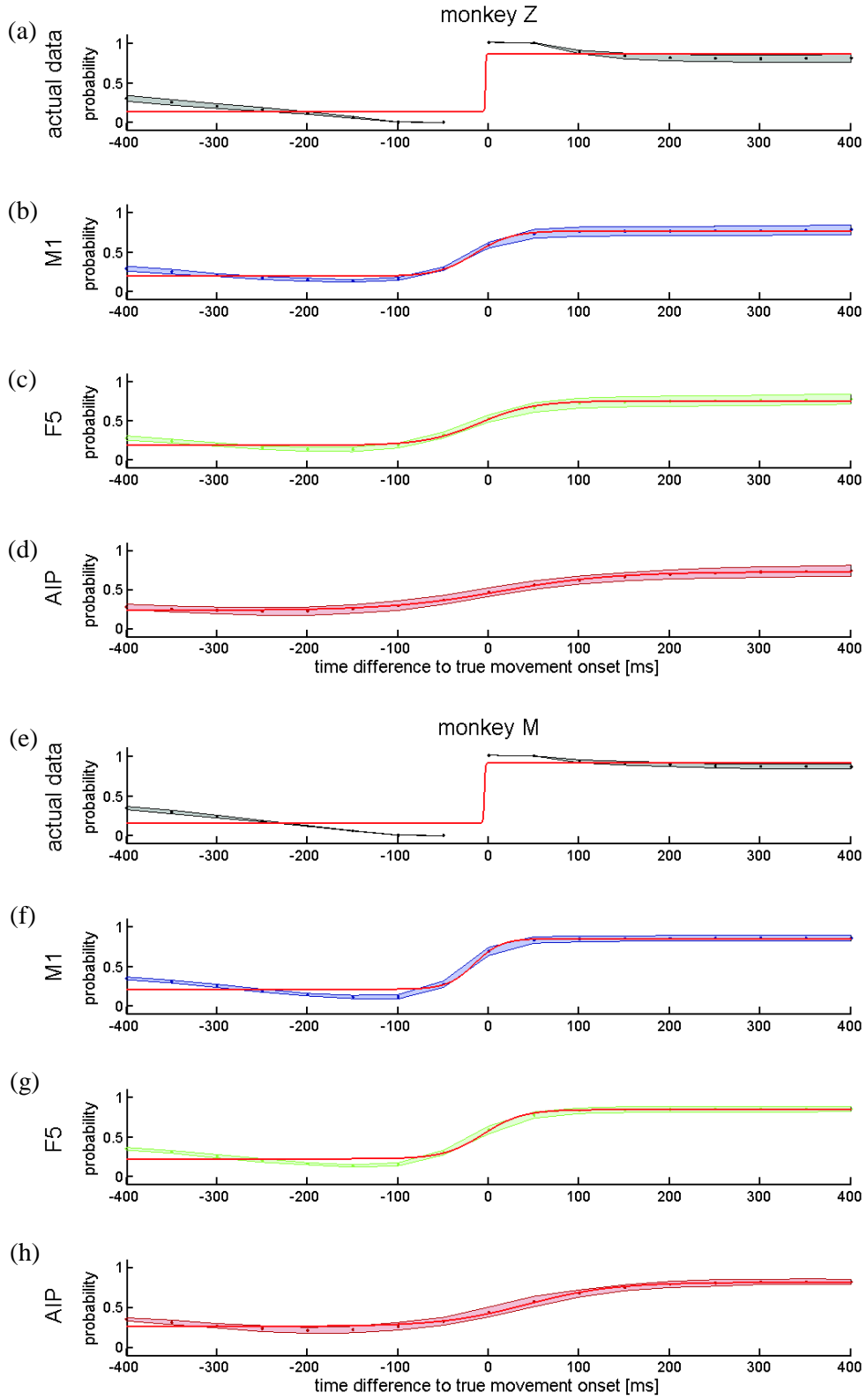
(figure 13 (c), (g)), and 0.02 and 0.02 when decoding when AIP (figure 13 (d), (h)). The decreasing values also indicate that decoding with M1 showed the most precise transition from resting to movement, whereas in state reconstruction with F5 and AIP more samples both before and after movement onset were incorrectly classified.

Next, we looked at the average time of movement onset prediction represented by the fit parameter  $c$ . Unfortunately, in the fit of the true data, this parameter cannot account for true movement onset: since we used discrete time samples with a sampling rate of 20 Hz for fitting the sigmoidal function, any number between -50 and 0 ms would have been a legitimate fitting value for  $c$ . Therefore, the actual value of  $c$  in the fit of the true data is meaningless to us.

This holds true to a certain extent also for  $c$  in the fitted functions of the decoded data. Nevertheless, we found that  $c$ , when decoding with either M1 or F5, also fell within this time window of -50 to 0 ms suggesting that movement onset could be captured on average within the precision of 50 ms ( $c = -15.5$  ms and  $-16.0$  ms when decoding from M1,  $c = -10.4$  ms and  $-6.4$  ms when decoding from F5, for monkey Z and M, respectively). In contrast, when decoding with AIP, we obtained values of  $c = 13.4$  ms and  $41.9$  ms for monkey Z and M, respectively, suggesting that

---

**Figure 13.** Probability of true and decoded movement states in a 800 ms time window around each actual movement onset (see Materials and Methods, section 5.5). Dots illustrate mean probability of true (a), (e) and predicted (b)-(d), (f)-(h) movement averaged across recordings, separately for monkey Z (a)-(d) and monkey M (e)-(h) whereas shaded regions show standard deviations. Red lines depict the respective fits.



movement onset prediction with AIP was delayed in comparison to the real movement onset.

In summary, movement onset was decoded on average most precisely with area M1: the distribution of time shifts compared to the real onset had the least variance and were therefore most reliable. Also, the average onset of predicted movement was very precise with respect to the resolution of the data. For F5, this was also the case; however, the predicted onsets also contained a higher variance and were therefore more inconsistent. AIP yielded again the lowest prediction accuracy: movement onset varied the most with respect to real onset and on average lagged behind true onset.

### ***6.5. Optimal decoding parameters***

As described in section 5.3, we tested various combinations of gap and bin lengths for decoding and evaluated the results with respect to decoding performance. For each recording, gap lengths from -1000 to 200 ms were examined together with bin lengths from 10-1400 ms and the combination yielding the highest percentage of correctly classified samples was determined (figure 14).

The cumulative distribution of optimal parameters is illustrated in figure 15 separately for bin (figure 15 (a)-(b)) and gap lengths (figure 15 (c)-(d)). In contrast to the Kalman filter decoding of continuous kinematics, optimal bin length varied among areas and was much longer than 10 ms. For all three areas, the median optimal bin lengths (pooled across all ten recordings) were significantly greater than zero (two-sided sign test,  $p < 0.002$ ). On average, they were similar for areas M1 and F5 (mean and standard deviation:  $270 \pm 71.49$  ms and  $295 \pm 79.76$  ms, respectively), whereas optimal bin lengths for decoding with AIP tended to be even longer (mean and standard deviation:  $580 \pm 198.89$  ms). Similarly, the medians between M1 and F5 (median: 250 ms for both areas, respectively) did not differ significantly, whereas there was a significant difference between the



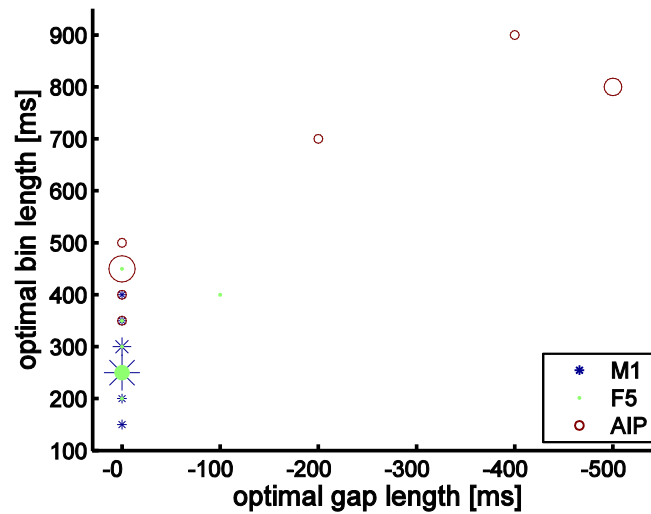


**Figure 14.** Scatterplot of optimal parameter combinations of each recording session and each area used for decoding. Blue stars, green dots, and red circles denote optimal parameter combinations for decoding with M1, F5, and AIP, respectively. Size of marker corresponds to number of recordings with respective optimal parameter combination.

median of optimal bin lengths for AIP (median: 475 ms) and the medians of the other two areas (Kruskal-Wallis test and Tukey-Kramer multicomparison test,  $p < 0.05$ ).

In contrast, optimal gap lengths were mostly very short (figure 15 (c)-(d)), especially when decoding with M1 or F5: for M1, optimal gap length was always -0 ms which was very similar to F5 with an average optimal gap length of -10 ms (standard deviation: 31.62 ms; median: -0 ms). Accordingly, neither of the median values was statistically different from zero (two-sided sign test, respectively,  $p = 1$ ). In contrast, when decoding with AIP, results were more mixed. Both gap lengths of -0 ms, as well as longer time lags were optimal for AIP (mean  $\pm$  standard deviation:  $-160 \pm 222.11$  ms; median: -0 ms). However, the median optimal gap length also did not differ significantly from zero (two-sided sign test,  $p = 0.125$ ). Furthermore, the variances of the distributions of optimal gap lengths were significantly different across the three areas (non-parametric Levene's test,  $p < 0.0001$ ).

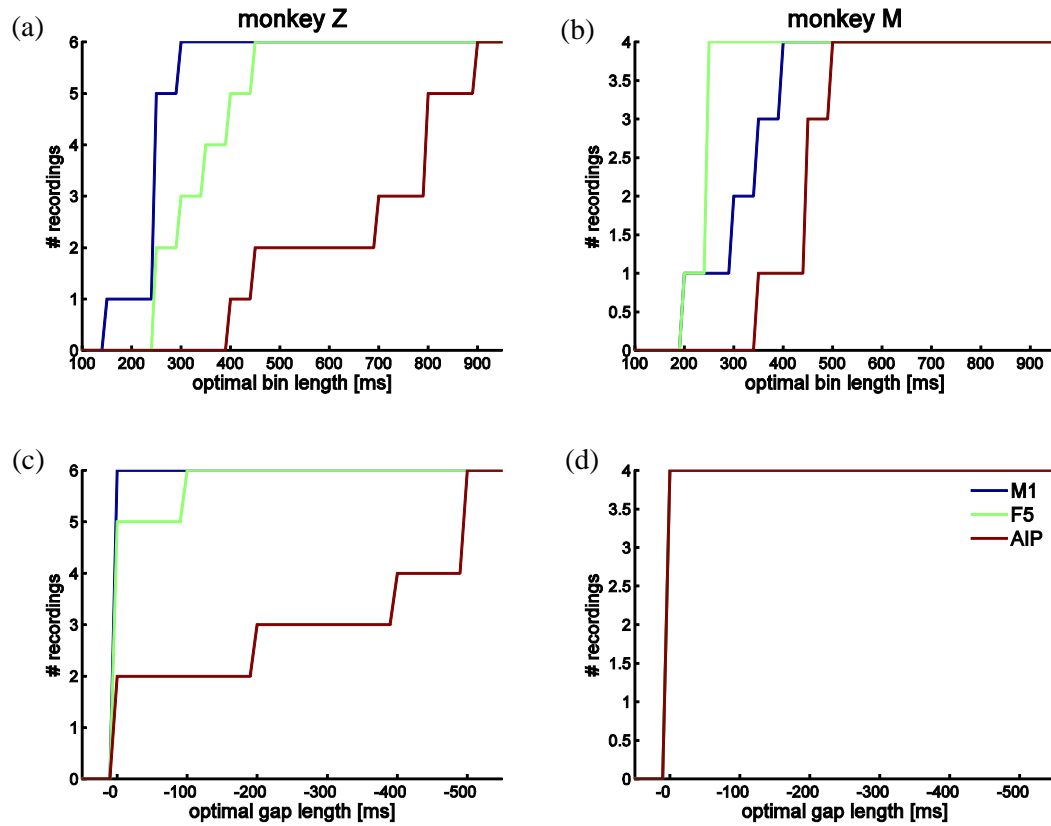


**Figure 15.** Bin (a)-(b) and gap (c)-(d) lengths yielding the highest decoding accuracy were determined for each recording and are shown as cumulative distributions separately for monkey Z (a), (c) and monkey M (b), (d). For monkey M, the optimal gap length was -0 ms for each area and recording. Therefore, only the line for area AIP is visible in (d).

In summary, results for M1 and F5 were comparable: bin lengths between 100 and 400 ms combined with no or only very short time lags yielded highest decoding performance. For decoding with AIP however, longer bin lengths of durations from 350 ms up to 900 ms were preferable combined with either also very short or long gap lengths of -200 to -500 ms.

## 7. Discussion

In addition to decoding 27 joint angles continuously over time, we predicted two different kinematic conditions (*resting* and *movement*) describing the state of the kinematics from single unit activity in M1, F5, and AIP. To our knowledge, this is the first study testing not only motor and premotor areas for state prediction, but also area AIP in the parietal cortex.

In short, we found that all three areas were well suited for state decoding. M1 and F5 yielded very similar results whereas prediction accuracy with activity from AIP was most often significantly lower. However, all areas exceeded chance level by far.

### ***7.1. State reconstruction with primary and premotor cortex***

Compared to Kalman filter decoding of 27 joint angles, we found very similar results for the prediction of states for the three different areas: we obtained best decoding performance with neural activity from M1, followed by F5 and AIP. All three areas were able to predict the state with high accuracy (figure 10), which was significantly better than chance level. Comparing the reconstructed state with actual trajectories (figure 9) confirmed that the predicted states matched the monkey's behaviour well. However, in contrast to the Kalman filter decoding, the differences in prediction accuracy were smaller between the three areas and were never significant between F5 and M1.

Previously, the motor and premotor cortices have been subject to investigations of their suitability for decoding kinematic and task-related categories. A variety of decoding algorithms have been employed to detect kinematic states (Aggarwal *et al* 2008, Darmanjian *et al* 2003, Ethier *et al* 2011, Lebedev *et al* 2008, Velliste *et al* 2014) or different kinds of trial epochs (Achtman *et al* 2007, Aggarwal *et al* 2013). However, in a neuroprosthetic application, detection of specific trial epochs will keep the patient restricted to a limited amount of motor actions within the respective task scheme, whereas the detection of kinematic states as *resting* or *movement* will provide the freedom of more natural and general ways to perform movements. To put this into practice, we

aimed to detect kinematic categories not only during correct trials but also during inter-trial periods and error trials.

So far, only one other study followed the same approach recently: Velliste *et al* (2014) distinguished between *idle* and *active* neural states during both trials and inter-trial intervals. In contrast to our definition of *resting* and *movement* state, their *idle* state corresponded only to our *passive resting* state, whereas our *active resting* state belonged to their *active* neural state. By utilizing a linear discriminant analysis (LDA) they were able to predict these states from spikes in M1 with a precision of approximately 98%. This was slightly higher than our average decoding performance of 94% when decoding from M1 (figure 10) and might be due to their different definition of states (see also discussion in section 7.4). Another study that decoded states only during correct trials used a more similar definition to our classification of kinematic states: Ethier *et al* (2011) set a velocity threshold to define data samples recorded during a centre-out reaching task performed with a cursor on a screen as *resting* or *movement* and achieved a prediction accuracy of approximately 90% when decoding from M1. There, LDA was used for state classification as well.

Other studies were only able to produce lower performances than the ones mentioned above or presented in this study: Aggarwal *et al* (2008) decoded *resting* and *movement* state of individual finger movements with a gating classifier (committee of neural networks) from neural activity in M1 and achieved an accuracy of about 85%. However, they only used sequentially recorded units for decoding which might have been disadvantageous compared to our simultaneous recordings from multiple arrays, in which additional information might have been encoded in the coherence or phase synchrony within the neuronal population (Averbeck and Lee 2004). Furthermore, their classifier might have been inferior to our wSVM method. This might also be the reason why Darmanjian *et al* (2003) only achieved a performance of approximately 80% when predicting *stationary* and *moving* states from M1 with a hidden Markov model. SVMs have been shown to outperform hidden Markov models in some cases (Miao *et al* 2007, Wissel *et al* 2013).

Aggarwal *et al* (2013) did not only decode from M1, but also included single and multiunit activity from premotor cortex (PM) into the data set for prediction of four different kinematic states during correct trials of a reach and grasp task. With LDA, they were only able to achieve a performance of about 70%. However, none of their states included our *passive resting* condition, since the monkey never placed its hand in a resting position during the task. Instead, as *baseline* state, the monkey had to actively pull a lever to initiate a trial before performing a reach and grasp to another object. This made their *baseline* state more comparable to our *active resting* state. The other states of their task (*reaction, move, hold*) also corresponded more to our *active resting* or *movement* state. As we showed in figure 11, *active resting* state was more difficult to distinguish from *movement* than *passive resting*, which could explain why Aggarwal and colleagues had more difficulty with distinguishing their four states with their decoder.

When comparing decoding performance separately for M1 and PM, Aggarwal and colleagues found that detection of states was more accurate with M1 than with PM. However, the difference was only significant for *baseline* state. These findings correspond well with our results where M1 performed insignificantly better in prediction than F5.

Lebedev *et al* (2008) also compared kinematic state prediction from spiking activity of M1 and PMd. Their two states of button *press* and *release* were comparable to the definition of our *passive resting* and *movement*, respectively. They predicted a value corresponding to the probability of a state and compared it to the true occurrence of states. By doing so, similarly to our results, they obtained a higher decoding performance for M1 ( $CC \approx 0.93$ ) than for PMd ( $CC \approx 0.87$ ).

## **7.2. State reconstruction with parietal cortex**

So far, this is the first study to investigate AIP as a potential area for detection of kinematic states as well as to compare the resulting decoding performance to other areas. Previously, only PRR in the parietal cortex encoding reaching movements has been subject to this analysis: Hudson and Burdick

(2007) decoded *baseline* and *reach* state with hidden Markov models from single and multiunits in PRR while a monkey was performing a delayed centre-out reaching task. Again, *baseline* state consisted of an active hand positioning over a centre target, which made it similar to our *active resting* state. Furthermore, Hudson and Burdick only demanded the decoding of *reach* state between go signal and beginning of hold phase during correctly performed trials in order to classify the prediction as successful. No attention was paid to the actual duration of predicted *reach* states as long as it stayed within the described interval. Furthermore, no comparison was made to the length of actual reaching movements. This way, they were able to decode with almost 80% accuracy. Assessment of the performance with our methods would most likely have yielded a substantially lower accuracy.

Shenoy *et al* (2003) also predicted the onset of movement during a delayed centre-out reaching task from activity in PRR. Similarly as in Hudson's and Burdick's study, all possible kinematic states again corresponded to either our *active resting* or *movement* state. There was no condition in their task comparable to our *passive resting* state. In approximately 85% of the trials, their decoder issued a movement command within the allowed time slot, however, again there was no direct comparison to actual movements.

In conclusion, we were able to show that not only motor and premotor areas are suited to predict kinematics states during reaching and grasping movements, but also area AIP in the parietal cortex seems to be an appropriate candidate. Although performance was inferior to the ones obtained by M1 or F5, it was still substantially higher than results reported previously in any other study utilizing signals from parietal cortex for state prediction.

### **7.3. Reconstruction of individual states**

For all three areas, *resting* state could be predicted more accurately than *movement* (figure 11). It is known that standard SVMs show a classification bias towards the category with the larger data set,

resulting in a classification bias towards that class (Chew *et al* 2000): since the upper limit of the classification error rate of a class is inversely proportionally related to its size (Huang and Du 2005), data sets with larger sizes will show a smaller classification error. To prevent this from happening in our decoding where *resting* state made up approximately two thirds of the data set, we employed a weighted SVM instead (Huang and Du 2005) to counter a potential bias towards that class (see also section 5.1 in Materials and Methods). In short, a weighted SVM introduces two different penalty parameters  $C$  for the two different classes (instead of one constant value for all training samples as in the standard SVM). Their values are set to the inverse ratio of the respective training class size. This way, the influence of data set size can be cancelled resulting in the same upper limit of classification error rate for each class. As a consequence, the boundary (hyperplane) separating the training samples of both classes is chosen in a way that more samples belonging to the smaller class are correctly assigned to their respective class (compared to the non-weighted SVM), with the potential risk of a higher misclassification of the samples of the opposite, now less important category. However, even with this modification, we still observed a prediction bias towards *resting* state.

Other studies in which *resting* and *movement* states were predicted did not find a bias towards one of the states (Darmanjian *et al* 2003, Ethier *et al* 2011, Velliste *et al* 2014). However, the two different states seemed to be more equally distributed within the data sets in at least two of the studies (Darmanjian *et al* 2003, Velliste *et al* 2014), which might be a reason why a bias did not occur. Furthermore, different algorithms were used for decoding (LDA and a hidden Markov model). The influence of decoding algorithm on the decoding performance of specific states needs to be tested in more detail in the future.

In a neuroprosthetic application, a potential bias of the wSVM could be accounted for from the theoretical side by adjusting the penalty parameters of both states even further as part of the training

step. This would modify the bias within the decoder and make the algorithm more sensitive towards the *movement* state (Huang and Du 2005).

Another way of sensitizing the decoder for *movement* state, which was not tested here, could be to decrease the velocity threshold determining which data sample is classified as movement in the training data. This way, more samples during transition periods from *resting* to *movement* and vice versa would be defined as *movement* and could produce a “counter-bias” in the training step towards *movement*. However, this could also lead to a misclassification of *resting* samples that were classified correctly before. The impact of this trade-off needs to be tested further in the future.

Moreover, our definition of *resting* and *movement* might have influenced the decoding performance of each state. As described in Materials and Methods (section 5.2), we first determined a kinematic information vector for each DOF by assigning each data sample to one of the two categories based on the respective velocity at a time instant. Then, a general kinematic information vector was constructed out of the individual ones by defining a time sample as *movement* if at least one third of the individual kinematic information vectors were categorized as *movement* at that time. This way, we classified samples with less than nine joints displaying *movement* as a general *resting* sample. The neural state for these samples however might have been (at least to some extent) a *movement* state. Thus, the decoder might have learned that some data samples are to be classified as *resting* although their neural state represented *movement*. In the decoding step, actual *movement* samples therefore might have been incorrectly classified as *resting* which, thus decreased the prediction accuracy of the *movement* state.

### **7.4. Active and passive resting**

Although kinematically similar (i.e. velocity below a certain threshold), we found that there were differences in prediction accuracy within the *resting* state category: Phases in which the monkey was waiting to perform the next movement could be decoded with higher precision (*passive resting*)



than phases in which the monkey held its hand and arm still while holding the grasped object (*active resting*). A reason for the lower precision during hold epochs could be that these phases of no movement were much shorter and embedded within a movement. Since our criterion to distinguish *resting* and *movement* was based on an empirically set velocity threshold, the state in transition phases from movement to no movement and vice versa is highly dependent on the defined threshold. Subsequently, this would impact the prediction accuracy within these phases (cf. above, section 7.3). Previous studies classifying *resting* and *movement* states also found transition periods from one state to the other to be the phases exhibiting the most prediction errors (Ethier *et al* 2011).

Another possibility for the difference in decoding accuracy could be that the actual neural state differed between periods of relaxed resting and periods of still hand position during a movement (Darmanjian *et al* 2003, Velliste *et al* 2014). Velliste *et al* (2014) recently showed that the neural activity of M1 between *passive* and *active resting* exhibited different tuning models and thus differed significantly. During *active resting*, the activity pattern of the recorded units resembled the pattern during *movement* state instead of the one during *passive resting*. This suggests that a division of data samples into *resting* and *movement* based on a mere velocity threshold without taking muscle activation into account (as in our study and several previous studies (Achtman *et al* 2007, Aggarwal *et al* 2013, Ethier *et al* 2011, Shenoy *et al* 2003)) does not necessarily reflect the actual difference in neural coding. Velliste and colleagues therefore divided their neural activity into *idle* (during *passive resting*) and *active* (during *active resting* and *movement*) state instead. Since the amount of *passive resting* was much higher in our data than *active resting*, the decoder probably associated *resting* state to a large extent with the neural tuning during *passive resting* and therefore classified phases in which the monkey was holding the object (*active resting*) to the opposite state, namely *movement*. In our definition of *resting* and *movement* states this resulted in low prediction accuracy during holding. However, if we had considered *idle* and *active* state as the

two different kinematic categories, the decoding performance might have been higher during hold phases.

In a neuroprosthetic application (where state and continuous kinematic prediction is combined) in which detection of *resting* state would mean overwriting any kinematic prediction with zero velocity, it might be even more desirable to keep the controlled actuator within an active (i.e. “on” state) state while the patient is engaged in an action even during phases of zero velocity (imagine for example holding a cup still while pouring coffee into it). This might help to improve the feeling of control over the prosthetic. A prosthetic that switched between *resting* and *movement* (i.e. switched “off” and “on”) during movement execution could confuse the patient and worsen the control. In contrast, during phases of relaxed resting (for example while watching tv) in which the prosthetic is not needed, it might be helpful to turn the prosthetic “off” by putting it into a *resting* state. This way the patient is not required be constantly engaged in prosthetic control to keep the arm and hand still.

### ***7.5. Decoding of movement onset***

Prediction of movement onset was on average very precise and close to the actual movement onset: whereas decoded onsets obtained with activity from F5 and M1 lay very close to the actual movement onset (within the resolution accuracy of the data), predicted onsets with AIP came slightly after real onsets. When looking at the variance of delay between real and decoded onsets, M1 performed better than F5, whereas decoding from AIP delivered the most variability in onset detection.

To our knowledge, this study compares the precision with which a decoder predicts movement onset for the first time comparatively for areas M1, F5, and AIP. The accuracy of state transition prediction has in general been barely described in the literature for any of the three areas. In the study of Aggarwal *et al* (2013), four different epochs of a behavioural reach and grasp task were

decoded from single and multiunit activity recorded in M1 and PM with LDA. To assess the latency of state transition prediction, the following method was employed: being in the current correct state, the decoder needed to have predicted the correct following state at least three out of five times. Only then, a transition into the next state was carried out. Furthermore, only transitions into the subsequent epoch (following the order as defined by the task) were allowed to take place. Most comparable to our transition from *resting* to *movement* (i.e. movement onset) was their transition from *reaction* state to *move*. There, Aggarwal and colleagues obtained an average delay of predicted transition of about 75 ms for M1, and 75 and 50 ms for PM for two monkeys, respectively. Since we did not impose any restrictions on the transition from resting to movement, as opposed to Aggarwal and colleagues, our transitioning times are much shorter and appear earlier.

In contrast, Kemere *et al* (2008) predicted transitions from *planning* to *movement* around 150 ms after an instructed go signal, which was 100 ms before actual movement onset. They decoded with spiking activity from caudal dorsal premotor cortex while the monkey was performing a reaching task. Here, a hidden Markov model was utilized for decoding.

The precision of transition prediction depends highly on the definition of when a respective prediction is allowed to occur. If a certain degree of certainty needs to be achieved as in Aggarwal and colleagues' study (where a subsequent state had to be predicted for a specific number of times before a state transition was allowed to happen), longer delays are likely to be introduced. In contrast, if the emphasis is laid on precision of onset prediction, an approach as presented in our study might be more appropriate.

Certainly, the selected decoding algorithm also plays a role in the precision of movement onset prediction. A decoder that takes into account the history of states for its prediction (like a hidden Markov model (Eddy 1996, Rabiner 1989)) might produce a different time lag than a predictor that treats each data sample independently (like an SVM (Huang and Du 2005)). However, the impact of decoding algorithm on performance needs to be further investigated in the future.

### **7.6. Optimal decoding parameters**

Optimal bin and gap lengths overlapped to a great extent for M1 and F5: windows with a length of up to 450 ms directly preceding the kinematic state sample to be predicted yielded highest decoding accuracies. On average, bin lengths were slightly longer for F5 than for M1. In contrast, when decoding with AIP, optimal parameter combinations showed much more variation. On the one hand, bin lengths of 350 to 400 ms directly preceding the kinematic state produced highest decoding accuracies, on the other hand bin lengths of 700-900 ms with times lags of -200 to -500 ms were optimal.

To our knowledge, no study so far has systematically reported the impact of bin and gap lengths on state decoding performance. Typically in decoding studies, the gap length was set to zero and a bin length preceding the time instant to be decoded was chosen without further justification or explanation. The bin lengths used for decoding with M1 ranged from 30 ms (Velliste *et al* 2014) up to 100 ms (Aggarwal *et al* 2008, Aggarwal *et al* 2013, Darmanjian *et al* 2003) and 500 ms (Ethier *et al* 2011) to predict kinematic or behavioural states. Contrary to our findings where bin lengths of slightly longer duration were optimal for F5 than for M1, most studies decoding from M1 and PM used the same parameters for both areas (Aggarwal *et al* 2013, Lebedev *et al* 2008). For state prediction from activity recorded in PM, we find bin lengths of 100-500 ms (Achtman *et al* 2007, Aggarwal *et al* 2013, Lebedev *et al* 2008) in the literature, for decoding with activity from parietal cortex (PRR) we find a bin of 250 ms (Shenoy *et al* 2003). These values correspond roughly with our findings, however we cannot decide if these values truly correspond to optimal bin lengths (and thus contradict or support our findings) or if they were chosen based on other, non-reported reasons.

However, the bin and gap lengths found to be optimal for state decoding differ from the ones found for the Kalman filter decoding in chapter II, section 3. There, highest prediction performances were obtained for very short bins (10 ms) preceding the kinematics in combination

with different gap lengths. Since the Kalman filter decoded continuous kinematics, where fast changes occurring in short time windows needed to be predicted, instantaneous monitoring of firing rates was important. This justifies the necessity of very short time windows. However for decoding kinematic states, which are categorical variables, small changes in neural activity were less important and therefore did not need to be strictly monitored by the decoder. Instead, categorical changes in neural patterns are better reflected in longer time intervals and thus longer bin lengths improved discrimination of kinematic states over short ones.

In general, our findings correspond to the general framework of the fronto-parietal network hypothesis (Jeannerod *et al* 1995 and section 1.1.5): visual information about the object to be grasped is first present in AIP, forwarded to F5 where a grip type is selected, which is then projected to M1. There, a motor command is issued and sent to the spinal cord. The optimal bin length, representing at what time most information with respect to the kinematic state is encoded in an area, follows this order for the three tested areas: bin lengths were longest for AIP, then F5, and shortest for M1. According to earlier studies and as discussed in section 4.5, AIP receives an efference copy from premotor and motor cortices, which can serve as a tool for the online control of movement (Mulliken *et al* 2008). This could explain why we did not only find bins to be optimal for AIP that were longer than the ones for M1 and F5, but we also obtained bin lengths that were similar to the ones for M1 and F5.

### **7.7. Conclusion**

Although we included both correct and incorrect trials as well as inter-trial intervals and did not restrict the decoder to any given structure of the task, we were able to achieve higher decoding accuracy with activity from AIP, F5, and M1 than most of the previous comparable studies could. Furthermore, our decoding paradigm allowed for unexpected and thus more natural behaviour (by including incorrect trials and inter-trial intervals) and it may therefore contribute towards the

development of neuroprosthetics that are not only usable in artificial lab conditions, but also in an everyday environment.

Contrary to our classification of *resting* and *movement* states based on a velocity threshold, further improvement of prediction performance might be achieved by classifying data samples into categories based on the active or passive engagement of the subject.

Moreover, the impact of decoding algorithms on prediction accuracy is not entirely clear at this stage. After the identification of the behavioural states that can be distinguished best based on their neural activity, the contribution of decoding algorithms to the accuracy of prediction should be assessed more precisely in the future.

Our results fit well into the framework of the fronto-parietal network hypothesis. For the first time, we were able to show the suitability of area AIP for predicting kinematic states and to put the respective decoding performance into context by comparing it to different cortical areas like motor and premotor cortex, which have already been accepted broadly as potential candidates for kinematic decoding (Schaffelhofer *et al* 2015). These findings contribute to the development and realization of future neuroprosthetic applications by providing information about the contribution of different cortical areas to motor coding as well as by providing information about their suitability for prediction of kinematic and behavioural states.

# **Chapter IV**

**- Conclusions**





## 8. Conclusions and Outlook

In this study, we were able to show for the first time that continuous decoding of hand, wrist, and arm kinematics over time was possible not only from areas M1 and F5, but also from parietal area AIP. Furthermore, our study presents the most complete decoding of finger, wrist, and arm joints so far. In addition, we not only predicted continuous movement, but were also able to detect in which behavioural state the animal was in. More precisely, we were able to decode *resting* and *movement* states with high precision from spiking activity in all three areas.

However, in this study we only tested the feasibility of both kinematic and state prediction separately. The next step would be the combination of decoding methods into one decoder, in which both state and kinematic prediction run in parallel and are able to influence each other.

The need for a combined decoder has already been expressed earlier by several researchers (Achtman *et al* 2007, Darmanjian *et al* 2003, Ethier *et al* 2011, Hudson and Burdick 2007, Kemere *et al* 2008). Since cortical activity patterns have been shown to be dependent on the cognitive state of the subject (Kemere *et al* 2008, Velliste *et al* 2014), it might be advantageous to detect those states in order to adjust the kinematic decoder to these changes and prevent or counteract false movement predictions.

Indeed, previous studies have shown that combined decoders have the potential to deliver predictions with higher accuracies than kinematic decoders without state detection: Aggarwal *et al* (2013) improved their decoding of 18 joint angles of the hand and wrist with a Kalman filter using from M1 and PM when they combined it with a state predictor detecting four different states of the behavioural task. However, the increase in performance was small and only observed if more than approximately 45 units were used for decoding.

In contrast, Ethier *et al* (2011) achieved a significant increase of decoding performance when they combined their prediction of 2D velocity of arm movements from activity in M1 with a state classifier detecting *resting* or *movement*. Similarly, Velliste *et al* (2014) combined a Laplace

Gaussian Filter decoding of 3D position, 3D velocity, and speed of the arm endpoint of a monkey performing reaching movements with an LDA detecting *idle* and *active* neural states with activity from M1. This way, they increased their prediction accuracy significantly compared to only using the Laplace Gaussian Filter for decoding. Also Darmanjian *et al* (2003) were able to improve their prediction of 3D arm position from M1 when they combined their kinematic decoder with a hidden markov Model for state detection.

However, the question of how to combine state and kinematic decoding is not trivial and offers many possible answers. If *resting* and *movement* states are detected by a state decoder to prevent unwanted movement predictions during phases of posture, a simple low-pass filtering during detected *resting* state could avoid noisy jittering in the kinematic prediction. Ethier *et al* (2011) tested this method for decoding 2D velocity from M1 in a centre-out reaching task using Wiener cascade model and an LDA for prediction. However, no significant increase of decoding performance was achieved this way. Instead, this was accomplished when two separate movement decoders were built with training data consisting of kinematics during either *movement* or *resting* state. In the decoding step, movement prediction was performed by switching between the two movement decoders based on the classification of the state decoder. The latter approach has also been successfully realized in combination with other state decoding algorithms like a hidden Markov model (Darmanjian *et al* 2003).

An additional way to combine decoders could be such that the kinematic prediction is stopped (kinematic output is kept constant or decoded velocity is overwritten with zero) if the state classifier detects a *resting* state (Velliste *et al* 2014, Wood *et al* 2005) or a corresponding task epoch (Aggarwal *et al* 2013).

Furthermore, the combination of a kinematic decoder with a state detector also offers the possibility to switch between different motor action patterns: whereas standard kinematic movement prediction is carried out during *movement* state, the kinematic decoding could pause

when a second behavioural or cognitive state is detected. Then, the prosthesis could perform a predefined grasp, a click (if the movement is performed on a virtual platform like a computer or smartphone), or another predefined action customized to the patient's needs. Moreover, the number of possible states could be increased to offer more flexibility in automated actions to be carried out.

These and other possibilities will have to be explored in the future. Our results contribute to the basic understanding about how well different brain areas in the fronto-parietal grasping network are suited for neuroprosthetic applications and how different types of decodings can be carried out with signals from these areas. In the future, these findings can contribute to the development and exploration of sophisticated types of neuroprostheses.



## 9. Summary

In this study, we performed two different kinds of decodings: first, we investigated the possibility of decoding complete hand, wrist, and arm movements that were represented by 27 DOF from single and multiunit activity in the hand areas of motor (M1), premotor (F5), and parietal cortex (AIP) in a comparative way. Second, we performed a detection of kinematic states, namely *resting* and *movement*, from the spiking activity in the same three cortical areas. To mimic more natural behaviour in which also unexpected movements could occur, we decoded both correct and error trials as well as inter-trial intervals and did not restrict the decoders to any given structure of the task.

To our knowledge, this is the first study that combines and compares areas M1, F5, and AIP for prediction of versatile, continuous hand kinematics as well as detection of respective behavioural states. Simultaneous recordings of population activity from the three areas by multi-electrode arrays gave us the possibility to examine the differences between the areas and evaluate the information content with respect to hand and arm kinematics in these areas.

We found that continuous trajectories of 27 joint angles could be reconstructed accurately over time by using single and multiunit activity from M1, F5, or AIP. The highest performance was achieved when using M1 for decoding, followed by F5 and area AIP. The same order of decoding accuracy was also true for the detection of kinematic states. All three areas were able to predict both joint angles and kinematic states significantly better than chance level. Furthermore, performances were similar to or even higher than reported in previous studies.

When combining activity from two or more areas for decoding of 27 joint angles, no significant increase of decoding performance was achieved. Furthermore, the differences in decoding performance between the three areas did not primarily depend on the number of neurons available for decoding, but strongly reflected the type of information encoded in these areas. No substantial

difference was found between decoding finger and wrist joints, whereas shoulder and arm movements were predicted with significantly higher accuracy.

For the decoding of joint angles, we found neural data from very short time bins preceding the kinematics to be suited best for decoding. However, the bin needed to be combined with an adequate time lag to find the optimal relation between brain activity and movement execution. These optimal gap lengths differed substantially between areas. Shorter gap lengths were ideal when decoding from M1, whereas optimal time gaps for F5 were longer than for M1, indicating that information about grasping is present earlier in F5 than in primary motor cortex. When decoding from area AIP, best decoding performance was obtained for gap lengths close to zero (with neural activity preceding kinematics) supporting the idea that AIP could represent a copy of the motor plan in F5 in order to compare it to the visual properties. All these findings are in line with the frontoparietal grasp network hypothesis (Jeannerod *et al* 1995). Similar results were obtained for the decoding of kinematic states, however, optimal bin lengths were longer than when predicting 27 joint angles.

*Resting* state could be detected with higher accuracy than *movement*. In addition, there was a difference in decoding accuracy between *passive resting*, when the monkey was waiting to perform the next movement, and *active resting*, when the animal held its hand still while holding the object: *passive resting* was detected by the classifier with higher precision than *active resting*. Nevertheless, movement onset was on average detected very precisely and the time lag between true and predicted movement onset lay within the resolution accuracy of the data when decoding from M1 and F5. When AIP was used for classification, movement onsets were detected shortly after real movement beginnings.

In conclusion, we found that all three areas were suited for decoding of both high-dimensional kinematics and kinematic states. Our findings contribute to the development of more sophisticated neuroprosthetics that will operate in a natural and intuitive way.

---

## References

- Achtman N, Afshar A, Santhanam G, Byron M Y, Ryu S I and Shenoy K V (2007) Free-paced high-performance brain-computer interfaces *J Neural Eng* **4** 336-347
- Aggarwal V, Acharya S, Tenore F, Shin H C, Etienne-Cummings R, Schieber M H and Thakor N V (2008) Asynchronous decoding of dexterous finger movements using M1 neurons *IEEE Trans Neural Syst Rehabil Eng* **16** 3-14
- Aggarwal V, Mollazadeh M, Davidson A G, Schieber M H and Thakor N V (2013) State-based decoding of hand and finger kinematics using neuronal ensemble and LFP activity during dexterous reach-to-grasp movements *J Neurophysiol* **109** 3067-3081
- Andersen R, Asanuma C, Essick G and Siegel R (1990a) Corticocortical connections of anatomically and physiologically defined subdivisions within the inferior parietal lobule *J Comp Neurol* **296** 65-113
- Andersen R A, Bracewell R M, Barash S, Gnadt J W and Fogassi L (1990b) Eye position effects on visual, memory, and saccade-related activity in areas LIP and 7a of macaque *J Neurosci* **10** 1176-1196
- Anderson K D (2004) Targeting recovery: priorities of the spinal cord-injured population *J Neurotrauma* **21** 1371-1383
- Ashe J (1997) Force and the motor cortex *Behav Brain Res* **87** 255-269
- Ashe J and Georgopoulos A P (1994) Movement parameters and neural activity in motor cortex and area 5 *Cereb Cortex* **4** 590-600
- Averbeck B B and Lee D (2004) Coding and transmission of information by neural ensembles *Trends Neurosci* **27** 225-230
- Bansal A K, Truccolo W, Vargas-Irwin C E and Donoghue J P (2012) Decoding 3D reach and grasp from hybrid signals in motor and premotor cortices: spikes, multiunit activity, and local field potentials *J Neurophysiol* **107** 1337-1355
- Bansal A K, Vargas-Irwin C E, Truccolo W and Donoghue J P (2011) Relationships among low-frequency local field potentials, spiking activity, and three-dimensional reach and grasp kinematics in primary motor and ventral premotor cortices *J Neurophysiol* **105** 1603-1619
- Batista A P and Andersen R A (2001) The parietal reach region codes the next planned movement in a sequential reach task *J Neurophysiol* **85** 539-544
- Baumann M A, Fluet M C and Scherberger H (2009) Context-specific grasp movement representation in the macaque anterior intraparietal area *J Neurosci* **29** 6436-6448

- Belmalih A, Borra E, Contini M, Gerbella M, Rozzi S and Luppino G (2009) Multimodal architectonic subdivision of the rostral part (area F5) of the macaque ventral premotor cortex *J Comp Neurol* **512** 183-217
- Ben Hamed S, Schieber M H and Pouget A (2007) Decoding M1 neurons during multiple finger movements *J Neurophysiol* **98** 327-333
- Bennett K M and Lemon R N (1996) Corticomotoneuronal contribution to the fractionation of muscle activity during precision grip in the monkey *J Neurophysiol* **75** 1826-1842
- Binkofski F, Dohle C, Posse S, Stephan K, Hefter H, Seitz R and Freund H (1998) Human anterior intraparietal area subserves prehension A combined lesion and functional MRI activation study *Neurology* **50** 1253-1259
- Borra E, Belmalih A, Calzavara R, Gerbella M, Murata A, Rozzi S and Luppino G (2008) Cortical connections of the macaque anterior intraparietal (AIP) area *Cereb Cortex* **18** 1094-1111
- Borra E, Belmalih A, Gerbella M, Rozzi S and Luppino G (2010) Projections of the hand field of the macaque ventral premotor area F5 to the brainstem and spinal cord *J Comp Neurol* **518** 2570-2591
- Bradberry T J, Gentili R J and Contreras-Vidal J L (2010) Reconstructing three-dimensional hand movements from noninvasive electroencephalographic signals *J Neurosci* **30** 3432-3437
- Brochier T, Spinks R L, Umiltà M A and Lemon R N (2004) Patterns of muscle activity underlying object-specific grasp by the macaque monkey *J Neurophysiol* **92** 1770-1782
- Carlsson K, Petrovic P, Skare S, Petersson K M and Ingvar M (2000) Tickling expectations: neural processing in anticipation of a sensory stimulus *J Cognitive Neurosci* **12** 691-703
- Carmena J M, Lebedev M A, Crist R E, O'Doherty J E, Santucci D M, Dimitrov D F, Patil P G, Henriquez C S and Nicolelis M A (2003) Learning to control a brain-machine interface for reaching and grasping by primates *PLoS Biol* **1** E42
- Chadwick E K, Blana D, Simeral J D, Lambrecht J, Kim S P, Cornwell A S, Taylor D M, Hochberg L R, Donoghue J P and Kirsch R F (2011) Continuous neuronal ensemble control of simulated arm reaching by a human with tetraplegia *J Neural Eng* **8** 034003
- Chang C-C and Lin C-J (2011) LIBSVM: A library for support vector machines *ACM Trans Intell Syst Technol* **2** 27:21-27:27
- Chang Y-W, Hsieh C-J, Chang K-W, Ringgaard M and Lin C-J (2010) Training and testing low-degree polynomial data mappings via linear SVM *JMLR* **11** 1471-1490
- Cheney P D and Fetz E E (1980) Functional classes of primate corticomotoneuronal cells and their relation to active force *J Neurophysiol* **44** 773-791



- Chew H-G, Crisp D J, Bogner R E and Lim C-C (2000) Target detection in radar imagery using support vector machines with training size biasing *Proceedings of the 6th international conference on Control, Automation, Robotics and Vision* Singapore
- Collinger J L, Wodlinger B, Downey J E, Wang W, Tyler-Kabara E C, Weber D J, McMorland A J, Velliste M, Boninger M L and Schwartz A B (2013) High-performance neuroprosthetic control by an individual with tetraplegia *Lancet* **381** 557-564
- Cortes C and Vapnik V (1995) Support-vector networks *Mach Learn* **20** 273-297
- Cutkosky M R and Wright P (1986) Modeling manufacturing grips and correlations with the design of robotic hands *Proceedings of the IEEE International Conference on Robotics and Automation* 1533-1539
- Darmanjian S, Kim S P, Nechyba M C, Morrison S, Principe J, Wessberg J and Nicolelis M A (2003) Bimodal brain-machine interface for motor control of robotic prosthetic *Proceedings of the IEEE/RSJ International Conference on Intelligent Robots and Systems (IROS)* Las Vegas, Nevada 3612-3617
- Debowy D J, Ghosh S, Ro J Y and Gardner E P (2001) Comparison of neuronal firing rates in somatosensory and posterior parietal cortex during prehension *Exp Brain Res* **137** 269-291
- Dum R P and Strick P L (1991) The origin of corticospinal projections from the premotor areas in the frontal lobe *J Neurosci* **11** 667-689
- Dum R P and Strick P L (2005) Frontal lobe inputs to the digit representations of the motor areas on the lateral surface of the hemisphere *J Neurosci* **25** 1375-1386
- Eddy S R (1996) Hidden markov models *Curr Opin Struc Biol* **6** 361-365
- Ethier C, Sachs N A and Miller L E (2011) Continuous state-dependent decoders for brain machine interfaces *5th International IEEE/EMBS Conference on Neural Engineering (NER)* Cancun, Mexico 473-477
- Fagg A H (1996) *A computational model of the cortical mechanisms involved in primate grasping*. Ph.D. Dissertation, University of Southern California, Computer Science Department.
- Fagg A H and Arbib M A (1998) Modeling parietal-premotor interactions in primate control of grasping *Neural Netw* **11** 1277-1303
- Faugier-Grimaud S, Frenois C and Stein D G (1978) Effects of posterior parietal lesions on visually guided behavior in monkeys *Neuropsychologia* **16** 151-168
- Fetz E E and Cheney P D (1980) Postspike facilitation of forelimb muscle activity by primate corticomotoneuronal cells *J Neurophysiol* **44** 751-772

- Flanagan J R and Wing A M (1993) Modulation of grip force with load force during point-to-point arm movements *Exp Brain Res* **95** 131-143
- Fluet M C, Baumann M A and Scherberger H (2010) Context-specific grasp movement representation in macaque ventral premotor cortex *J Neurosci* **30** 15175-15184
- Fogassi L, Gallese V, Buccino G, Craighero L, Fadiga L and Rizzolatti G (2001) Cortical mechanism for the visual guidance of hand grasping movements in the monkey: A reversible inactivation study *Brain* **124** 571-586
- Fogassi L and Luppino G (2005) Motor functions of the parietal lobe *Curr Opin Neurobiol* **15** 626-631
- Fridman E A, Hanakawa T, Chung M, Hummel F, Leiguarda R C and Cohen L G (2004) Reorganization of the human ipsilesional premotor cortex after stroke *Brain* **127** 747-758
- Fulton J F (1949) *Physiology of the nervous system*. University of Michigan: Oxford University Press.
- Galea M P and Darian-Smith I (1994) Multiple corticospinal neuron populations in the macaque monkey are specified by their unique cortical origins, spinal terminations, and connections *Cereb Cortex* **4** 166-194
- Gallese V, Murata A, Kaseda M, Niki N and Sakata H (1994) Deficit of hand preshaping after muscimol injection in monkey parietal cortex *Neuroreport* **5** 1525-1529
- Georgopoulos A P, Schwartz A B and Kettner R E (1986) Neuronal population coding of movement direction *Science* **233** 1416-1419
- Gerbella M, Belmalih A, Borra E, Rozzi S and Luppino G (2011) Cortical connections of the anterior (F5a) subdivision of the macaque ventral premotor area F5 *Brain Struct Funct* **216** 43-65
- Gnadt J W and Andersen R A (1988) Memory related motor planning activity in posterior parietal cortex of macaque *Exp Brain Res* **70** 216-220
- Goodale M A, Meenan J P, Bulthoff H H, Nicolle D A, Murphy K J and Racicot C I (1994) Separate neural pathways for the visual analysis of object shape in perception and prehension *Curr Biol* **4** 604-610
- Goodale M A and Milner A D (1992) Separate visual pathways for perception and action *Trends Neurosci* **15** 20-25
- Goodale M A, Milner A D, Jakobson L S and Carey D P (1991) A Neurological Dissociation between Perceiving Objects and Grasping Them *Nature* **349** 154-156

- Hauschild M, Mulliken G H, Fineman I, Loeb G E and Andersen R A (2012) Cognitive signals for brain-machine interfaces in posterior parietal cortex include continuous 3D trajectory commands *Proc Natl Acad Sci U S A* **109** 17075-17080
- He S Q, Dum R P and Strick P L (1993) Topographic organization of corticospinal projections from the frontal lobe: motor areas on the lateral surface of the hemisphere *J Neurosci* **13** 952-980
- Hochberg L R, Bacher D, Jarosiewicz B, Masse N Y, Simeral J D, Vogel J, Haddadin S, Liu J, Cash S S, van der Smagt P and Donoghue J P (2012) Reach and grasp by people with tetraplegia using a neurally controlled robotic arm *Nature* **485** 372-375
- Hochberg L R and Donoghue J P (2006) Sensors for brain-computer interfaces *IEEE Eng Med Biol Mag* **25** 32-38
- Holdefer R N and Miller L E (2002) Primary motor cortical neurons encode functional muscle synergies *Exp Brain Res* **146** 233-243
- Hsu C-W, Chang C-C and Lin C-J (2003) *A practical guide to support vector classification*. Technical report, National Taiwan University, Taipei 106, Taiwan, Department of Computer Science.
- Huang Y-M and Du S-X (2005) Weighted support vector machine for classification with uneven training class sizes *Proceedings of the 4th International Conference on Machine Learning and Cybernetics* Guangzhou, China 4365-4367
- Hubel D H and Wiesel T N (1968) Receptive fields and functional architecture of monkey striate cortex *J Physiol* **195** 215-243
- Hudson N and Burdick J W (2007) Learning hybrid system models for supervisory decoding of discrete state, with applications to the parietal reach region *3rd International IEEE/EMBS Conference on Neural Engineering* Kohala Coast, Hawaii, USA 587-592
- Humphrey D R, Schmidt E M and Thompson W D (1970) Predicting measures of motor performance from multiple cortical spike trains *Science* **170** 758-762
- Hwang E J and Andersen R A (2009) Brain control of movement execution onset using local field potentials in posterior parietal cortex *J Neurosci* **29** 14363-14370
- Janssen P, Vogels R, Liu Y and Orban G A (2001) Macaque inferior temporal neurons are selective for three-dimensional boundaries and surfaces *J Neurosci* **21** 9419-9429
- Jeannerod M (1988) *The neural and behavioural organization of goal-directed movements*. New York: Oxford University Press.
- Jeannerod M, Arbib M A, Rizzolatti G and Sakata H (1995) Grasping objects: the cortical mechanisms of visuomotor transformation *Trends Neurosci* **18** 314-320

- Johansson R and Westling G (1984) Roles of glabrous skin receptors and sensorimotor memory in automatic control of precision grip when lifting rougher or more slippery objects *Exp Brain Res* **56** 550-564
- Johansson R S and Flanagan J R (2009) Coding and use of tactile signals from the fingertips in object manipulation tasks *Nat Rev Neurosci* **10** 345-359
- Kakei S, Hoffman D S and Strick P L (1999) Muscle and movement representations in the primary motor cortex *Science* **285** 2136-2139
- Kakei S, Hoffman D S and Strick P L (2001) Direction of action is represented in the ventral premotor cortex *Nat Neurosci* **4** 1020-1025
- Kalman R E (1960) A new approach to linear filtering and prediction problems *J Basic Eng-T ASME* **82** 35-45
- Kandel E R, Schwartz J H and Jessell T M (2000) *Principles of neural science*. New York: McGraw-Hill.
- Kasser R J and Cheney P D (1985) Characteristics of corticomotoneuronal postspike facilitation and reciprocal suppression of EMG activity in the monkey *J Neurophysiol* **53** 959-978
- Kemere C, Santhanam G, Byron M Y, Afshar A, Ryu S I, Meng T H and Shenoy K V (2008) Detecting neural-state transitions using hidden Markov models for motor cortical prostheses *J Neurophysiol* **100** 2441-2452
- Kim J H, Bießmann F and Lee S W (2014) Decoding Three-Dimensional Trajectory of Executed and Imagined Arm Movements from Electroencephalogram Signals *IEEE Trans Neural Syst Rehabil Eng* **PP** 1
- Kirsch S R, Schilling C and Brunner G (2006) Assessment of metallic distortions of a electromagnetic tracking system *P Soc Photo-Opt Ins* **6141** J1410-J1410
- Kubanek J, Miller K, Ojemann J, Wolpaw J and Schalk G (2009) Decoding flexion of individual fingers using electrocorticographic signals in humans *J Neural Eng* **6** 066001
- Lal T N, Hinterberger T, Widman G, Schröder M, Hill J, Rosenstiel W, Elger C, Schölkopf B and Birbaumer N (2005) *Methods towards invasive human brain computer interfaces*. In: *Advances in Neural Information Processing Systems*. Cambridge, MA: MIT Press. Saul L K, Weiss Y and Bottou L Eds.
- Lebedev M A, O'Doherty J E and Nicolelis M A (2008) Decoding of temporal intervals from cortical ensemble activity *J Neurophysiol* **99** 166-186
- Lehmann S J and Scherberger H (2013) Reach and gaze representations in macaque parietal and premotor grasp areas *J Neurosci* **33** 7038-7049

- Lemon R N (1999) Neural control of dexterity: what has been achieved? *Exp Brain Res* **128** 6-12
- Lemon R N, Mantel G W and Muir R B (1986) Corticospinal facilitation of hand muscles during voluntary movement in the conscious monkey *J Physiol* **381** 497-527
- Lin J, Wu Y and Huang T S (2000) Modeling the constraints of human hand motion *IEEE WHM* 121-126
- Liu Y, Sharma M, Gaona C M, Breshears J, Roland J, Freudenburg Z, Weinberger K Q and Leuthardt E (2010) Decoding Ipsilateral Finger Movements from ECoG Signals in Humans *Adv Neur In* **23** 1468-1476
- Luppino G, Murata A, Govoni P and Matelli M (1999) Largely segregated parietofrontal connections linking rostral intraparietal cortex (areas AIP and VIP) and the ventral premotor cortex (areas F5 and F4) *Exp Brain Res* **128** 181-187
- Matelli M, Camarda R, Glickstein M and Rizzolatti G (1986) Afferent and efferent projections of the inferior area 6 in the macaque monkey *J Comp Neurol* **251** 281-298
- Maynard E M, Nordhausen C T and Normann R A (1997) The Utah intracortical electrode array: a recording structure for potential brain-computer interfaces *Electroencephalogr Clin Neurophysiol* **102** 228-239
- McKiernan B J, Marcario J K, Karrer J H and Cheney P D (1998) Corticomotoneuronal postspike effects in shoulder, elbow, wrist, digit, and intrinsic hand muscles during a reach and prehension task *J Neurophysiol* **80** 1961-1980
- Menz V K, Schaffelhofer S and Scherberger H (2015) Representation of continuous hand and arm movements in macaque areas M1, F5, and AIP: a comparative decoding study *J Neural Eng* (subm.)
- Miao Q, Huang H-Z and Fan X (2007) A comparison study of support vector machines and hidden Markov models in machinery condition monitoring *J Mech Sci Technol* **21** 607-615
- Morrow M M and Miller L E (2003) Prediction of muscle activity by populations of sequentially recorded primary motor cortex neurons *J Neurophysiol* **89** 2279-2288
- Muakkassa K F and Strick P L (1979) Frontal lobe inputs to primate motor cortex: evidence for four somatotopically organized 'premotor' areas *Brain Res* **177** 176-182
- Mulliken G H, Musallam S and Andersen R A (2008) Forward estimation of movement state in posterior parietal cortex *Proc Natl Acad Sci U S A* **105** 8170-8177
- Murata A, Fadiga L, Fogassi L, Gallese V, Raos V and Rizzolatti G (1997) Object representation in the ventral premotor cortex (area F5) of the monkey *J Neurophysiol* **78** 2226-2230

- Murata A, Gallese V, Luppino G, Kaseda M and Sakata H (2000) Selectivity for the shape, size, and orientation of objects for grasping in neurons of monkey parietal area AIP *J Neurophysiol* **83** 2580-2601
- Musallam S, Corneil B D, Greger B, Scherberger H and Andersen R A (2004) Cognitive control signals for neural prosthetics *Science* **305** 258-262
- Mushiake H, Saito N, Sakamoto K, Itoyama Y and Tanji J (2006) Activity in the lateral prefrontal cortex reflects multiple steps of future events in action plans *Neuron* **50** 631-641
- National Research Council (2003) *Guidelines for the care and use of mammals in neuroscience and behavioral research*. Washington, D.C.: National Academies Press.
- Neumann N and Kubler A (2003) Training locked-in patients: A challenge for the use of brain-computer interfaces *IEEE Trans Neural Syst Rehabil Eng* **11** 169-172
- Norman J (2002) Two visual systems and two theories of perception: An attempt to reconcile the constructivist and ecological approaches *Behav Brain Sci* **25** 73-144
- Nudo R J (2007) Postinfarct cortical plasticity and behavioral recovery *Stroke* **38** 840-845
- O'Doherty J E, Lebedev M A, Hanson T L, Fitzsimmons N A and Nicolelis M A (2009) A brain-machine interface instructed by direct intracortical microstimulation *Front Integr Neurosci* **3** 20
- O'Doherty J E, Lebedev M A, Ifft P J, Zhuang K Z, Shokur S, Bleuler H and Nicolelis M A (2011) Active tactile exploration using a brain-machine-brain interface *Nature* **479** 228-231
- Paninski L, Fellows M R, Hatsopoulos N G and Donoghue J P (2004) Spatiotemporal tuning of motor cortical neurons for hand position and velocity *J Neurophysiol* **91** 515-532
- Pesaran B, Nelson M J and Andersen R A (2006) Dorsal premotor neurons encode the relative position of the hand, eye, and goal during reach planning *Neuron* **51** 125-134
- Pesaran B, Pezaris J S, Sahani M, Mitra P P and Andersen R A (2002) Temporal structure in neuronal activity during working memory in macaque parietal cortex *Nat Neurosci* **5** 805-811
- Petrides M and Pandya D N (1984) Projections to the frontal cortex from the posterior parietal region in the rhesus monkey *J Comp Neurol* **228** 105-116
- Pistohl T, Schmidt T S, Ball T, Schulze-Bonhage A, Aertsen A and Mehring C (2013) Grasp detection from human ECoG during natural reach-to-grasp movements *PLoS One* **8** e54658
- Pistohl T, Schulze-Bonhage A, Aertsen A, Mehring C and Ball T (2012) Decoding natural grasp types from human ECoG *Neuroimage* **59** 248-260

- Platt J (1999) *Fast training of support vector machines using sequential minimal optimization*. In: *Advances in kernel methods—support vector learning*. Cambridge, MA: MIT Press. Schölkopf B, Burges C J C and Smola A J Eds.
- Poliakov A V and Schieber M H (1999) Limited functional grouping of neurons in the motor cortex hand area during individuated finger movements: A cluster analysis *J Neurophysiol* **82** 3488-3505
- Quiroga R Q, Nadasdy Z and Ben-Shaul Y (2004) Unsupervised spike detection and sorting with wavelets and superparamagnetic clustering *Neural Comput* **16** 1661-1687
- Raab F H, Blood E B, Steiner T O and Jones H R (1979) Magnetic position and orientation tracking system *IEEE T Aero Elec Sys* **15** 709-718
- Rabiner L (1989) A tutorial on hidden Markov models and selected applications in speech recognition *Proc IEEE* **77** 257-286
- Raos V, Umiltà M A, Murata A, Fogassi L and Gallese V (2006) Functional properties of grasping-related neurons in the ventral premotor area F5 of the macaque monkey *J Neurophysiol* **95** 709-729
- Raspopovic S, Capogrosso M, Petrini F M, Bonizzato M, Rigosa J, Di Pino G, Carpaneto J, Controzzi M, Boretius T and Fernandez E (2014) Restoring natural sensory feedback in real-time bidirectional hand prostheses *Sci Transl Med* **6** 222ra219
- Rathelot J A and Strick P L (2006) Muscle representation in the macaque motor cortex: an anatomical perspective *Proc Natl Acad Sci U S A* **103** 8257-8262
- Rathelot J A and Strick P L (2009) Subdivisions of primary motor cortex based on corticomotoneuronal cells *Proc Natl Acad Sci U S A* **106** 918-923
- Reed C L, Shoham S and Halgren E (2004) Neural substrates of tactile object recognition: an fMRI study *Hum Brain Mapp* **21** 236-246
- Rehg J M and Kanade T (1994) Visual tracking of high dof articulated structures: an application to human hand tracking *3rd European Conference on Computer Vision* Stockholm, Sweden 35-46
- Rizzolatti G, Camarda R, Fogassi L, Gentilucci M, Luppino G and Matelli M (1988) Functional organization of inferior area 6 in the macaque monkey. II. Area F5 and the control of distal movements *Exp Brain Res* **71** 491-507
- Rizzolatti G and Fadiga L (1998) *Grasping Objects and Grasping Action Meanings: the Dual Role of Monkey Rostroventral Premotor Cortex (Area F5)*. In: *Sensory Guidance of Movement*. Chichester: Wiley. Novartis Foundation Symposium 218

- Rizzolatti G, Gentilucci M, Fogassi L, Luppino G, Matelli M and Ponzoni-Maggi S (1987) Neurons related to goal-directed motor acts in inferior area 6 of the macaque monkey *Exp Brain Res* **67** 220-224
- Rizzolatti G and Luppino G (2001) The cortical motor system *Neuron* **31** 889-901
- Rossini P M, Micera S, Benvenuto A, Carpaneto J, Cavallo G, Citi L, Cipriani C, Denaro L, Denaro V and Di Pino G (2010) Double nerve intraneural interface implant on a human amputee for robotic hand control *Clin Neurophysiol* **121** 777-783
- Saito N, Mushiake H, Sakamoto K, Itoyama Y and Tanji J (2005) Representation of immediate and final behavioral goals in the monkey prefrontal cortex during an instructed delay period *Cereb Cortex* **15** 1535-1546
- Sakata H, Taira M, Kusunoki M, Murata A and Tanaka Y (1997) The TINS Lecture. The parietal association cortex in depth perception and visual control of hand action *Trends Neurosci* **20** 350-357
- Sakata H, Taira M, Kusunoki M, Murata A, Tsutsui K, Tanaka Y, Shein W N and Miyashita Y (1999) Neural representation of three-dimensional features of manipulation objects with stereopsis *Exp Brain Res* **128** 160-169
- Sakata H, Taira M, Murata A and Mine S (1995) Neural mechanisms of visual guidance of hand action in the parietal cortex of the monkey *Cereb Cortex* **5** 429-438
- Schaffelhofer S, Agudelo-Toro A and Scherberger H (2015) Decoding a wide range of hand configurations from macaque Motor, Premotor, and Parietal Cortices *J Neurosci* **35** 1068-1081
- Schaffelhofer S and Scherberger H (2012) A new method of accurate hand- and arm-tracking for small primates *J Neural Eng* **9** 026025
- Schwartz M L and Goldman-Rakic P S (1984) Callosal and intrahemispheric connectivity of the prefrontal association cortex in rhesus monkey: relation between intraparietal and principal sulcal cortex *J Comp Neurol* **226** 403-420
- Shenoy K V, Meeker D, Cao S, Kureshi S A, Pesaran B, Buneo C A, Batista A P, Mitra P P, Burdick J W and Andersen R A (2003) Neural prosthetic control signals from plan activity *Neuroreport* **14** 591-596
- Smola A J and Schölkopf B (2004) A tutorial on support vector regression *Stat Comput* **14** 199-222
- Snyder L, Batista A and Andersen R (1997) Coding of intention in the posterior parietal cortex *Nature* **386** 167-170



- Stark E, Asher I and Abeles M (2007) Encoding of reach and grasp by single neurons in premotor cortex is independent of recording site *J Neurophysiol* **97** 3351-3364
- Taira M, Boline J, Smyrnis N, Georgopoulos A P and Ashe J (1996) On the relations between single cell activity in the motor cortex and the direction and magnitude of three-dimensional static isometric force *Exp Brain Res* **109** 367-376
- Thach W T (1978) Correlation of neural discharge with pattern and force of muscular activity, joint position, and direction of intended next movement in motor cortex and cerebellum *J Neurophysiol* **41** 654-676
- Townsend B R, Subasi E and Scherberger H (2011) Grasp movement decoding from premotor and parietal cortex *J Neurosci* **31** 14386-14398
- Travis A M (1955) Neurological deficiencies after ablation of the precentral motor area in *Macaca mulatta* *Brain* **78** 155-173
- Tsutsui K-I, Jiang M, Yara K, Sakata H and Taira M (2001) Integration of Perspective and Disparity Cues in Surface-Orientation-Selective Neurons of Area CIP *J Neurophysiol* **86** 2856-2867
- Tsutsui K-I, Sakata H, Naganuma T and Taira M (2002) Neural correlates for perception of 3D surface orientation from texture gradient *Science* **298** 409-412
- Umiltà M A, Brochier T, Spinks R L and Lemon R N (2007) Simultaneous recording of macaque premotor and primary motor cortex neuronal populations reveals different functional contributions to visuomotor grasp *J Neurophysiol* **98** 488-501
- Vargas-Irwin C E, Shakhnarovich G, Yadollahpour P, Mislow J M, Black M J and Donoghue J P (2010) Decoding complete reach and grasp actions from local primary motor cortex populations *J Neurosci* **30** 9659-9669
- Velliste M, Kennedy S D, Schwartz A B, Whitford A S, Sohn J W and McMorland A J (2014) Motor cortical correlates of arm resting in the context of a reaching task and implications for prosthetic control *J Neurosci* **34** 6011-6022
- Velliste M, Perel S, Spalding M C, Whitford A S and Schwartz A B (2008) Cortical control of a prosthetic arm for self-feeding *Nature* **453** 1098-1101
- Wang Z, Gunduz A, Brunner P, Ritaccio A L, Ji Q and Schalk G (2012) Decoding onset and direction of movements using Electrocorticographic (ECoG) signals in humans *Front Neuroeng* **5** 15
- Welch G and Bishop G (2006) *An Introduction to the Kalman Filter*. Chapel Hill, NC: University of North Carolina.

- Wessberg J, Stambaugh C R, Kralik J D, Beck P D, Laubach M, Chapin J K, Kim J, Biggs S J, Srinivasan M A and Nicolelis M A (2000) Real-time prediction of hand trajectory by ensembles of cortical neurons in primates *Nature* **408** 361-365
- Williams J C, Rennaker R L and Kipke D R (1999) Long-term neural recording characteristics of wire microelectrode arrays implanted in cerebral cortex *Brain Res Protoc* **4** 303-313
- Wilson F A, Scalaidhe S P and Goldman-Rakic P S (1993) Dissociation of object and spatial processing domains in primate prefrontal cortex *Science* **260** 1955-1958
- Wissel T, Pfeiffer T, Frysch R, Knight R T, Chang E F, Hinrichs H, Rieger J W and Rose G (2013) Hidden Markov model and support vector machine based decoding of finger movements using electrocorticography *J Neural Eng* **10** 056020
- Wolpaw J R and McFarland D J (2004) Control of a two-dimensional movement signal by a noninvasive brain-computer interface in humans *Proc Natl Acad Sci U S A* **101** 17849-17854
- Wood F, Donoghue J P and Black M J (2005) Inferring attentional state and kinematics from motor cortical firing rates *Proceedings of the 2005 IEEE Engineering in Medicine and Biology 27th Annual Conference* Shanghai, China 149-152
- Wu W, Gao Y, Bienenstock E, Donoghue J P and Black M J (2006) Bayesian population decoding of motor cortical activity using a Kalman filter *Neural Comput* **18** 80-118
- Wu W, Shaikhouni A, Donoghue J P and Black M J (2004) Closed-loop neural control of cursor motion using a Kalman filter *Proceedings of the 26th Annual International Conference of the IEEE EMBS* San Francisco, CA, USA 4126-4129

**Abbreviations**

<b>AIP</b>	anterior intraparietal area
<b>AS</b>	arcuate sulcus
<b>CIP</b>	caudal intraparietal sulcus
<b>CS</b>	central sulcus
<b>DLPF</b>	dorsolateral prefrontal cortex
<b>DO</b>	dorsal opercular area
<b>DOF</b>	degree of freedom
<b>DP</b>	dorsal prelunate area
<b>ECoG</b>	electrocorticogram
<b>EEG</b>	electroencephalogram
<b>F1</b>	primary motor cortex (M1)
<b>F5</b>	rostral part of ventral premotor area
<b>F5a</b>	anterior (and ventral) part of the postarcuate bank in F5
<b>F5c</b>	postarcuate convexity in F5
<b>F5p</b>	posterior (and dorsal) part of the postarcuate bank in F5
<b>FEF</b>	frontal eye field
<b>GrF</b>	granular frontal area
<b>IAS</b>	inferior arcuate sulcus
<b>IFS</b>	inferior frontal sulcus
<b>IPD</b>	inferior precentral dimple
<b>IPS</b>	intraparietal sulcus
<b>IT</b>	inferotemporal lobe
<b>LDA</b>	linear discriminant analysis
<b>LGN</b>	lateral geniculate nucleus

<b>LIP</b>	lateral intraparietal area
<b>LS</b>	lateral sulcus / lunate sulcus
<b>ISTS</b>	lateral superior temporal sulcus
<b>M1</b>	primary motor cortex
<b>MIP</b>	medial intraparietal sulcus
<b>MT</b>	middle temporal area
<b>PM</b>	premotor cortex
<b>PMd</b>	dorsal premotor cortex
<b>PMv</b>	ventral premotor cortex
<b>PPC</b>	posterior parietal cortex
<b>PRR</b>	parietal reach region
<b>PS</b>	principle sulcus
<b>S</b>	spur of the arcuate sulcus
<b>SII</b>	secondary somatosensory area
<b>SAS</b>	superior arcuate sulcus
<b>SMA</b>	supplementary motor area
<b>STS</b>	superior temporal sulcus
<b>SVM</b>	Support Vector Machine
<b>V1</b>	primary visual cortex
<b>VIP</b>	ventral intraparietal area
<b>wSVM</b>	weighted Support Vector Machine

# Curriculum Vitae

## Personal information

**Name** Veera Katharina Menz  
**Affiliation** Research Group Primate Neurobiology  
German Primate Center  
Kellnerweg 4, 37077 Göttingen  
**Phone** +49 551 3851 484  
**Email** kmenz@dpz.eu  
Katharina.Menz@gmx.de

**Date of birth** August 20, 1984  
**Place of birth** Hünfeld, Germany

## Education

2011 – present PhD student at the Research Group Primate Neurobiology, German Primate Center, Göttingen, Germany  
Title of PhD thesis: *“Continuous detection and prediction of grasp states and kinematics from primate motor, premotor, and parietal cortex”*  
Participant of the GGNB doctoral program *“Theoretical and Computational Neuroscience” (PTCN)*, thesis committee:

- Prof. Dr. Hansjörg Scherberger (German Primate Center)
- Prof. Dr. Fred Wolf (Max Planck Institute for Dynamics and Self-Organization)
- Prof. Dr. Alexander Gail (German Primate Center)

2004 – 2010 Studies of mathematics with physics as second subject (Diplom: 1,0),  
Mathematical Institute, University of Cologne, Germany  
Title of diploma thesis: *“Modelling of Synaptic STDP and Analysis in a Two-Neuron Model”*

1995 – 2004 Wigbertschule Hünfeld, Abitur (1,6)

## Languages

German Native speaker  
Finnish Second mother tongue  
English Excellent  
Latin Latin proficiency certificate

## Professional Experience

- 2010 – 2011            Research Assistant, Research Group of Prof. Dr. Tassilo Küpper,  
Mathematical Institute, University of Cologne
- 2009 – 2010            Undergraduate Assistant, Research Group of Prof. Dr. Tassilo Küpper,  
Mathematical Institute, University of Cologne

## Teaching Experience

- 2012 – 2013            Supervision Master Thesis “*Principal component analysis for Kalman filter decoding of grasping movements from area AIP, F5, and M1*”
- 2012                      Supervision lab rotation “*Systemic Neurobiology*”: “*The influence of spike sorting on decoding of grasping movements with a Kalman Filter from area AIP, F5 and M1*”
- 2012                      Teaching assistant, “*Motor Systems*” lecture and seminar
- 2010 – 2011            Tutor of mathematics students

## Certificates

- Mar 2012                “*Scientific integrity & the responsible conduct of research*”, German Primate Center, Göttingen
- Feb 2012                40-hours course in Laboratory Animal Science according to the recommendations of the FELASA (Category B)
- May 2011                Communication training “*Sag's klar*” for scientists, organized by the Klaus Tschira Stiftung

## Publications

Menz VK\*, Schaffelhofer S\*, and Scherberger H (2015): Representation of continuous hand and arm movements in macaque areas M1, F5, and AIP: a comparative decoding study. *J Neur Eng* (submitted)

Menz VK, Schaffelhofer S, and Scherberger H (2012): Decoding of reach and grasp kinematics from primate premotor, motor, and parietal cortex. *Front Comput Neurosci Conference Abstract: Bernstein Conference 2012*.

doi: 10.3389/conf.fncom.2012.55.00111

Menz VK, Popovych S, and Küpper T (2012): Modelling of Synaptic STDP and Analysis in a Two-Neuron Model. *Discontinuity, Nonlinearity and Complexity*, 1(2): 147-159.

## Programming skills

Microsoft Office, LaTeX, Matlab, Maple, basic knowledge in C++, Photoshop, Adobe Illustrator and Gimp

## Talks

- Sep 2011 *“Modelling of Synaptic STDP and Analysis in a Two-Neuron Model”*,  
Minisymposium “Modellierung und Analyse neuraler Netzwerke zum  
Verständnis sensorischer Reizverarbeitungsstörungen”,  
Annual Meeting of the Society of German Mathematicians DMV, Cologne,  
Germany
- Jan 2011 *“Modelling of Synaptic STDP and Analysis in a Two-Neuron Model”*, Max  
Planck Institute for Dynamics and Self-Organization, Göttingen, Germany
- Nov 2010 *“Modelling of Synaptic STDP and Analysis in a Two-Neuron Model”*,  
German Primate Center, Göttingen, Germany
- Nov 2009 *“Modelling of Synaptic STDP and Analysis in a Two-Neuron Model”*,  
School of Engineering, Computing and Mathematics, University of Exeter,  
UK

## Conferences

- Sep 2014 Bernstein Conference on Computational Neuroscience, Göttingen,  
Germany with poster presentation “Continuous detection and prediction  
of complete hand and arm kinematics from primate motor, premotor, and  
parietal cortex”
- Mar 2014 7<sup>th</sup> Primate Neurobiology Meeting, Tübingen, Germany with poster  
presentation “Detection and prediction of continuous hand and arm  
kinematics from primate motor, premotor, and parietal cortex”
- Dec 2013 GGNB Science Day, Göttingen, Germany with poster presentation  
„Detection and decoding of continuous hand and arm movements from  
primate motor, premotor, and parietal cortex“
- Nov 2013 Annual Meeting of the Society for Neuroscience, San Diego, CA with poster  
presentation “Decoding of movement states and continuous kinematics of  
hand and arm motions from primate motor, premotor and parietal cortex”
- Mar 2013 10<sup>th</sup> Meeting of the German Neuroscience Society, Göttingen, Germany  
with poster presentation “Decoding continuous reach and grasp  
movements from primate premotor, motor, and parietal cortex”
- Mar 2013 6<sup>th</sup> Primate Neurobiology Meeting, Göttingen, Germany with poster  
presentation “Decoding continuous reach and grasp movements from  
primate premotor, motor, and parietal cortex”
- Oct 2012 Annual Meeting of the Society for Neuroscience, New Orleans, LA with  
poster presentation “Decoding of reach and grasp kinematics from primate  
premotor, motor, and parietal cortex”
- Sep 2012 Bernstein Conference on Computational Neuroscience, Munich, Germany  
with poster presentation “Decoding of reach and grasp kinematics from  
primate premotor, motor, and parietal cortex”

Sep 2012 BCCN/BFNT SAB-Meeting, Göttingen, Germany with poster presentation  
“Decoding of reach and grasp kinematics from primate premotor, motor,  
and parietal cortex”

Mar 2012 5<sup>th</sup> Primate Neurobiology Meeting, Tübingen, Germany

Sep 2011 Annual Meeting of the Society of German Mathematicians DMV,  
Cologne, Germany

Mar 2011 9<sup>th</sup> Meeting of the German Neuroscience Society, Göttingen, Germany

Mar 2011 4<sup>th</sup> Primate Neurobiology Meeting, Göttingen, Germany

Nov 2009 “Mathematische Analyse nichtlinearer Phänomene” Meeting,  
Oberwolfach, Germany

### Workshops

Mar 2013 Excellence Workshop “Towards Long-Term Cortical Neurointerfaces”,  
Delmenhorst, Germany with poster presentation “Decoding continuous  
reach and grasp movements from primate premotor, motor, and parietal  
cortex”

Apr 2012 “Nonlinear Dynamics and Applications”, Mathematical Institute, University  
of Cologne, Cologne, Germany

Göttingen, February 27, 2015



Katharina Menz